MINISTRY OF NATIONAL EDUCATION
AND SCIENTIFIC RESEARCH

THE ANNALS OF "DUNAREA DE JOS" UNIVERSITY OF GALATI

Fascicle IX
METALLURGY AND MATERIALS SCIENCE

YEAR XXXIV (XXXIX)
September 2016, no. 3

ISSN 1453-083X

2016
GALATI UNIVERSITY PRESS

EDITORIAL BOARD

Table of Contents

THE ANNALS OF "DUNAREA DE JOS" UNIVERSITY OF GALATI
FASCICLE IX. METALLURGY AND MATERIALS SCIENCE
N°. 3 - 2016, ISSN 1453 – 083X

TRIBOLOGICAL STUDIES REGARDING THE CRUDE RAPESEED OIL PRESS

Liviu Cătălin ŞOLEA
"Dunarea de Jos" University of Galati, Romania
e-mail: csolea@ugal.ro

ABSTRACT

The aim of this paper is to present a tribology test conducted on crude rapeseed oil press. The experiments were carried out with four-ball machine. The oil was tested at speed of 1000 rot/min and loads of 140 N and 200 N. Times of the test were 1200, 2400 and 3600 seconds. During the action of the 140 N load, the friction force has an almost linear increase, unlike the friction force recorded at the load of 200 N, when it was noticed a sharp increase in the range of 0 to 800 seconds, followed then by a stabilization of the friction force.

KEYWORDS: lubricant, rapeseed oil, friction force, four-ball machine

1. Introduction

In the recent years, tribological and rheological behavior studies of vegetable oils have been the subject of research both from our country and other countries. The gradual replacement of conventional lubricants with fast biodegradable lubricants aroused the interest of many researchers [1-8].

The tribological behavior of the vegetable oils was tested on various tribology testers [9-12], but in particular on the four-ball machine [13-21].

The four-ball machine can be used to perform studies of the resistance to wear and resistance to galling. In the work [22] the authors studied the tribological behavior of sunflower oils, obtained from the six stages of processing in comparison with the hydraulic oil H32.

Jayadas [23] compared the wear resistance of coconut oil with the SAE 20W50 mineral oil. Chiong Ing *et al.* [14], using the four-ball machine, conducted a tribology study for an oil palm refined in comparison with a paraffinic mineral oil.

Farooq *et al.*, in the work [24], using the entire machine with four balls, have examined the tribological behavior for the sesame oil and castor oil. Masjuki *et al.* [25] have studied resistance to wear for both mineral oils SAE10 and the ESA30 additives (varying percentages) with methyl ester of oil palm on the four-ball machine. Husnawan *et al.* [26], using the four-ball machine have studied the influence of the oil palm and the additive amino phosphates in a mineral oil (SN 500). It was noted that the palm oil caused a sign of wear less than mineral oil while the mixture of mineral oil with oil palm 30% and additive by 3% amino phosphates causes the smaller wear diameter.

2. Experimental procedure

Tribology tests have been carried out on the four-ball machine (Fig. 1).

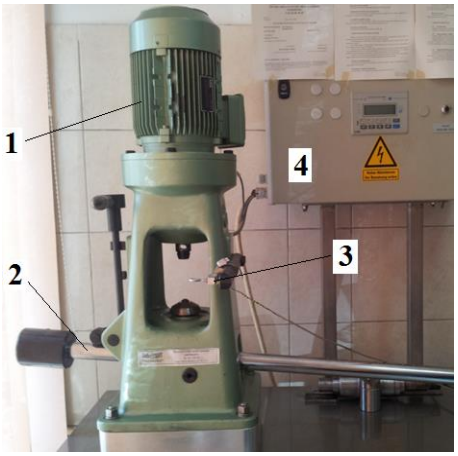

Fig. 1. *Four-ball machine*

This machine is located within the laboratory "Lubritest" of Department of Mechanical Engineering of the Engineering Faculty from "Dunarea de Jos" University of Galati.

In Figure 1 is presented an overall picture of the four-ball machine, together with the acquisition

system data, in accordance with standard SR EN ISO 20623:2004.

The four-ball machine components (fig. 1) are: the electric motor drive (1), the charging system (2), the force transducer (3), the electronic panel for programming the parameters of the work (4).

Using the four-ball machine was tested a lubricant that is introduced between the four balls (Fig. 2), a ball, (2) what rests on three other balls, (1) carrying a rotating movement; at the same time a system of loading (Fig. 1, pos. 2) ensures a contact pressure between the four balls [27].

Fig. 2. *All the four balls*

Fig. 3. *The acquisition system and processing of experimental data*

The friction force was measured using a tens sensor (3) (Fig.1), fixed between the support frame and the cup mounting arm of the three-ball system. The signal sent by the tens sensor is captured by a Scout type 55 system (2) (Fig. 3) and sent to a computer (1) (Fig. 3). The CATMAN® Express 4.5 system was used for data acquisition and processing.

Table 1. The chemical composition EN31 (%) [26]

Material	C	Cr	Mn	Si	S	P	VHN
EN31	1.0	1.3	0.5	0.35	0.05	0.05	805

The four balls have a diameter of 12.7 mm made of steel with the composition and the hardness presented in Table 1. The balls are especially treated and have a very small tolerance of the diameter (± 0.0005 mm), hardness and the quality of the surface: Ra = 0.02 ... 0.03 mm.

3. Experimental results

In this paper was performed a tribological tests on crude rapeseed oil press. The experiments have been performed on the four-ball machine. It was measured the friction force obtained as a result of the contact between the ball located in the rotational motion and on the three fixed balls.

The oil has been tested at speed of 1000 rot/min and loads of 140 N and 200 N. The period of the tests has been 1200, 2400 and 3600 seconds.

Figure 4 represented the variation of friction force for 1200 seconds, on 140 N. It can be noticed a linear increase of the friction force through the analyzed time interval.

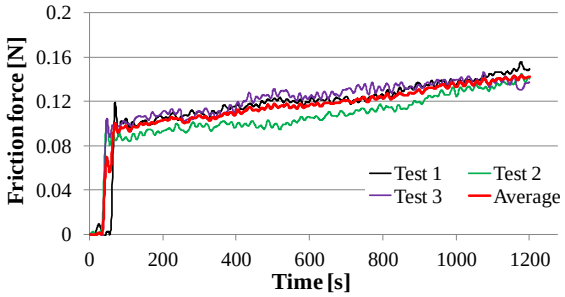

Fig. 4. *Friction force variation with time at 140 N, 1200 seconds*

In Figure 5 were represented the variations of friction force in time for 1200 seconds, for the load with 200 N. Increasing the load from 140 N to 200 N it is notable an increase of the friction force. In the first part of the tests (0-800 s) was recorded a sharp increase of the friction force. In the range 800-1200 seconds it is observed a slight stabilization of the friction force.

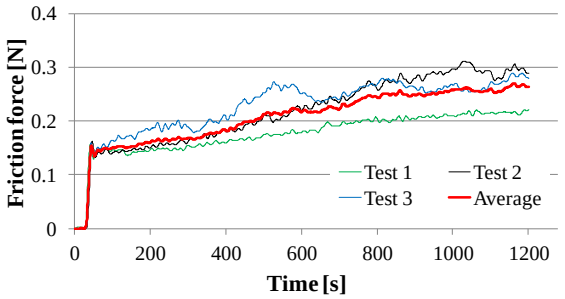

Fig. 5. *Friction force variation with time at 200 N, 1200 de seconds*

In Figure 6 were represented the variations in time of friction for 2400 seconds, for the load of 140

N. Increasing the time of the test is to be noted that the growth of the linear trend of the friction force remains the same.

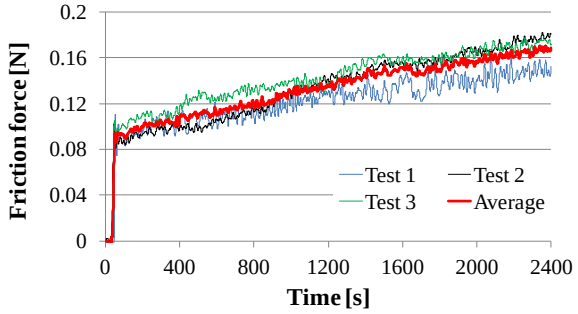

Fig. 6. *Friction force variation with time at 140 N, 2400 de seconds*

In Figure 7 were represented the variations in the time of friction force for 2400 s, for the load of 200 N. It is observed a stabilization trend of the friction force after 1200 seconds.

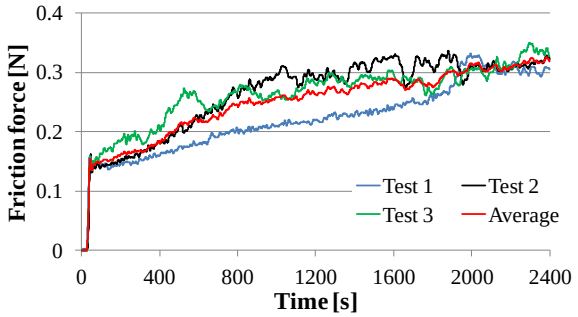

Fig. 7. *Friction force variation with time at 200 N, 2400 seconds*

In Figure 8 were represented the variations of friction force for 3600 seconds, for the two loads for which were carried out the tests.

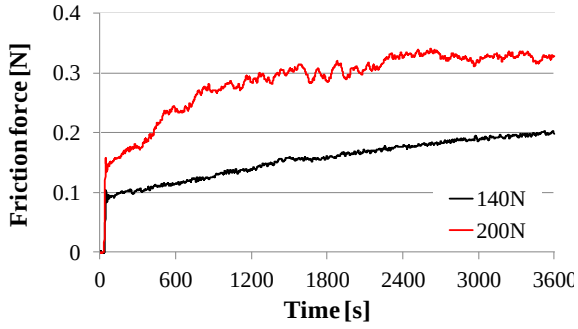

Fig. 8. *Friction force variation with time, at 140 N and 200 N loads*

The tests conducted with load of 140 N indicate an almost linear increase of the friction force, on the whole period analyzed. In the case of the tests carried out at the load of 200 N, there appears a sharp increase in the range 0-800 seconds followed by a slight increase until the final of the tests.

In Figure 9 were represented the variations of the friction force with time for 140 N and 200 N loads. So, were calculated average values of the result of friction force for the last 300 seconds of each test.

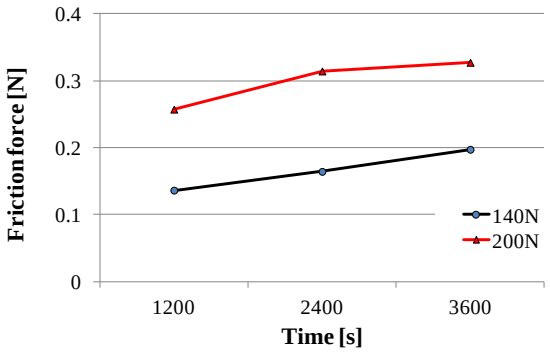

Fig. 9. *Friction force variation with time, both loads of testing, average values*

The friction force increases with the load increases, for all periods of the test. Also, the friction force increases with time trial, for both loads.

An increase of the load with 43%, from 140 N to 200 N, causes, for the test of 1200 seconds, an increase of the friction force with 87.8%. For the test of 2400 seconds, the increase is 91.3% and for the test of 3600 seconds, the increase is 65.5%.

For the tested oil on 140 N, in the period 1200 - 2400 s, the friction force increases with 19.96%, while in the last period of time the increase is 20.41%, comparable to that of the first period of time.

For the tested oil on 200 N, in the period of 1200 – 2400 s, the friction force increases with 22.18% while in the last period of time the growth is much smaller, representing 4.2%. After this last period of time, the friction force registers a tendency of stabilization.

4. Conclusions

The friction force varies with the increase of load at which the oil has been tested. During the action of the 140 N load, the friction force has an almost linear increase, unlike the friction force recorded at the load of 200 N, when it was noticed a sharp increase in the range of 0 to 800 seconds, followed then by a stabilization of the friction force. In order to determine the time after which takes place the stabilization of the friction force, for rapeseed oil

tested to load on 140 N, it is necessary to make tests for further periods of 3600 minutes.

References

[1]. Bogatu L., Ciupariu D., Tănăsescu C., *Improving the oxidation stability and biodegradability of environmentally friendly lubricants*, Revista de Chimie, 61, no. 10, 2010.
[2]. Bogatu L., Dragomir E. R., *Influence of additives on antiwear and extreme pressure behavior of vegetable oils*, Revista de Chimie, 67, no. 4, 2016.
[3]. Bhaumik S., Pathak S. D., *A comparative experimental analysis of tribological properties between commercial mineral oil and neat castor oil using Taguchi method in boundary lubrication regime*, Tribology in Industry, vol. 38, issue 1, p. 33-44, 2016.
[4]. Hassan M., Ani F. N., Syahrullail S., *Tribological features of refined, deodorized and bleached palm oil with mineral oil blend*, Tribology Transactions, 2015.
[5]. Calixto Rodríguez-Martínez, Francisco Lafargue-Pérez, José Ángel Sotolongo-Pérez, Annarella Rodríguez-Poveda, Juliano Chitue de Assuncao Nascimento, *Determinación de las propiedades físicas y carga crítica del aceite vegetal Jatropha curcas L.*, Ingeniería Mecánica, vol. 15, no. 3, p. 170-175, Havana, ISSN 1815-5944, 2012.
[6]. Calixto Rodríguez-Martínez, Francisco Lafargue-Pérez, *Comparación experimental de un aceite vegetal y un aceite mineral básico como lubricantes en el par tribológico acero-babbit*, Tecnologia Quimica, Havana, vol. 33, no. 1, p. 74-80, 2013.
[7]. Stanciu I., *A study of rheological behavior for refined rapeseed oil*, Ovidius University Annals of Chemistry, vol. 24, no. 1, p. 51-54, 2013.
[8]. Stanciu I., *New relationship to describe the rheology of sunflower oil*, Ovidius University Annals of Chemistry, vol. 25, issue 1, p. 28-31, 2014.
[9]. Arnsek A., Vizintin J., *Lubricating properties of rapeseed-based oils*, Journal Synth Lubr, 16 (4), p. 281-296, 1999.
[10]. Kalin M., Vizintin J., *The tribological performance of DLC-coated gears lubricated with biodegradable oil in various pinion/gear material combinations*, Wear, 259, p. 1270-1280, 2005.
[11]. Maru M. M., Trommer R. M., Almeida F. A., Silva R., Achete C. A., *Assessment of the lubricant behavior of biodiesel fuels using stribeck curves*, Fuel Processing Technology, 116, p. 130-134, 2013.
[12]. Salih N., Salimon J., Yousif E., *The physicochemical and tribological properties of oleic acid based triester biolubricants*, Industrial Crops and Product, 34, p. 1089-1096, 2011.
[13]. Spânu C., Rîpă M., Ciortan S., *Study of wear evolution for a hydraulic oil using a four-ball tester*, The Annals of University "Dunărea de Jos" of Galati, Fascicle VIII, Tribology, p. 186, 2008.
[14]. Chiong Ing T., Rafiq A. K. M., Ayli Z., Syahrullail S., *Tribological behavior of refined bleached and deodorized palm olein in different loads using a four-ball tribotester*, Scientia Iranica B, 19 (6), p. 1487-1492, 2012.
[15]. Haseeb A. S. M. A., Sia S. Y., Fazal M. A., Masjuki H. H., *Effect of temperature on tribological properties of palm biodiesel*, Energy, 35, p. 1460-1464, 2010.
[16]. Ing T. C., Rafiq A. K. M., Azli Y., Syahrullail S., *The effect of temperature on the tribological behavior of RBD palm stearin*, Tribology Transactions, 55, p. 539-548, 2012.
[17]. Rounds F., *Effects of hydroperoxides on wear as measured in four-ball wear tests*, Tribology Transactions, 36 (2), p. 297-303, 1993.
[18]. Shahabuddin M., Masjuki H. H., Kalam M. A., Bhuiya M. M. K., Mehat H., *Comparative tribological investigation of bio-lubricant formulated from a non-edible oil source (Jatropha oil)*, Industrial Crops and Products, 47, p. 323-330, 2013.
[19]. Zulkifli N. W. M., Kalam M. A., Masjuki H. H., Shahabuddin M., Yunus R., *Wear prevention characteristics of a palm oil-based TMP (trimethylolpropane) ester as an engine lubricant*, Energy, 54, p. 167-173, 2013.
[20]. Zeng X., Wu H., Yi H., *Tribological behavior of three novel triazine derivates as additives in rapeseed oil*, Wear, 262, p. 718-726, 2007.
[21]. Zhu F., Fan W., Wang A., Zhu Y., *Tribological study of novel S-N style 1,3,4-thiadiazole-2-thione derivatives in rapeseed oil*, Wear, 266, p. 233-238, 2009.
[22]. Calomir C., Ştefănescu I., Şolea L. C., Chiriţă G., *Vegetal oils as lubricating materials*, The Annals of „Dunarea de Jos" University of Galati, Fascicle VIII, Tribology, p. 154-160, (XV), ISSN 1221-4590, Galati University Press, 2008.
[23]. Jayadas N. H., Prabhakaran N., Ajithkumar G., *Tribological evaluation of coconut oil as an environment-friendly lubricant*, Tribology International, 40, p. 350-354, 2007.
[24]. Farooq M., Ramil A., Gul S., Muhammad N., *The study of wear behavior of 12-hydroxystearic acid in vegetable oil*, Journal of Applied Sciences, 11 (8), p. 1381-1385, 2011.
[25]. Masjuki H. H., Maleque M. A., *Investigation of the anti-wear characteristics of palm oil methyl ester using a four-ball tribotester test*, Wear, 206, p. 179-186, 1997.
[26]. Husnawan M., Saifullah M. G., Masjuki H. H., *Development of friction force model for mineral oil basestock containing palm olein and antiwear additive*, Tribology International, 40, p. 74-81, 2007.
[27]. ***, *Micro Photonics Inc., Friction & Wear Testing, Four Ball Wear*, online at http://www.microphotonics.com/tribomt.html (12.08.2008).

THE ANNALS OF "DUNAREA DE JOS" UNIVERSITY OF GALATI
FASCICLE IX. METALLURGY AND MATERIALS SCIENCE
Nº. 3 - 2016, ISSN 1453 – 083X

THE INFLUENCE OF THE CARBON CONTENT ON THE DEPTH OF THE CARBONITRURAT LAYER IN FLUIDIZED LAYER FOR 1C15, 1C25 AND 1C45 STEELS

Marian-Iulian NEACȘU, Sorin DOBROVICI, Nicolae DIACONU
"Dunarea de Jos" University of Galati
e-mail: uscaeni@yahoo.com

ABSTRACT

This paper presents the experimental research of carbonitriding thermochemical processing in fluidized layer performed on some samples of carbon steel with different carbon contents, the fluidized layer being made up of a mixture of quartz sand and gases (methane, ammonia and air).

The thermochemical treatments have been carried out over a time period of two hours and thirty minutes for all temperatures considered for the study. An important parameter of this type of thermochemical processing was also represented by the ratio of methane and ammonia that influenced the final results of the research.

The research results revealed the influence of the carbon content of the steels investigated on the thickness values of the carbonitrided layer for samples investigated.

KEYWORDS: carbo nitriding, fluidized bed, hardness, surface layer

1. Introduction

Carbonitriding is the thermochemical treatment that is normally applied on carburizing carbon steels, in a temperature range between 830...870 °C. The treatment environments used are various (solid, liquid, gaseous, plasma, vacuum) so that the concentration of carbon at the surface to be brought to 0.8...0.9% and that of the nitrogen to 0.3...0.4% [1].

The structure of the carbonitrided layer at these temperatures is much closer to that of the carburated layers because at high temperatures, carbon diffusion is more intense than that of nitrogen [2].

The durability of the carbonitrurate parts being one of the most important objectives in the construction of cars, by carbonitriding this objective is successfully accomplished.

The most desired and most used properties complex in technological applications consists in [3]:

- high toughness in the middle of the piece;
- high hardness at the surface of the piece.

Fluidized layer carbonitriding involves achieving an active carbonitriding environment inside a fluidized bed by overlapping two categories of phenomena:

- fluidization (transformation of a fixed bed of inert beads of firebrick with 0.10...0.16 mm average size in a fluidized bed gas mixture)
- carbonitriding, which involves choosing a gas mixture (methane and ammonia, in varying proportions) allowing the accelerated implementation of this treatment at the working temperature specific to carbonitriding.

Developing and extending the use of fluidized bed heat treatment facilities was and is determined by a number of advantages offered by such facilities. Technical and economic aspects related to the construction (acquisition) and the operation of such plants show that there are advantages over other types of equipment used in heat treatment [4].

The gas mixture for carburizing serves to generate at the treatment temperature the active carbon atoms which are adsorbed and then dispersed in the material. This mixture can be obtained from:

- natural gas,
- endogas purified by natural gas addition,
- exogas purified by natural gas addition,
- gaseous atmosphere obtained from the gasification of liquid hydrocarbons [3].

Active carbon atoms are obtained by a reaction of endothermic dissociation of methane gas as soon

as it enters the high temperature fluidized bed as a result of contact with hot sand grains [5].

$$CH_4 \leftrightarrow C + 2H_2 \quad (1)$$

Methane easily dissociates at high temperatures and therefore the amount of methane that is placed in the oven must be very well controlled to avoid the production of the so-called hydrocarbon black. Active carbon excess that is not adsorbed becomes a layer of amorphous carbon and slows much the further process kinetics [6].

Ammonia is introduced into the workspace to generate nitrogen atoms that are active and also adsorbed and then diffused towards the interior of the material. Dissociation of ammonia occurs after an endothermic reaction [7] and at temperatures of 500 °C, under the presence of dissociation energy, the decomposition is total:

$$2NH_3 \leftrightarrow N_2 + 3H_2 \quad (2)$$

Also in the case of fluidized layer carbonitriding, the main chemical reactions that occur inside the furnace working atmosphere, which is a gaseous atmosphere (homogeneous systems) and between this and the parts surfaces (heterogeneous systems) are:

$$2CO = C_{(\gamma)} + CO_2 \quad (3)$$

$$CO + H_2O = CO_2 + H_2 \quad (4)$$

$$CH_4 = C_{(\gamma)} + 2H_2 \quad (5)$$

$$NH_3 = N_{(\gamma)} + 3/2H_2 \quad (6)$$

Carbonitriding in a fluidized bed is in fact a gas carbonitriding with conditions in the theoretical treatment, respectively the reactions of dissociation in the components of the medium, adsorption of the carbon and nitrogen atoms and finally their diffusion.

Carburized steels are carbon steels with a maximum carbon content of 0.25%, but may also be higher concentrations steels. After carburizing, the surface carbon concentration can reach 0.7...1.2%.

2. Materials and method of research

Samples of 3 carbon steel grades - OLC 15, OLC 25 and OLC 45, whose chemical composition is shown in Table 1, were subjected to experimental research.

Table 1. *Chemical composition of steel grades subject of research*

Nr. crt.	Mark	Chemical composition, % mass								
		C	Mn	Si	P	S	Cu	Cr	Ni	Ti
1	1C 15	0.14	0.53	0.22	0.017	0.023				
2	1C25	0.22	0.48	0.32	0.025	0.450	0.21	0.17	0.10	
3	1C45	0.201	0.951	0.281	0.014	0.016	-	1.05	-	0.06

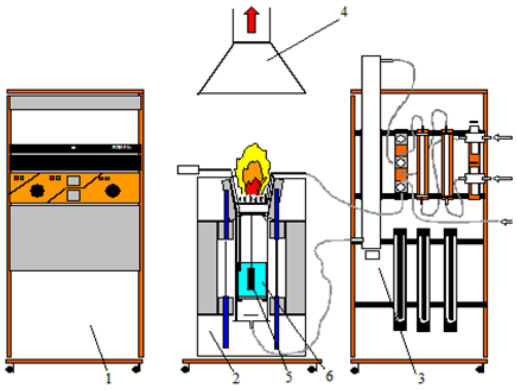

Fig. 1. *Laboratory installation for fluidized bed thermochemical treatments: 1 - system of power supply and temperature control, 2 - fluidized-bed furnace, 3 - technological gas supply rack, 4 - flue gas hood, 5 - sample, 6 - fluidized bed*

The laboratory scale installation for the thermochemical treatment of carbonitriding in a fluidized bed with the aid of which experiments have been performed is shown schematically in Figure 1.

The carbonitriding regimes that have been experienced at laboratory scale are shown in Table 2. The tests carried out had in view the influence of carbon content of the three steel grades considered in research, on the size of the carbonitrided layer depth, depending on process parameters.

With the chosen experimental regimes, the low, medium and high carbonitriding temperatures were covered, at the same value of maintaining duration of 2 hours and 30 minutes for three values of the ammonia percentage (5%, 15%, 25%) introduced in the system.

Table 2. *Thermochemical treatment regimes tested*

Nr. crt.	Proportion of ammonia [%]	Temperature [°C]	Duration of carbonitriding h, min
1	25	900	2h 30min
2		750	
3		650	
4		550	
5	15	900	2h 30min
6		750	
7		650	
8		550	
9	5	950	2h 30min
10		750	
11		650	
12		550	

The technology is based on mass and energy transfer from medium to pieces. This is why a good circulation of the gaseous medium is particularly important for a successful treatment.

The carbonitriding medium is a fluidized bed made of quartz sand grains, the fluidizing agent being an atmosphere resulting from decomposition of methane and ammonia at the working temperature.

The chemical composition of the fluidizing agent is amended by the proportions of gas at the entrance. Dissociation reactions take place quickly due to the contact of the gases introduced into the working chamber of the treatment furnace at ambient temperature and the hot granular solids. The fluidized bed is characterized by a high carbon potential and the absence of the occurrence of deposits of carbon black which inhibits carburization. Deposition of carbon black on the surface of the samples is removed from the fluidized bed of solid granules which come into contact with the surface of the sample permanently.

Methane and ammonia flow rates, the working temperature and other technological parameters were determined by preliminary experiments. Carbonitriding experiments were done on the same plant on the basis of a program in which variations of the important technological parameters were established (Table 2). The humidity of methane and ammonia was retained by a silica gel column.

3. Experimental results

After conducting experimental research on the samples, there were conducted investigations of the carbonitrided layers made without subsequent tempering (at the balance) in order to highlight the carbonitrided layer thickness variation according to the parameters of the thermochemical treatment regime for the three types of steel studied. The carbonitrided layer measurement was made in metallographic format.

Figure 2 shows the variation of the carbonitrided layer thickness at a temperature of 550 °C depending on the percentage of ammonia for the three steel types studied. The highest value of the carbonitrided layer thickness in these conditions was obtained for samples of 1C25 at a rate of 5% ammonia. The shallowest carbonitriding was recorded on samples of 1C45 at a rate of 5% ammonia. For the value of 15% ammonia, the carbonitrided layer depth decreases with the decrease in carbon content for the three grades of steel undergoing thermochemical processing. At 25% ammonia, the layer depth is increases in the following order: 1C45, 1C15, 1C25.

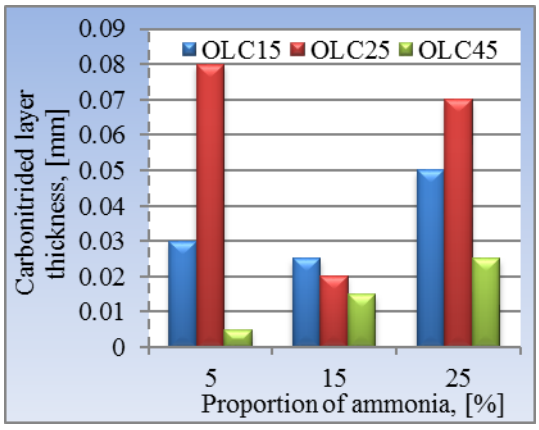

Fig. 2. *Variation of the carbonitrided layer thickness at 550 °C according to the proportion of ammonia for the three steel types studied*

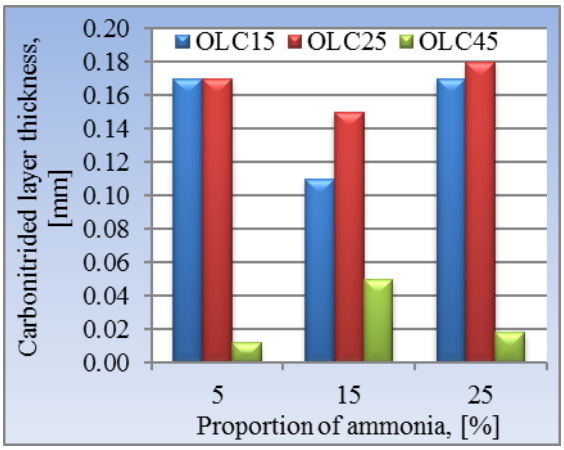

Fig. 3. *Variation of the carbonitrided layer thickness at 650 °C according to the proportion of ammonia for the three steel types studied*

The variation of the carbonitrided layer thickness at 650 °C according to the percentage of ammonia for the three steel types studied is shown in Figure 3.

At this thermo-chemical treatment temperature, for samples of 1C15 and 1C25 it has been observed that the depth of the carbonitrided layer has the same value when the ratio of ammonia is 5%. For both steels, the layer depth decreases when the ammonia percentage increases to 15%, but with a greater decrease for 1C15. At a rate of 25% ammonia, an increase in the thickness of the carbonitrided layer can be observed in both steels, at levels higher than those recorded when the percentage of ammonia is 5%.

The samples of 45 1C reach a maximum depth of the carbonitrided layer in the conditions shown in Figure 3, where the percentage of ammonia is 15%.

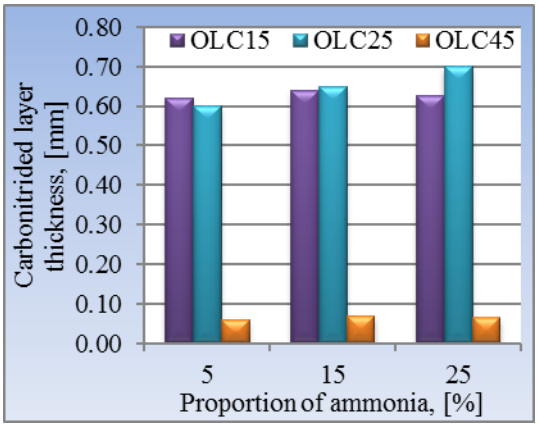

Fig. 4. *Variation of carbonitrided layer thickness at 750 °C, according to the proportion of ammonia for the three steel types studied*

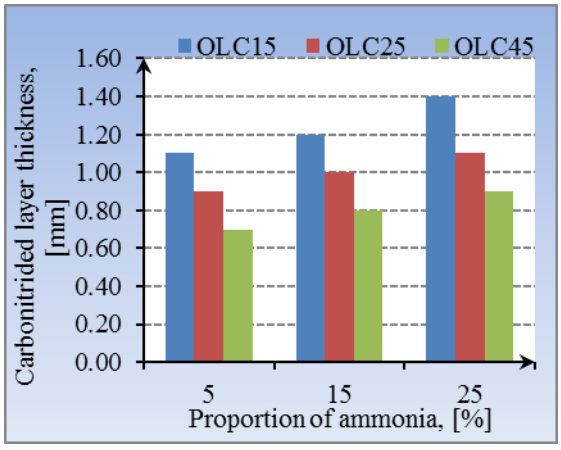

Fig. 5. *Variation of the carbonitrided layer thickness at 900 °C, according to the proportion of ammonia for the three steel types studied*

The results obtained by processing the samples at treatment temperature of 750 °C is shown in Figure 4. At this temperature of thermochemical treatment, for the samples of 1C25 it was observed that the carbonitrided layer depth increases with increasing the proportion of ammonia in the system. For the other two steels, a maximum in the depth of the layer can be noticed when the percentage of ammonia is 15%. Layer depth values for the samples of 1C15 are superior to those obtained for the samples of 1C45 steel.

Figure 5 shows the variation in thickness of the carbonitrided layer at 900 °C, according to the proportion of ammonia for the three steel types studied. The carbonitrided layer thickness increases with the increasing of ammonia percentage, for all three types of steel studied. The highest values were obtained for 1C15 in all cases, while the lowest values were obtained for steel 1C 45. In this case, it can be concluded that the carbonitrided layer thickness decreases as the percentage of carbon in the samples studied increases. At this temperature of 900°C, the nitriding process prevails and, normally, the increase of the proportion of ammonia makes its pervading to take place deeper in the samples.

Figure 6 shows the microstructure of a OLC 15 steel sample with the highest carbonitrided layer (1.4 mm) obtained at a temperature of 900 °C for a percentage of 25% ammonia.

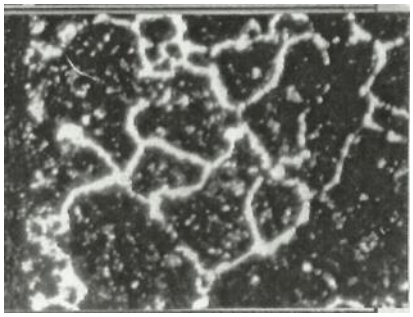

Fig. 6. *1C15 steel microstructure carbonitrided in fluidized layer at 900 °C / 2 h, 30min, 100 X magnification, attack NITAL 2%*

Figure 7 shows the microstructure of a sample of OLC 25 thermo-processed at a temperature of 750 °C with a hold time of two hours and 30 minutes, and with an intake of ammonia 25% in the carbonitriding. At 750 °C, for this sample it was obtained the highest carbonitrided layer of all samples from the three steels studied.

Figure 8 shows the microstructure of the OLC 45 sample with the greatest thickness of the carbonitrided layer, which was obtained by processing at a temperature of 900 °C / 2h, 30min with a content of 25% ammonia.

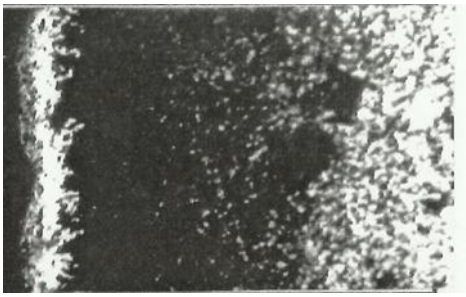

Fig. 7. *1C25 steel microstructure carbonitrided in fluidized layer at 750 °C / 2h, 30min, 100 X magnification, attack NITAL 2%*

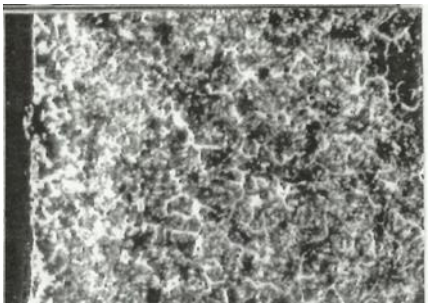

Fig. 8. *Microstructure of 1C45 steel carbonitrided in fluidized layer at 900 °C / 2h, 30 min, 100 X magnification, attack NITAL 2%*

4. Conclusions

Experimental research conducted revealed that at a fluidized bed carbonitriding temperature of 900 °C, for a processing time of 2 hours and 30 minutes and with a percentage of ammonia of 25%, there were obtained the highest depths of carbonitrided layer for the samples of three steel grades studied.

For the regimes at 900 °C, the carbonitrided layer thickness increases as the carbon content decreases in the samples investigated. At this temperature, the highest layer thickness is recorded for the samples of 1C 15. Also at 900 °C it is observed that with increasing the proportion of ammonia in the system, there occurs an increased thickness of the carbonitrided layer, too.

At 750 °C for IC 25 samples, it can be noticed that with the increase of the percentage of ammonia, there is an increase in the thickness of the carbonitrided layer. However, the difference between the maximum thickness of the carbonitrided layer in similar conditions of time and percentage of ammonia, at 900 °C and 750 °C is of 0.5 mm, which is not a neglectable difference.

An important advantage owned by heat treatment and fluidized bed thermochemical facilities is the large range of operating temperatures. Another advantage is the ability to vary within wide limits the initial composition of the gas, respectively the actual composition of the fluidized bed. Therefore, a single installation can make a large number of thermochemical treatments simply by altering the composition of gases entering the fluidized bed.

References

[1]. Dulcy M., Gantois M., *Principe de base de la cementation et de la carbo-nitruration*, Traitements termique, no. 289, p. 46-54, 1996.
[2]. Dulămilă T., Florian E., *Tratamente termice si termochimice*, Editura Didactică și Pedagogică, București, 1982.
[3]. Dobrovici S., Cazacu N., Bâclea A., *Carbonitrurarea în strat fluidizat*, Editura Fundației Universitare "Dunărea de Jos" din Galați, 2001.
[4]. Kunii D., *Fluidization engineering*, John Wiley & Sons, Inc., New York, 1991.
[5]. Samoilă C., Ionescu M. S., Drugă L., *Tehnologii și utilaje moderne de încălzire*, Editura Tehnică, București, 1986.
[6]. Hoffman R., Vogel W., *Cementation-Tempre. Oxidation marginale. Origines, etendue et effets*, Traitement thermique, no. 309, 1998.
[7]. Oprea F., Taloi D., Constantin I., Roman R., *Teoria proceselor metalurgice*, Editura Didactică și Pedagigică, București, 1978.

THE ANNALS OF "DUNAREA DE JOS" UNIVERSITY OF GALATI
FASCICLE IX. METALLURGY AND MATERIALS SCIENCE
N°. 3 - 2016, ISSN 1453 – 083X

INFLUENCE OF SOME TECHNOLOGICAL PARAMETERS OF FLUIDIZED BED CARBONITRIDING ON THE SURFACE HARDNESS OF CARBONITRIDED PARTS FROM LOW ALLOY STEELS

Marian-Iulian NEACȘU, Sorin DOBROVICI
"Dunarea de Jos" University of Galati
e-mail: uscaeni@yahoo.com

ABSTRACT

The paper describes the experimental research of thermos-chemical treatment of carbonitriding performed on samples of different brands of low alloy steels.

The technological parameters whose influence on the carbonitrided surfaces hardness was studied are thermo-chemical treatment temperature and the percentage of ammonia in the carbonitriding medium. Thermo-chemical treatments of carbonitriding have been carried out at low, medium and high temperatures.

The investigations were conducted with three values for the ammonia percentage, which lead to different results for the surface hardness of the samples subjected to the investigations.

The duration of treatment of two hours and thirty minutes, constant for all experiments performed, was chosen as the one commonly used in gas carbonitriding technologies.

KEYWORDS: thermo-chemical treatment, carbonitriding, temperature, hardness

1. Introduction

Ensuring sustainability of parts used in machine building is achieved through thermo-chemical treatment of carbonitriding.

The complex of properties most desired and most used in technological applications consists of [1]:

- high surface hardness of the piece;
- high toughness in the middle of the piece.

The thermochemical treatment of fluidized bed carburizing is used mainly in areas where heat transfer, mass transfer and heat or mass transfer are required [2, 3]. Among the most important applications of the fluidized bed are:

- chemical industry (catalytic reactions in which the catalyst is fluidized);
- oil industry (heavy oil catalytic cracking);
- thermal power (coal fluidized bed combustion).

The chemical activity of the medium is dependent on:

- proportion of gas at the furnace inlet
- the chemical composition at the working temperature because gases (methane and ammonia) undergo chemical reactions.

Thus, it is formed a gas mixture composed of hydrogen, nitrogen, ammonia and methane (in small portions), which ensures fluidity of sand grains at the working temperatures, in compliance with fluidization conditions. Practically, the properties specific to fluidized beds are achieved [4, 5].

The main chemical reactions in the case of fluidized bed carbonitriding which occur inside the furnace working atmosphere, which is a gas atmosphere, and between the latter and the surfaces of the parts, are:

$$2CO = C_{(\gamma)} + CO_2 \quad (1)$$

$$CO + H_2O = CO_2 + H_2 \quad (2)$$

$$CH_4 = C_{(\gamma)} + 2H_2 \quad (3)$$

$$NH_3 = N_{(\gamma)} + 3/2H_2 \quad (4)$$

Ammonia in atomic condition, necessary to the carbonitriding treatment, results from the phenomenon of dissociation of ammonia that takes place after an endothermic reaction [6] and, at temperatures of 500 °C, under the presence of dissociation energy, decomposition is complete:

$$2NH_3 \leftrightarrow N_2 + 3H_2 \quad (5)$$

After an endothermic dissociation reaction of methane gas active carbon atoms are obtained which enter the high temperature fluidized bed as a result of the contact with the hot sand grains [7].

$$CH_4 \leftrightarrow C + 2H_2 \quad (6)$$

In order to carry on the role for which the fluid bed is introduced into the system, the fluidization conditions must be fulfilled: the fluidization velocity, the properties of the grain solid, the fluidizing agent thermophysical properties, the characteristics of the fluidization chamber [5].

The technical and economic aspects offered by such facilities led to the development and expansion of the use of such heat treatment fluidized bed facilities [4, 8].

Due to the fact that at high temperatures the diffusion of carbon is higher than that of nitrogen, the carbonitrided layers structure at these temperatures is much close to that of the carbide layers [2, 8].

2. Materials and research method

The fluidized bed carbonitriding experiments were done on samples of 21TiMnCr12, 18MnCr10, 13CrNi40 steel whose chemical composition is shown in Table 1.

Table 1. *Chemical composition of grades of steel subject to research*

Nr. crt.	Mark	Chemical composition, % mass							
		C	Mn	Si	P	S	Cr	Ni	Ti
1	21TiMnCr12	0.2	0.95	0.28	0.014	0.016	1.05	-	0.06
2	18MnCr10	0.18	1.05	0.22	0.035	0.035	1.05	-	-
3	13CrNi40	0.13	0.45	0.22	0.035	0.035	1.45	4.00	-

The thermochemical treatment regimens studied at laboratory scale are shown in Table 2. In choosing these regimes, the recommendations from literature were taken into account and low, mid and high carbonitriding temperatures were covered for the same maintaining time of 2 hours and 30 minutes. The proportion of ammonia introduced into the system at a time was of 5%, 15%, 25%, in each variant of treatment carried out.

Table 2. *Thermochemical treatment regimes tested*

Nr. crt.	Proportion of ammonia [%]	Temperature [°C]	Duration of carbonitriding [min]
1	5	550	150
2		650	
3		750	
4		900	
5	15	550	
6		650	
7		750	
8		900	
9	25	550	
10		650	
11		750	
12		900	

In Figure 1 is shown in section the furnace in which the thermochemical treatment regimes described above were carried out.

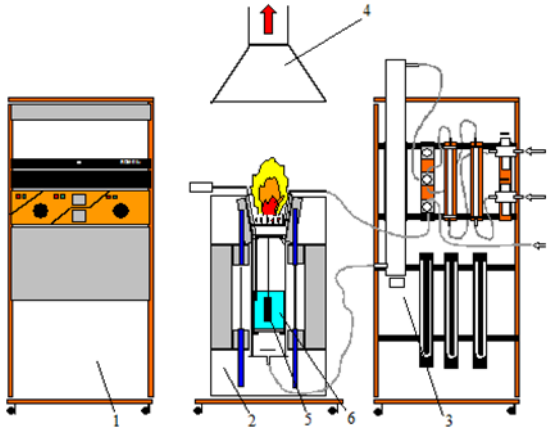

Fig. 1. *Laboratory installation for fluid bed thermo-chemical treatments: 1 - system of power supply and temperature control, 2 - the fluidized-bed furnace, 3 - technology gas supply rack, 4 - flue gas hood, 5 - sample, 6 - fluidized bed*

The thermochemical treatment technology is based on energy and mass transfer from piece to the environment and therefore a good circulation of the gaseous medium is very important to attain the objective of the thermochemical treatment.

The fluidized bed, which is made of granules of quartz sand, represents the carbonitriding environment, while the fluidizing agent is the atmosphere resulting from decomposition of methane and ammonia at the working temperature.

Changing the ratio between the two gases, ammonia and methane, lead to changes in the chemical composition of the fluidizing agent.

The contact between the gases introduced into the working chamber of the treatment furnace at the ambient temperature and the hot granular solids results in a decrease in the time of the dissociation reaction, which is an advantage of the treatment in the fluidized bed.

The fluidized bed is characterized by a high carbon potential, and the absence of the occurrence of deposits of carbon black which inhibits carburization. During the technological process, deposits of carbon black occur on the samples surface, but are removed by the solid granules from the fluidized bed, which are constantly moving and permanently gets in contact with the sample surface.

By conducting some preliminary experiments, the flow rates of methane and ammonia were established. Carbonitriding thermochemical processing regimens were made on the same plant, on the basis of a program in which variations of important technological parameters were established: the treatment temperature and the percentage of ammonia in the system. By means of a silica gel column, moisture was retained from methane and ammonia.

3. Research results

The experiments conducted have studied the influence of temperature and ammonia percentage on the surface hardness of the samples subjected to carbonitriding.

In order to determine the hardness of the carbonitrided samples surface obtained, after preliminary preparation, hardness test was performed by Vickers method with a load of 5 kg force.

Figure 2 shows the variation of the Vickers type hardness, HV5, for 21TiMnCr12 steel, depending on the temperature of treatment and the percentage of ammonia.

The highest value of hardness was obtained from samples that have been treated under the conditions: temperature of 550 °C and an ammonia concentration of 15%. The lowest values of surface hardness of this steel sample were registered in the processing regime characterized by temperature of 650 °C at a rate of 5% NH_3 and at the temperature of 750 °C with 25% NH_3.

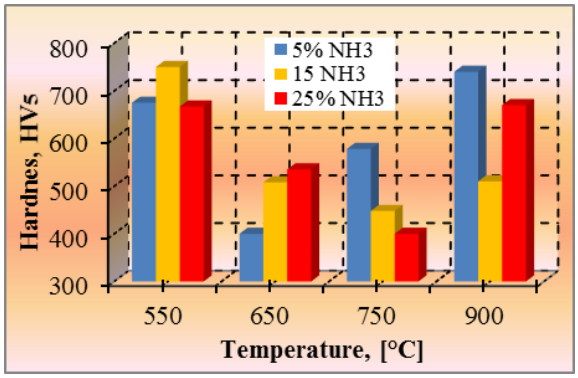

Fig. 2. *Variation of the surface hardness of 21MoMnCr12 steel samples, carbonitrided in fluidized bed for different proportions of ammonia*

For the samples of 18MnCr10 steel carbonitrided according to the regimens chosen, the change in surface hardness values is illustrated in Figure 3. At a temperature of 550 °C, the hardness corresponding to 15% NH_3 system is the highest for this temperature. Following the thermochemical processing at a temperature of 750 °C, the hardness values obtained when the percentage of NH_3 is 5 to 15% are very close. Increasing temperature to 900 °C makes the surface hardness to record hardness values of samples around 600 daN/mm^2 for all three concentrations of ammonia.

The lowest hardness value was obtained for the samples treated at 750 °C when the supply of NH_3 was of 25%.

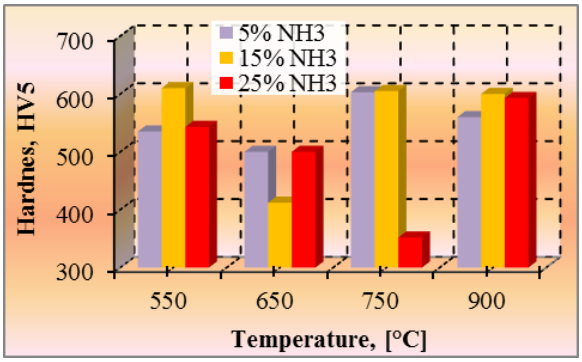

Fig. 3. *The surface hardness variation of the 18MnCr10 steel samples carbonitrided in fluidized bed for various proportions of ammonia*

Figure 4 shows for the samples of 13CrNi40 steel how hardness varies on the surface of the carbonitrided samples. In this case, it is noted that the hardness obtained is less than that for 18MnCr10 steel and also than that for 21TiMnCr12 steel.

The highest values of surface hardness of 13CrNi40 steel samples were obtained under the conditions of 750 °C treatment temperature and for an ammonia content of 5 to 25%.

For a content of 5% ammonia, an increase of the treatment temperature from 550 to 750 °C results in an increase in the hardness of the steel surfaces for these 13CrNi40 steel samples, and from 750 °C to 900 °C the hardness is slightly decreased. When the ammonia content is 15%, the highest hardness was recorded for 13CrNi40 steel samples treated at 750 °C.

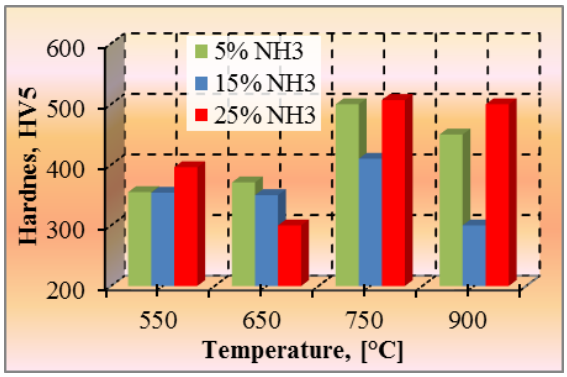

Fig. 4. *Variation of the surface hardness of the 13CrNi40 steel samples carbonitrided in fluidized bed for various proportions of ammonia*

Figures 5, 6 and 7 present the microstructures for one sample of each steel grade studied, Fig. 5 - 21TiMnCr12 steel, Fig. 6 - 18MnCr10 steel, Fig. 7 - 13Cr10Ni40 steel, for which the highest values of the surface hardness were obtained after processing according to one of the fluidized bed carbonitriding regimes experimented.

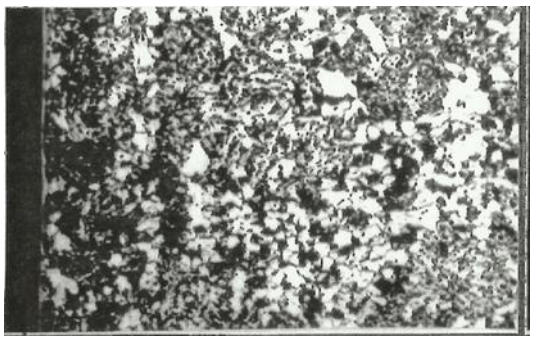

Fig. 5. *The microstructure of a 21TiMnCr12 steel sample carbonitrided at t = 550 °C, 5% NH_3, 100 X magnification, attack NITAL 2%*

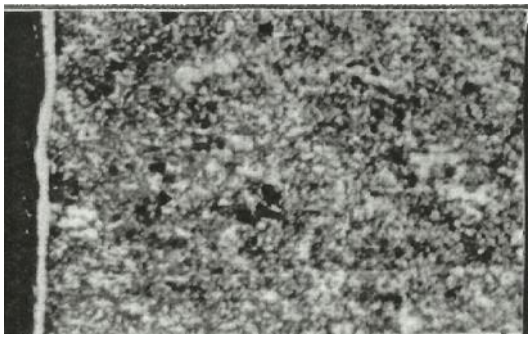

Fig. 6. *The microstructure of a18MnCr10 steel sample carbonitrided at t = 550 °C, 15% NH_3, 100 X magnification, attack NITAL 2%*

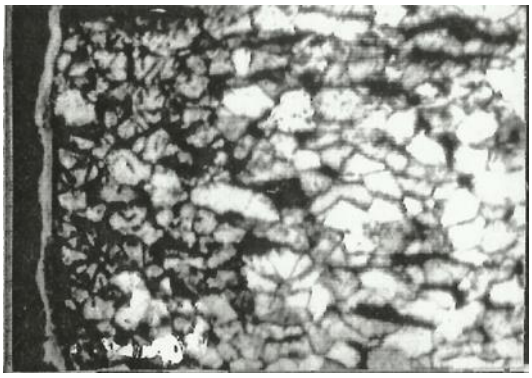

Fig. 7. *Microstructure of a 13CrNi40 steel sample carbonitrided at t = 750 °C, 25% NH3, 100 X magnification, attack NITAL 2%*

The structures present on the surface nitride layers and carbonitrides layers with various thicknesses.

4. Conclusion

Noting the variation of the HV5 type surface hardness values of the samples from the 3 studied low alloy steels, we can say that:

• decreasing the content of C resulted in the production of softer surfaces;

• for a content of 5% ammonia for 13CrNi40 steel surfaces are obtained with hardness increasing with the increase of the treatment temperature within the interval 550 °C – 750 °C, while for the interval between the 750 °C – 900 °C, the hardness is decreasing with increasing the temperature;

• at 650 °C, for samples of 13CrNi40 steel, hardness decreases as the values of the percentage of NH_3 are increasing from 5% to 25%, as opposed to what is recorded for the samples of 21TiMnCr12 steel, when at the same treatment temperature of 650 °C, the increase in the percentage of NH_3 increases hardness;

• for the samples of steel 18MnCr10 carbonitrided at 550 °C, the surface hardness increases when ammonia increases from 5 to 15% and decreases when ammonia increases from 15 to 25%, while for the samples annealed at 650 °C, the situation is exactly the opposite;

• a treatment temperature of 750 °C for steel 21TiMnCr12 highlights a decrease in hardness as the content of ammonia in the system is increasing;

• for 21TiMnCr12 steel samples, where the percentage of ammonia is 5%, the hardness increases proportionally with the increase of the treatment temperature between 650 °C - 900 °C;

• a concentration of 15% and 25% NH_3 during the carbonitriding of 21TiMnCr12 steel results in a decrease in hardness with increasing the treatment temperature in the temperature range 550 °C – 750 °C, after which the hardness increases in the range 750 °C – 900 °C;

The results of the experiments conducted to the confirmation of the special properties of fluidized beds (dispersed gas-solid medium) and the possible industrial application of the proposed technology and of the different variants derived from it.

References

[1]. Dobrovici S., Cazacu N., Bâclea A., *Carbonitrurarea în strat fluidizat*, Editura Fundației Universitare "Dunărea de Jos" Galați, 2001.

[2]. Dulcy M., Gantois M., *Principe de base de la cementation et de la carbo-nitruration*, Traitements termique, no. 289, p. 46-54, 1996.

[3]. Pye D., *Practical nitriding and ferritic nitrocarburizing*, ASM International, Materials Park, OH, 2003.

[4]. Kunii D., *Fluidization engineering*, John Wiley & Sons, Inc., New York, 1991.

[5]. Winter K.-M., *Gaseous nitriding: in theory and in real life*, United Process Controls, Heiningen, Germany, 2009.

[6]. Oprea F., Taloi D., Constantin I., Roman R., *Teoria proceselor metalurgice*, Editura Didactică și Pedagigică, București, 1978.

[7]. Samoilă C., Ionescu M. S., Drugă L., *Tehnologii și utilaje moderne de încălzire*, Editura Tehnică, București, 1986.

[8]. ***, Handbook of Thermal Process Modeling of Steels 190X_C012 Page Proof, p. 635, *Modeling of Case Hardening*, Gustavo Sánchez Sarmiento and María Victoria Bongiovanni, 2008.

THE ANNALS OF "DUNAREA DE JOS" UNIVERSITY OF GALATI
FASCICLE IX. METALLURGY AND MATERIALS SCIENCE
Nº. 3 - 2016, ISSN 1453 – 083X

PHYSICAL -MECHANICAL AND TECHNOLOGICAL CHARACTERISTICS OF Ti10Zr ALLOY FOR DENTAL APPLICATIONS

Vlad Gabriel VASILESCU[1], Elisabeta VASILESCU[2]
[1] "Carol Davila" Medicine and and Pharmacy University, Faculty of Dentistry, Bucharest, Romania
[2] "Dunarea de Jos" University of Galati, Romania
e-mail: elisabeta.vasilescu@yahoo.com

ABSTRACT

Progress reported over time in dentistry can be attributed largely to the dynamics of acquiring new materials. A biomaterial is considered ideal in the absence of any biomaterial-tissue interaction, which means a biomaterial totally inert to the biological medium. Biomaterials currently used as implants that come in contact with the tissues and substances and fluids in the body must meet two basic characteristics, called bio-functionality and biocompatibility. They define both the ability to fulfill its function properly and the compatibility of the implant biomaterial with the tissue that it incorporates. The most common are metallic biomaterials (metals and alloys) due to their very good mechanical properties and their accepted biocompatibility. Issues related to the use of metallic materials in dental biomaterials (prostheses, implants) include mainly corrosion, release of toxic metal ions and wear. The toxicity of the metal ions as particles resulting from wear is a major disadvantage in the use of metallic biomaterials as they may induce multiple tissue reactions, such as osteolysis, damage the normal structure of the bone, severe reaction of macrophages, granuloma, fibrous capsule, inflammatory and immune reactions. All this can lead to implant destabilization and loosening.

This paper summarizes the physical-mechanical and technological characteristics of a new titanium-based alloy having high biocompatibility due to the chemical composition. The alloy is composed of 10% zirconium designed to improve fatigue strength in corrosive environment and does not contain harmful elements present in conventional titanium-based alloys composition.

KEYWORDS: biocompatibility implant, melting, cold crucible, casting, titanium-zirconium, microstructure

1. Introduction

In dentistry, metals and especially alloys have important broad applications, some are processed by casting in dental labs, other alloys are industrially cast and used such as implants, or after cold processing in laboratory for the manufacturing of the metal components of the various types of metal orthodontic appliances or partial movable acrylic dentures [1-4]. The term of Dental Metallurgy acquires new meanings through the modernization of the alloy making and processing techniques [5]. Dental alloys are part of a special class of biocompatible materials which, by their properties, should provide resistance to the phenomena specific to the oral environment. Of these, the most important is the corrosion process of the surfaces by biological, chemical, especially electrochemical action. Also, wear surfaces to form metal particles and release harmful metal ions that can migrate into tissues [6-10].

Dental alloys commonly used are: noble alloys (Au-Pt with 80% Pt), semi-noble alloys (Au-Pd with 50-60% Au), low noble alloys (Ag-Pd with 50-60% Pd) and not noble alloys (Ni-Cr with 75-85% Ni and 11-15% Cr; Co-Cr with 40-70% Co and 20-30% Cr; Fe-Cr with 59% Fe and 26% Cr; stainless steel with 18% Cr and 8% Ni, Co-Cr-Mo with 10-60% Co, 2-80% Ni and 10-30% Cr); Cu-Al alloys.

Generally, use is made of metals and alloys that are easily passivated. Although the passive oxide layer of such biomaterials remains intact, however, in the neighboring tissues, higher concentrations of

metal ions occur which may affect the biomaterial-tissue interaction and can cause tissue damage over time. Stainless steel is very susceptible to salt corrosion environments, such as the tissue fluid. By corrosion, steel becomes a metal with low resistance to fatigue, the main cause of implant failure [10, 11]. Release of corrosion products ($Ni^{2+,}$ $Cr^{3+,}$ Cr^{6+}) causes inflammatory reactions. In endosseous implants, inflammation prevents osseointegration and favors the formation of a fibrous capsule [12-14].

Modern alloys based on Co-Cr, due to superior mechanical properties and advantageous cost price, have replaced noble alloys of class IV in the traditional (metal-polymer) and modern (metal and metal-ceramic composite) technology [4]. Chromium is the main alloying element that provides corrosion resistance and oxidation by forming oxide films (Cr_2O_3) adherent and continue that protect the surface. In dentistry, the cobalt-chromium-molybdenum alloys were used as subperiosteal implants, endosseous plates and transosseous implants.

Limiting the use of stainless steels only for temporary devices was called for by the appearance of superior titanium alloys ((Ti, Ti-Al-V, Ti-Ni, Ti-Al, Ti-Al-Nb) [15-17].

Although titanium is considered a biocompatible metal, Ti^{4+} ions inhibit in vitro the activity of osteoclasts and reduce osteoblasts protein synthesis; In a study using human osteoblast cell line MG-63, defined as proliferative osteoblast, Shida and his collaborators have shown that the Ti^{4+} ions induce the production of IL-6 and thus activates osteoclastogenesis.

Titanium alloy implants have significantly lower corrosion rates than those of other metallic implants, but they release metals in organism; Aluminum and Vanadium are elements released into the tissues. The metal ions released as a result of corrosion and wear process can induce denture loss after a long period of implantation, especially because of the potential adverse effects of vanadium. Release of vanadium ions in the body may cause serious diseases of breathing organs and the systems producing platelets [15-17].

For this reason, it is preferred the alloy of Ti-Al-Nb instead of Al-Ti-V [18-21]. In vitro studies have shown that cells behave differently in the presence of wear debris generated from the two alloys. Therefore, it is found an increased release of prostaglandin E2 in response to Ti-6Al-4V particles contact and an increase in the release of other inflammatory cytokines compared with Ti-Al-Nb particles. These data suggest that Ti-6Al-4V stimulate phagocytic cells more than the Ti-Al-Nb or pure Ti. Exposure of bone marrow cells derived from Ti-6Al-4V particles induces a significantly increased release of pro-inflammatory and osteolytic mediators which are responsible for the loss of denture [22].

It should be noted that the insertion of an implant lead to wound, and the healing success is closely related to the tissue response which depends, among other, on the surrounding tissue and the ability of the affected tissues to regenerate.

To summarize, in terms of materials and their effects, there are the following categories: materials with toxic response tissue (e.g. iron, nickel, cobalt, chromium, cadmium), materials that generate fibrous tissue (e.g. zinc, silver, aluminum, stainless steel, chrome - cobalt alloys), materials that induce vital reaction (e.g. titanium, ceramic, aluminum, zirconium ceramic).

Lately, in the dentistry world have appeared non-noble dental alloys complex allies helping to improve their specific properties, primarily their biocompatibility and the toxic effects of metals (Ni, Cr, Co, Ti, Al) released by the prosthetic implants are intensely studied.

2. Materials and experimental conditions

Titanium- based alloy (Ti10Zr) was developed in cold crucible furnace at R & D Consulting and Services SRL Bucharest. Magnetic levitation melting in cold crucible furnace applies to difficult fusible melted and very reactive metals such as titanium, niobium, tantalum, molybdenum, zirconium, etc. Given the alloy destination for medical applications, it is necessary to strictly comply with the quality of the metal materials used in its preparation. The chemical composition of the Ti10Zr alloy is shown in the Figure 1 and in the Table 1.

Table 1. *EDAX ZAF Quantification (Standard less), element normalized*

Elements	Wt. %	At. %	K-Ratio	Z	A	F
Ti-K	**87.72**	93.15	0.8271	1.0084	0.9350	1.0000
Zr-K	**12.28**	6.85	0.1111	0.9113	0.9933	1.0000
Total	100.00	100.00	-	-	-	-

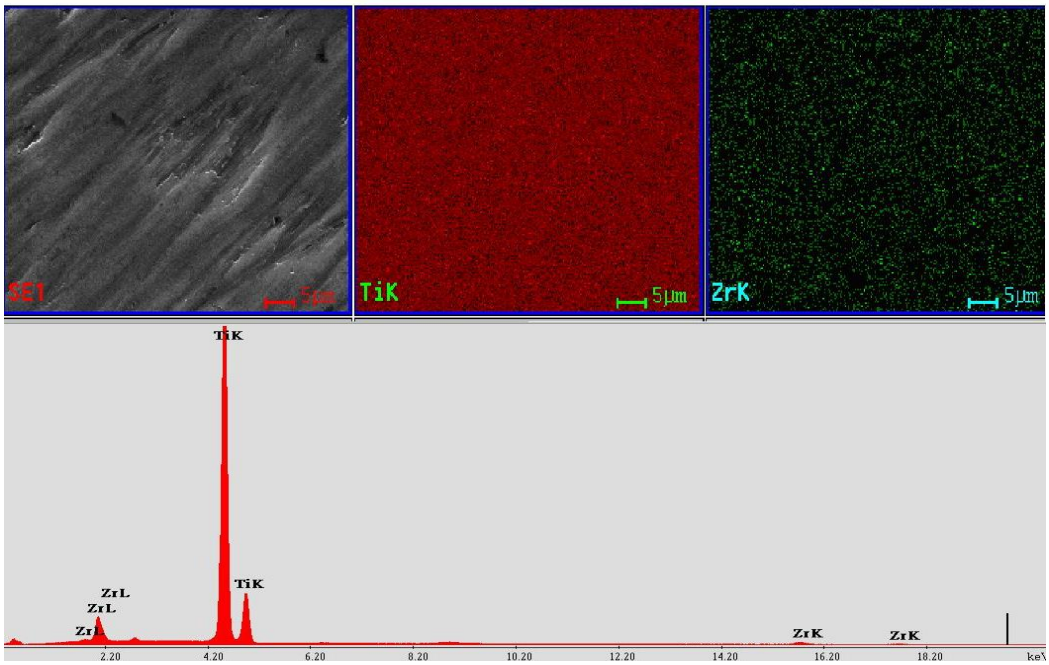

Fig. 1. *Scanning Electron Microscopy image (SEM) and EDX Spectrum of samples taken from Ti10Zr Alloy* Castings [5, 23-25]

3. Experimental results

Final ingots have a diameter of about 19 mm and length of 70 mm (Fig. 2). The implant was designed and made at SC TEHNOMED Bucharest (Fig. 1).

a b

Fig. 2. *Cast alloy blank of Ti10Zr (ingot) (a) and dental implants (b)*

Knowing the behavior of the bio-alloy metallurgical processing (technical features) and under stress required analysis and laboratory tests, which evaluated the use potential of the alloy Ti10Zr as biomaterial for applications in dentistry.

In the following are presented the conditions for determining the mechanical characteristics of the alloy studied, in accordance with standards and regulations.

From initial ingot (Figure 1) were made standard samples (Figure 3), which were tested on the machine static axial tensile (Mechanical Testing Laboratory of AM Galati, Figure 3, Figure 4).

a b

Fig. 3. *Standard test specimen of alloy Ti10Zr tensile testing: before (a) and after the test (b)*

Fig. 4. *Tensile test machine to determine the mechanical properties of the alloy Ti10Zr (making the specimen from the initial blank and the tensile test)*

To study the behavior of the bio-alloy metallurgical processing by plastic deformation hot and cold, blank was processed initially by turning and subjected to heat to a temperature of 850 ºC. Heated preform was subjected to hot extrusion, the initial diameter of 10 mm then the Φ5 mm, followed by cold rolling to gauges respectively Φ4 mm diameter and Φ3 mm [23-25].

Research on structural changes and assessment of properties (micro-hardness) during processing (molding, extrusion 1 extrusion 2 cold rolling) described above were performed on samples cut from the blanks by milling undergo initial processing. Metallographic analysis shows a gradual finishing the structure and uniformity and homogenization of it [Fig. 6, Fig. 7].

Applied technology highlighted good deformation behavior of the alloy, a good plasticity and a trend of reduced hardening.

Processing by plastic deformation provides a fine structure and an increase of about 50% of the properties of hardness and strength [5]. In fact, the analysis carried out on fractographic bio-alloy samples, and the test results of tensile test (the study of the fracture surface at different magnifications Figure 8) show a ductile fracture, the investigated fracture surface being clean and free of cracks and inclusions, without confirming good behavior of the hot and cold plastic deformation processing of the bio-alloy.

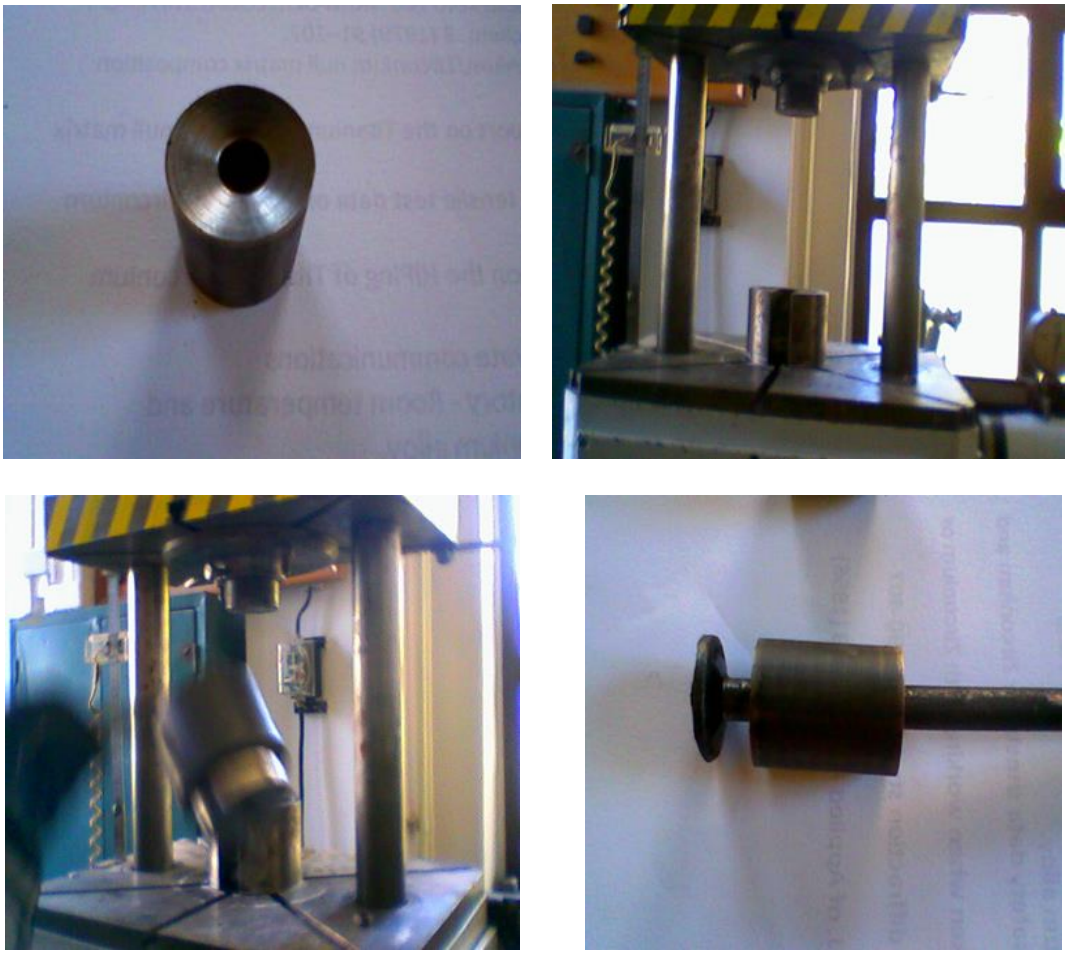

Fig. 5. *Aspects of the stages of hot extrusion molding to a diameter of 10 mm of the blank having 18 mm diameter and 35 mm length; the new blank of Φ10x35 mm was subject to heating at 850 °C then hot extruded at the Φ5 mm diameter. Finally, the Φ5 mm extruded blank was cold rolled to a diameter of Φ3 mm*

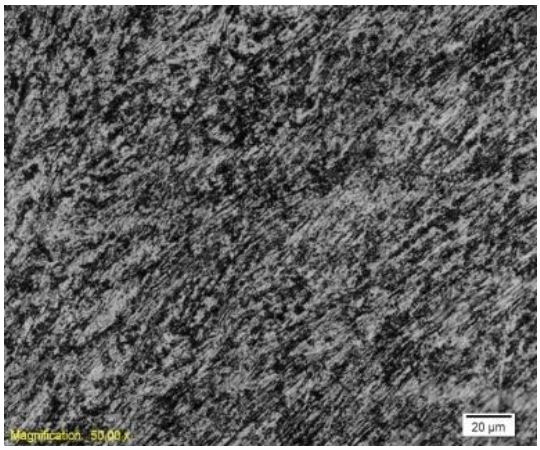

Fig. 6. *Microstructural aspects condition: extruded from Φ10 mm to Φ5 mm* [23-25]

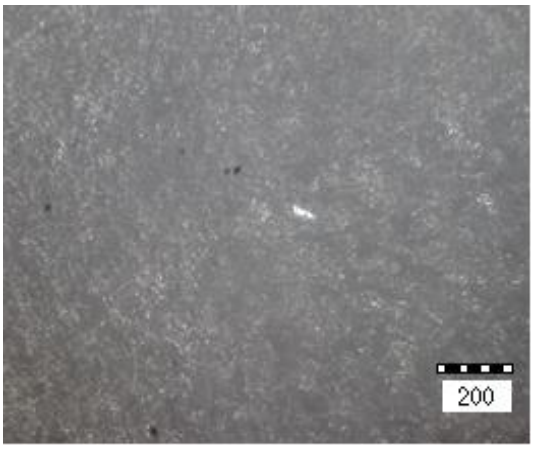

Fig. 7. *Microstructural aspects (optical microscopy, structural condition – cold rolled: a.) to d = 4 mm; b.) to d = 3 mm* [5]

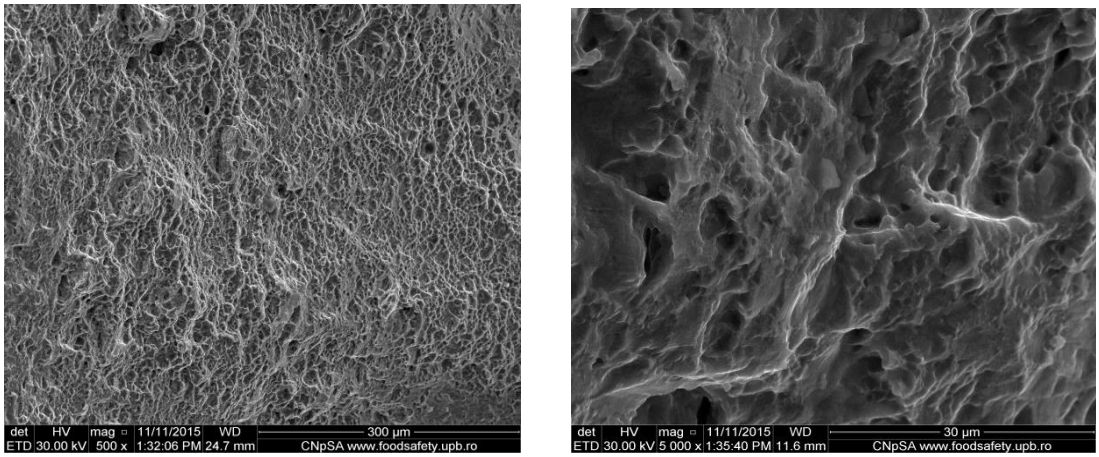

X500 X5000

Fig. 8. *Characteristics of ductile fracture samples from the bio-alloy Ti10Zr (SEM analysis at different magnifications)* [5]

3.1. Determination of Young's modulus and hardness using the micro-indentation [5]

Experimental alloys studied were tested for hardness and elastic modulus determination. We used a hardness tester for determining hardness on the principle Martens, ultra-micro-hardness testing device DUH-211S Shimadzu from Laboratory Testing and Material Characterization of the Faculty of Food Engineering of the University "Stefan cel Mare" Suceava.

3.2. Universal Hardness test - HU

Compared to the conventional method of testing for hardness (Brinell, Vickers and Rockwell) in which the values specific to deformation is determined only after removal of the load, i.e. the calculation of the hardness is only used for part of the plastic universal deformation hardness test (HU), and the size of specific deformation under load is determined. Also, the universal hardness is used for the calculation of the component as plastic deformation as well as elastic deformation component. The test was carried out under loading and unloading the progressive indenter reading, and memorizing pairs of values: force (F) - depth of penetration; (h) offers the possibility of determining not only the hardness HU, but also of important mechanical characteristic units such as: modulus of elasticity, which is elastic deformation, tend to creep tendency seating capacity of hardening of the material, etc. [documentation on testing conditions was carried out in the Laboratory of testing and material characterization at the University "Stefan cel Mare" Suceava]. During the test, load is measured both at discharge and at pairs value force (F) and depth of penetration (h).

Table 2. *Mechanical characteristics of the samples from Ti10Yr bio-alloy (Shimadzu DUH 211S)* [5]

Sample Type	**F_{max}**	**h_{max}**	**HMV**	**HM_s**	**H_{it}**	**E_{it}**	**C_{it}**	**n_{it}**	**HV***	**HV**
	[mN]	[µm]	[N/mm^2]	[N/mm^2]	[N/mm^2]	[N/mm^2]	[%]	[%]		
Ti10Zr	1000	48.794	1599.956	998.015	2054.839	7.574e+004	1.623	17.863	194.18	228.36
		49.369	1563.539	1052.730	1968.489	8.091e+004	1.759	16.855	186.02	214.47
		49.393	1562.355	1188.072	1992.908	7.604e+004*	1.588	17.796	188.33	221.51
Average value		**49.185**	**1575.283**	**1079.606**	**2005.412**	**78325**	**1.656**	**17.504**	**189.51**	**221.44**

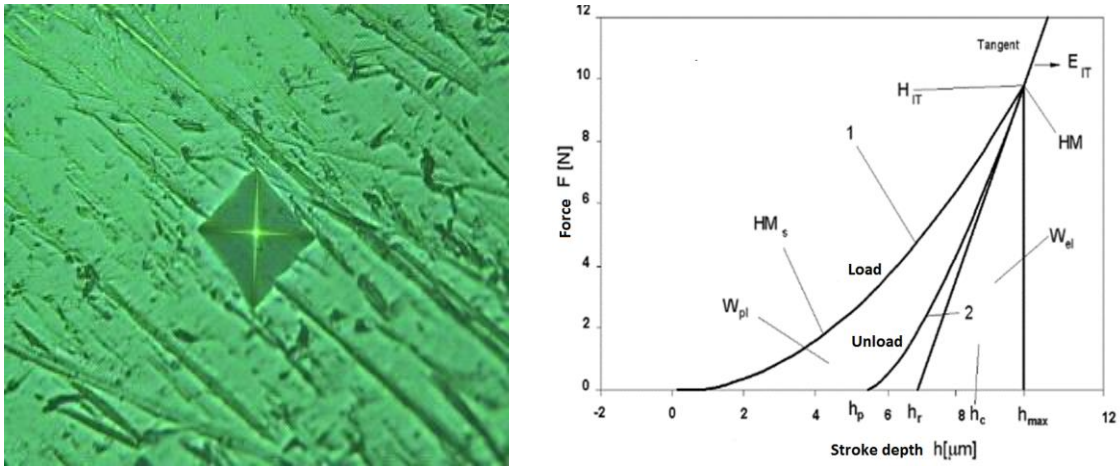

a b

Fig. 9. *Footprint indenter (The impression) on the sample alloy Ti10Zr (a), the graphic representation of the evolution of pairs of values, force (F) - penetration depth (h) (b), if the charging process (1) - Download (2) to test the hardness Martens* [5]

The experimental results are presented regarding the measured characteristic parameters for Ti10Zr alloy hardness testing, using the Shimadzu DUH-211S device.

4. Conclusions

The analysis of physico-chemical and technological characteristics of the new alloy (Ti10Zr) with high biocompatibility in terms of composition (chemical elements such as vanadium and aluminum were removed etc.) shows the following:

a. comparable physical and mechanical properties of titanium alloys commonly used in dental applications respectively:

- low density (4.7 g / cm^3), comparable to pure titanium (4.51 g / cm^3) and conventional titanium alloys;

- relatively low modulus of elasticity (E = 94.2 - 113 GPa, depending on the method of determination);

- mechanical characteristics: Rm = 636 MPa, Rc = 527 MPa, A = 31.2%.

b. metallurgical hot and cold processing of the Ti10Zr alloy showed good deformation behavior of the alloy, good plasticity (an increase of about 50% of hardness and resistance) and reduced hardening tendency.

References

[1]. Kenneth J., *D.M.D. Anusavice*, Phillips' Science of Dental Materials, Tenth Edition, 1996.

[2]. Park J. B., *et al.*, *Biomaterials, Principles and Applications*, MA: CRC Press, 2003.

[3]. Craig R. G., *Materiale dentare restaurative*, Ed. All Educational, Bucuresti, p. 22, 2001.

[4]. Vasilescu E., *Research on the Behaviour of the Tooth- Crowns Assembly Made of Different Materials in Solutions simulating the Oral Environment*, The Annals of "Dunarea de Jos" University of Galati Fascicle lX. Metallurgy and Materials Science, no. 3, p. 27, 2015.

[5]. Vasilescu V. G., *Contribuţii la studiul materialelor metalice biocompatibile utilizate în implantologia orală*, Teză de doctorat susţinută la U.M.F. "Carol Davila" Bucureşti, 2016.

[6]. Anderson J. M., *et al.*, *Host reactions to biomaterials and their evaluation*, Ratner B. D., *et al.*, eds. Biomaterials Science: An Introduction to Materials in Medicine London, Elsevier, 2004.

[7]. Khan M. A., Williams R. L., Williams D. F., *In vitro corrosion and wear of titanium alloys in the biological environment*, Biomaterials, 17, p. 2117, 1996.

[8]. Patrascu I., Vasilescu E., Gatin E., Cara-Ilici R. R., *Corrosion of Biomaterials Used in Dental Reconstruction Dentistry*, Chapter 26, 2014.

[9]. Patrascu I., Vasilescu V. G., Milicescu St., *Modern methods for assessing the corrosion resistance of dental alloys used in dentistry*, Chapter 9, 2014.

[10]. Gadea S., Petrescu M., *Metalurgie fizica si studiul metalelor*, vol. 3, EDP Bucuresti, 1983.

[11]. Ghiban B., *Metallic Biomaterials*, Editura Printech, Bucuresti, 1999.

[12]. Fleck C., Eifler D., *Corrosion, fatigue and corrosion fatigue behaviour of., metal implant materials, especially titanium alloys*, International Journal of Fatigue, 32, p. 929-935, 2010.

[13]. Montes C. C., Pereira F. A., Thome G., Alves E. D. M., Acedo R. V., Renato de Souza J., Moreira Melo A. C., Trevilatto P. C., *Osseointegrated Dental Implant Loss.*, Implant Dentistry, vol. 16, no. 4, 2007.

[14]. Hadi S. A., Ashfaq N., Bey A., Khan S., *Biological factors responsible failure of osseointegration in oral implants*, Biology and Medicine, 3 (2), Special Issue, p. 164-170, 2011.

[15]. Rack H. J., Qazi J. I., *Titanium alloys for biomedical applications*, Materials Science and Engineering C 26 Elsevier, p. 1269-1277, 2006.

[16]. Imam M. A., Fraker A. C., *Titanium alloys as implant materials*, In: Brown SA, American Society for Testing and Materials, p. 3-16, 1996.

[17]. Vlad Gabriel Vasilescu, Elisabeta Vasilescu, *Consideraţii asupra compoziţiei aliajelor cu baza titan utilizate in implantologia orala*, Congresul National GALMED, Editia a-V-a, 13-16 noiembrie 2014 Galati Romania (volum de abstracte/prezentare poster).

[18]. Moranta C., Lopez M. F., Gutierrez A., Jimenez J. A., *AFM and SEM Characterization of non-toxic vanadium-free Ti alloys used as biomaterials*, Applied Surface Science 220 Elsevier, p. 79-87, 2003.

[19]. Okazaki Y., Gotoh E., *Comparison of metal release from various metallic biomaterials in vitro*, Biomaterials, 26, 11, 2005.

[20]. Khan M., Williams R., Williams D., *The corrosion behaviour of Ti–6Al–4V, Ti–6Al–7Nb and Ti–13Nb–13Zr in protein solutions*, Biomaterials, 20 (7), p. 631-637, 1999.

[21]. Drăgan (Raileanu) L. A., Petreus T., Tudoran L. B., Munteanu C., Mareci D., Cotrutz C. E., Chelariu R., *Cytocompatibility evaluation of two new Ti-Nb-Zr-Al alloys for medical applications*, Elsevier Editorial System(tm) for Materials Science and Engineering C.

[22]. Campos M. I., Godoy dos Santos, Leme M. S., Trevilatto P. C., *Interleukin-2 and Interleukin-6 gene promoter polymorphisms, and early failure of dental implants*, Implant Dentistry, vol. 14(4), p. 391-398, 2005.

[23]. Vasilescu V. G., Patrascu I., Cotruț C., Vasilescu E., *Experimental Research on the Behavior of the Alloy Ti10Zr in Simulated Oral Environment*, Rev. Chim. (Bucharest), no. 2, p. 263, 2016.

[24]. Dima O., Alexandru P., Gurău G., Vlad Gabriel Vasilescu, Elisabeta Vasilescu, *Studies and Research on Treatment of Titanium Alloys*, UgalMat 2014, Galati, The Annals of "Dunarea de Jos" University of Galati. Fascicle IX. Metallurgy and Materials Science no. 1, 2014.

[25]. Vasilescu Vlad Gabriel, Patrascu Ion., Vasilescu Elisabeta, *Studies and Research Regarding the Influence of Metallurgical Processing on the Structure and Properties of* some *Titanium Based Alloys Used in Dentistry*, The VIth Edition of International Conference UgalMat 2014, Advanced Technologies and Material Section, May 29-31, Dunărea de Jos" University of Galati, Romania, 2014.

[26]. Vlad Gabriel Vasilescu, Elisabeta Vasilescu, *Aliaj Ti-Zr utilizat in implantologia orala*, Congresul National cu participare internationala pentru studenti si tineri medici rezidenti, GALMED Editia a V-a, 13-16 noiembrie 2014, Galati, Romania (volum de abstracte/prezentare poster).

THE ANNALS OF "DUNAREA DE JOS" UNIVERSITY OF GALATI
FASCICLE IX. METALLURGY AND MATERIALS SCIENCE
N°. 3 - 2016, ISSN 1453 – 083X

STUDIES AND RESEARCHES REGARDING THE OBTAINING AND CHARACTERIZATION OF COMPOSITE NICKEL COATINGS- Ni/Al_2O_3, Ni/KAOLIN ELECTROCHEMICALLY PRODUCED

Simona BOICIUC, Petrică ALEXANDRU
"Dunarea de Jos" University of Galati, Romania
e-mail: simonaboiciuc@yahoo.com

ABSTRACT

This study presents the composite nickel coatings electrochemically obtained using as disperse phases Al_2O_3 particles and kaolin. There were used Watts electrolytes, with a pH = 4, current density of 4 A/dm^2, a concentration of the disperse phase of 20 g/l, a speed of agitation of 300 rpm, deposit strokes of 60, 90, 120 minutes. The characterization of those has been done microstructurally and also from the point of view of the film thickness and microhardness. The existing of the disperse phase particles has led to the shrinking of the nickel dimensions of crystalites, which has determined a decrease in roughness and an increase in hardness.

KEYWORDS: Ni composite coatings, electrodeposition, Al_2O_3, kaolin, microhardness

1. Introduction

Composite coatings are considered revolutionary materials, with real improvement perspectives of their properties and multiple utilizations in the aerospatial industry, marine industry, automotive industry, electric industry and electronic industry.

The major advantage, essential for composites is the possibility of properties modulation and by that obtaining a wide variety of materials. In most cases, the composite material comprises a core matrix in which is dispersed a material complementary to the form of fibers or particles.

Composite materials in the nickel matrix electrochemically obtained are characterized by high hardness, good wear behavior and high resistance to corrosion. As complementary materials, can be used the following types of disperse phases: oxides such as TiO_2, SiO_2, Al_2O_3, CeO_2, ZrO_2, SnO_2 and Cr_2O_3, carbides such as WC, TiC and SiC, nitrides such as Si_3N_4 and BN, carbon nanotubes [1].

Composite coatings Ni - Al_2O_3 are used in applications which require a high resistance to wear, corrosion, temperature, so they can be used as an alternative to chrome coatings. They can be used in the case of high pressure cylinder engines, molds, components of musical instruments, accessories machinery, electrical components, electronic microdevice [2].

Composite materials Ni – kaolin are used in the aerospatial industry, automotive industry, in applications which require a good behavior to wear, abrasion, fatigue, corrosion [3].

The properties of the composite materials depend on the type, structure, shape, the size, morphology and the content of the additional phase particles and their distribution in the metal matrix.

The functional properties of composite coatings are strongly influenced by their structure, tensions developed in the layer and also by the orientation and complementary phases which may cause the anisotropy of the properties.

Nickel has been chosen as a covering material because it is one of the most common industrial coverings used for decorative and functional applications [4].

Technical alumine used in experimental researches has almost 98.5% γ - Al_2O_3 and a maximum of 10% α - Al_2O_3.

α - Al_2O_3 crystallizes into a hexagonal lattice, has a density of 3.66 to 3.99 g/cm^3, a good resistance to high temperatures (T_t = 2054 °C), with higher mechanical properties (modulus of elasticity E = 440 GPa hardness H = 30 GPa). It has the form of colorless crystals or white and it is chemically inert.

γ - Al_2O_3 crystallizes in a face-centered cubic lattice, has a density of 3.65 to 3.67 g/cm^3, a modulus of elasticity of approx. 275 GPa, and a stability limit of 1200 °C.

Kaolin - Al_2O_3 * $2SiO_2$ * $2H_2O$ – is a clay (mineral) very fine-grained, white, with a density of 2.65 g/cm^3, low plasticity, with high resistance to high temperatures and by burning it becomes solid and very compact. A mineral layer has a triclinic crystal symmetry made of octahedral configurations composed of Al_2O_3 and SiO_2 tetrahedral parties that share a common plan-made of oxygen atoms. The layers thus formed are connected to each other by the links of hydrogen atoms [3].

Electro-co-deposition of the dispersed particles which is obtained in parallel with the electro crystallization of pure metal is presented in five steps [4]:

- the forming of the double electric layer around each of the particles after their introduction into the electrolyte;
- the transport of the particles to the hydrodynamic limit;
- the diffusion of the positively charged particles to the cathode;
- the reduction of free electroactive species or adsorbed by the particles;
- the embedding of the particles in the metal matrix.

The researches presented in this study have as a general objective the development of a technology of an electrochemical coatings of nickel composite matrix technique using Al_2O_3 as a dispersed phase with a size of approx. 5 μm and kaolin with a particle size of approx. 2 μm and their characterization in terms of microstructure of the layer thickness and hardness.

2. Experimental condition

In order to obtain nickel coatings and composite nickel coatings in nickel matrix it has been used a direct current source, a device provided with a magnetic stirrer and a temperature regulation system and a cell for the electrolyte bath. It has been used a solution volume of 300 ml, and the experiments have been made at 50 ºC temperatures.

There were used electrolyte Watts-type consisting of $NiSO_4 \cdot 6H_2O$ - 300 g/l, $NiCl_2 \cdot 6H_2O$ - 50 g/l and H_3BO_3 - 40 g/l, pH = 4, with a current density of 4 A/dm^2, with the concentration of the dispersed phase 20 g/l, a stirring speed of 300 rpm, with a deposition time of 60, 90, 120 minutes.

The electrodepositions were conducted by the vertical arrangement of the electrodes at a distance of 14 mm from each other. As anode was used nickel in high purity (99%), the cathode being of copper strip, representing the support material for depositions at the size of 76 x 20 x 1 mm.

The copper strip used was prepared by degreasing (with organic solvents - trichlorethylene), etching (HNO_3 + HCl at the room temperature for 1 to 2 minutes) followed by washing with distilled water.

The metallographic analysis of samples was performed on a Neophot 2 microscope with the data acquisitions on a computer and it highlighted the appearance of the surface of the nickel depositions compared to composite coatings, their adherence, how they grew the electrodeposited crystals and the presence of flaws such as pores, cracks, exfoliations.
To determine hardness was used a microdurimeter PMT-3, with a load of 50 g.

3. Experimental results

The characterization of ACE composite coatings was performed compared to pure nickel coatings and consisted of macro and microstructural analysis, determinations of the layer thickness, microhardnesses.

3.1. The characterization of the nickel matrix composite coatings with a dispersed Al_2O_3 phase electrochemically obtained

Fig. 1 shows the appearance of pure nickel coatings obtained at different electrodeposition times of coating. It can be seen that the deposited layers are homogeneous, no crackings and good adhesion to substrates of copper. It can be seen that by increasing the time of electrodeposition, the coating thickness increases, the current density and stirring speed being maintained constant.

Fig. 2 shows the microstructural appearance of the composite coatings, electrochemically obtained nickel matrix as particles of Al_2O_3 by embedding the dispersed phase into Ni matrix.

By looking at Fig. 2 it can be seen that the obtained composite electrochemical coatings in nickel matrix using as disperse phases Al_2O_3 particles exhibit good adhesion to the substrate, homogeneity and compactness. It can be seen that the presence of disperse phase particles, the best inclusion being at a time of deposition of 90 minutes. Al_2O_3 particles led to decreased crystallite size (compared to pure nickel deposits), which decreased the roughness deposits and increased hardness (it simultaneously occurs the blocking of the dislocations movements in the nickel matrix) (Fig 4).

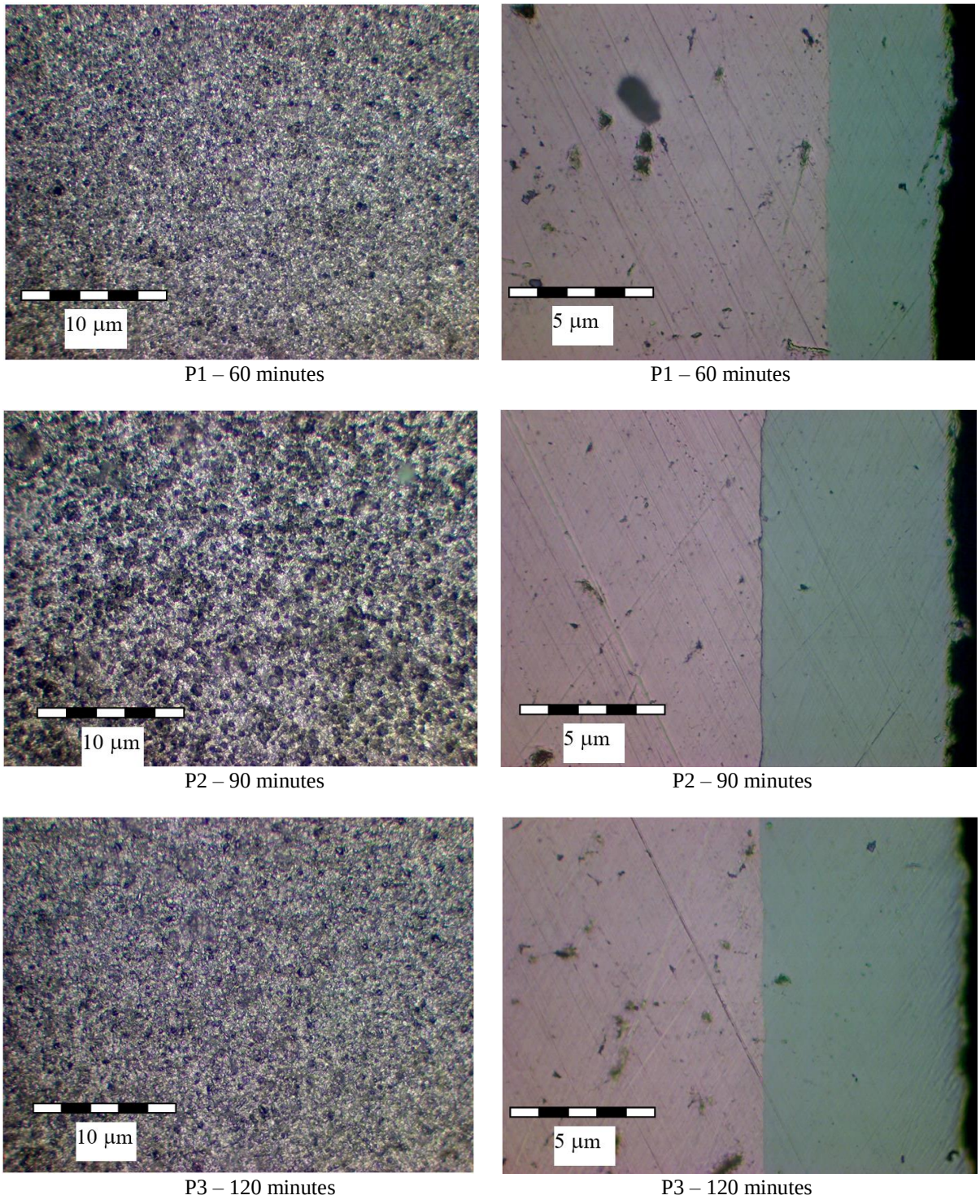

P1 – 60 minutes | P1 – 60 minutes

P2 – 90 minutes | P2 – 90 minutes

P3 – 120 minutes | P3 – 120 minutes

Fig. 1. *The microstructure of the pure nickel coatings*

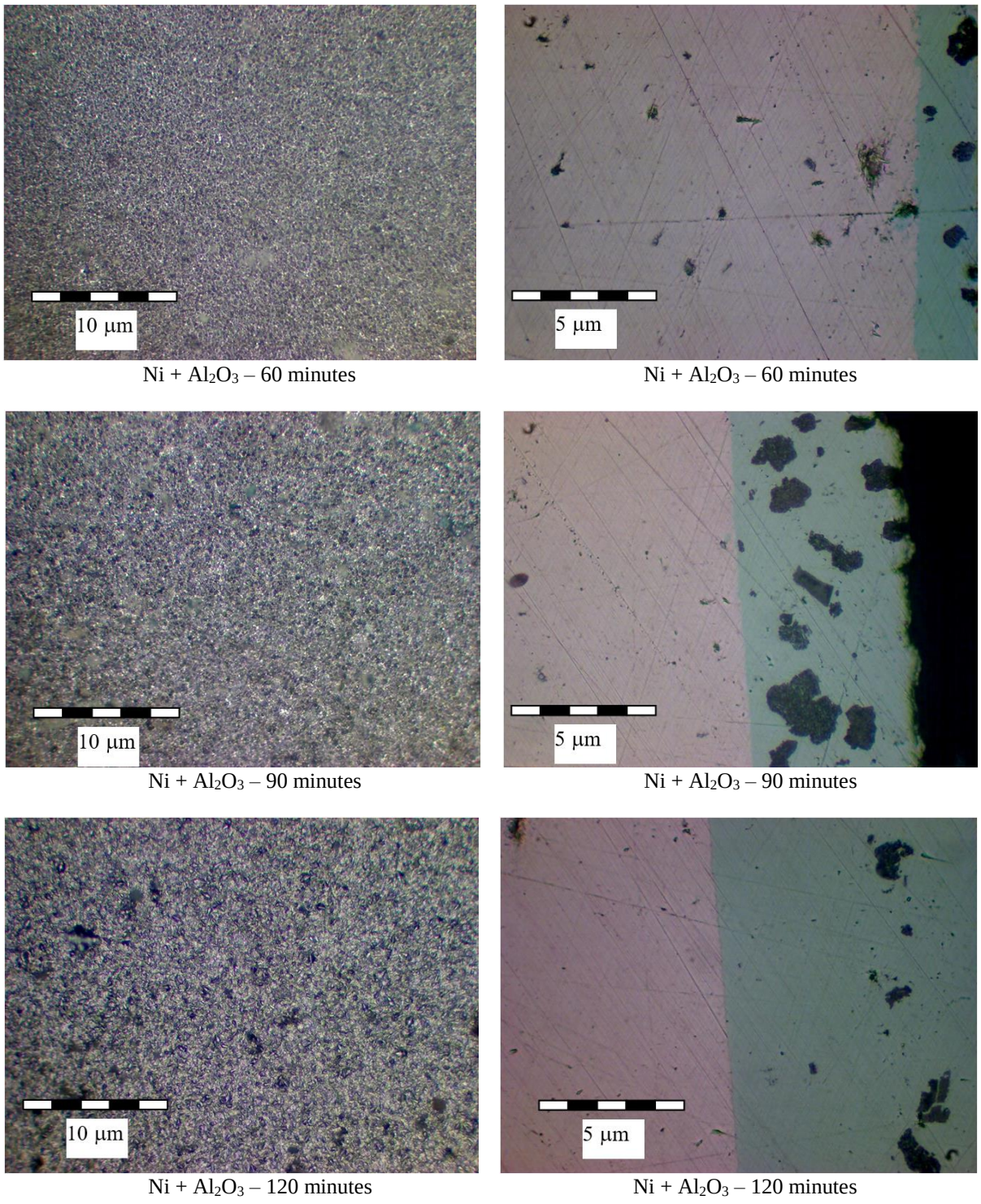

Ni + Al_2O_3 – 60 minutes | Ni + Al_2O_3 – 60 minutes

Ni + Al_2O_3 – 90 minutes | Ni + Al_2O_3 – 90 minutes

Ni + Al_2O_3 – 120 minutes | Ni + Al_2O_3 – 120 minutes

Fig. 2. *The microstructure of the electrochemically composite coatings obtained in nickel matrix by using Al_2O_3 particles as dispersed phases*

Fig. 3 shows the deposition time influence on the thickness of pure nickel coatings and on composite coatings electrochemically obtained in nickel matrix using as disperse phases Al_2O_3 particles. It can be seen that by increasing the time of electrodeposition the coating thickness increases, the current density and stirring speed is maintained constant.

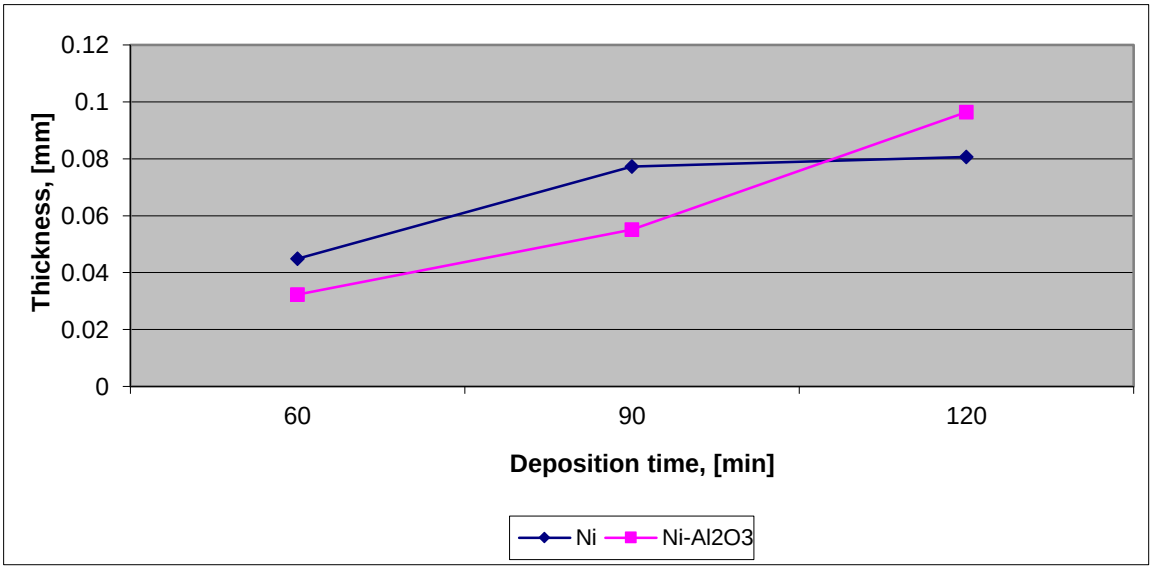

Fig. 3. *The influence of deposition time on the thickness of pure nickel coatings and on composite coatings electrochemically obtained in nickel matrix using as disperse phases Al_2O_3 particles*

Fig. 4 shows the deposition time influence on the microhardness of pure nickel coatings and on composite coatings electrochemically obtained in nickel matrix using as disperse phases Al_2O_3 particles. It may be noticed that in the case of pure nickel coatings and also in composite coatings electrochemically produced, in nickel matrix using as dispersed phases Al_2O_3 particles, it can be seen an increase of microhardness compared with cooper substrate which has a microhardness of 126.7 daN/mm^2. Increased hardness of pure nickel coatings with increased time deposition growth might be attributed to internal stresses in the deposited coating.

However, it appears that the presence of the Al_2O_3 dispersed phase leads to a further increase in the microhardness of obtained coatings compared to pure nickel coatings.

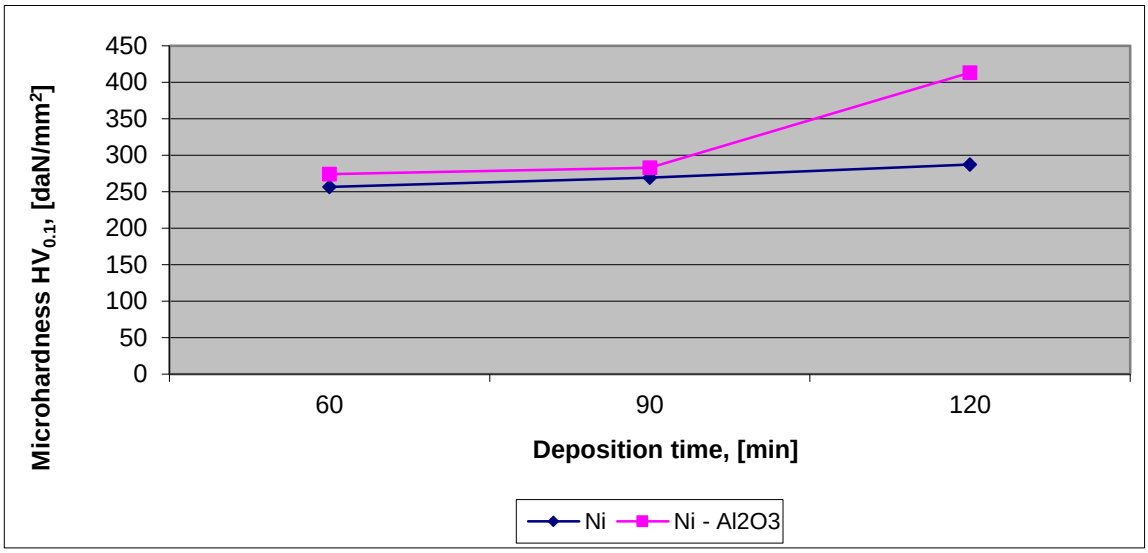

Fig. 4. *The influence of deposition time on the microhardness pure nickel coatings and also on the composite coatings electrochemically obtained in nickel matrix using as dispersed phases particles of Al_2O_3*

3.2. The characterization of composite coatings in nickel matrix electrochemically obtained at the disperse phase of kaolin $Al_2O_3 * 2SiO_2 * 2H_2O$

Fig. 5 shows the appearance of microstructural the coatings composition obtained electrochemically in the matrix of nickel using as the dispersed phase particles of kaolin.

It can be seen that the deposited layers are homogeneous, no crackings and good adhesion to substrates of copper. The presence of particles of kaolin modifies the growth of crystals of nickel affording coatings smoother (as compared to coatings of the pure nickel), compact and continuous.

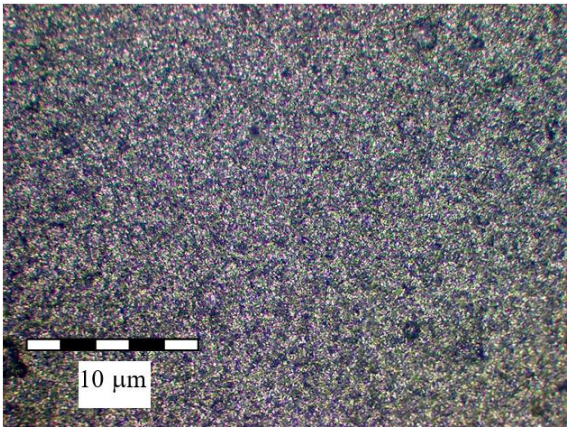

Ni – kaolin - 60 minutes

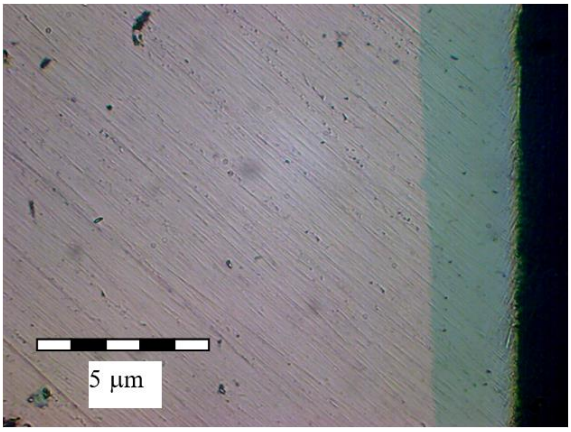

Ni – kaolin – 60 minutes

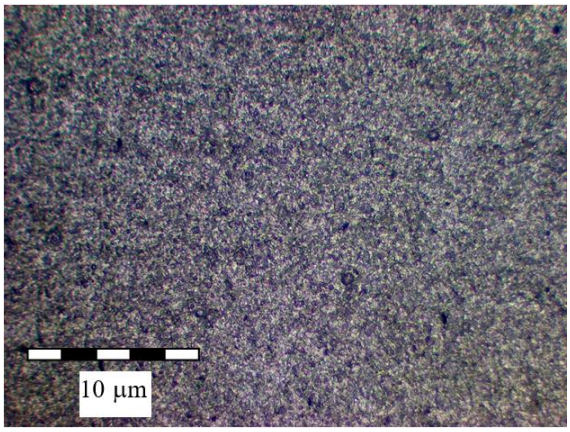

Ni – kaolin - 90 minutes

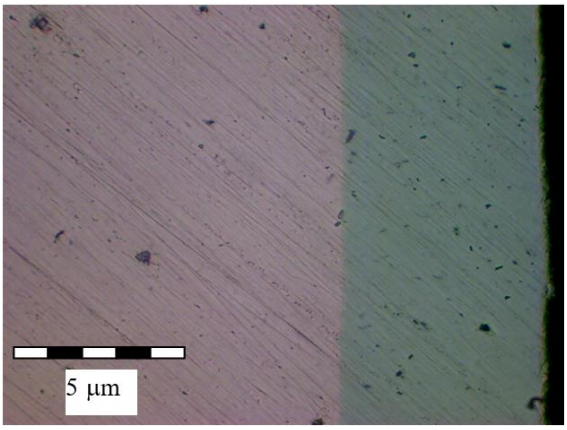

Ni – kaolin – 90 minutes

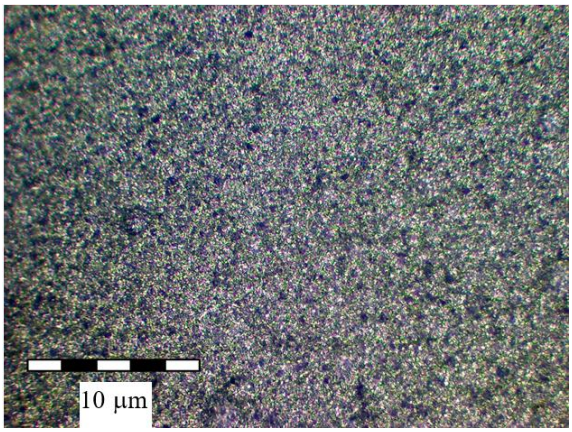

Ni – kaolin – 120 minutes

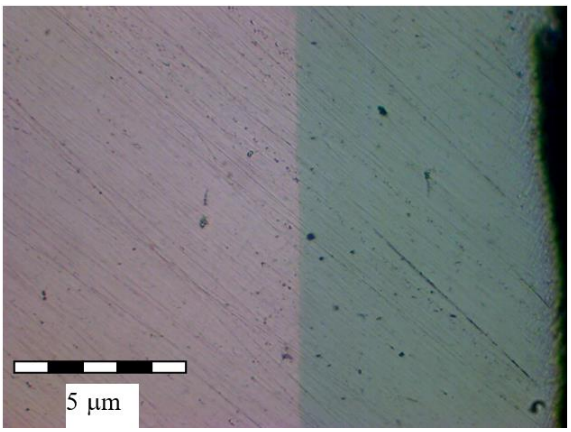

Ni – kaolin – 120 minutes

Fig. 5. *The microstructure of the electrochemically composite coatings obtained in nickel matrix by using the kaolin particles as dispersed phases*

Fig. 6 shows the influence of the time of deposition on the thickness of coatings composites produced electrochemically in the matrix of nickel using the phase dispersed kaolin clay particles. It may be noted that the increase in time deposit increases the thickness of the deposited layer.

Comparing the layer thickness of the deposit obtained at different times for the two types of dispersed phase particles it can be stated that the use of kaolin which has submicroscopic dimensions, resulting in a layer thickness higher than the case of using alumina particles, Fig. 7. So, kaolin particles show a better ability than embedding the alumina particles.

Regarding the microhardness of the obtained composite, electrochemical coatings in nickel matrix using as kaolin clay particles dispersed phases, we find that the increase in time deposit increases their hardness (Fig. 8). This increase is due to the increase in tension on the one hand during the deposition of the layer, and on the other hand a good embedding of the particles of the dispersed phase in the coating.

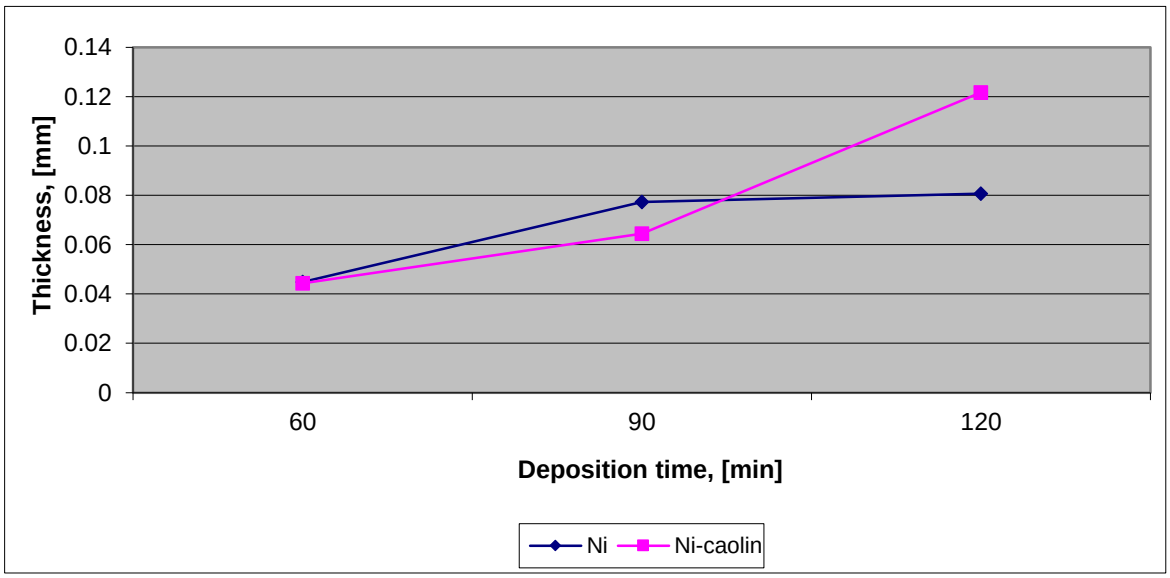

Fig. 6. *The influence of deposition time on the thickness of pure nickel layer coatings and composite coatings on electrochemically produced in nickel matrix using as dispersed phases kaolin particles*

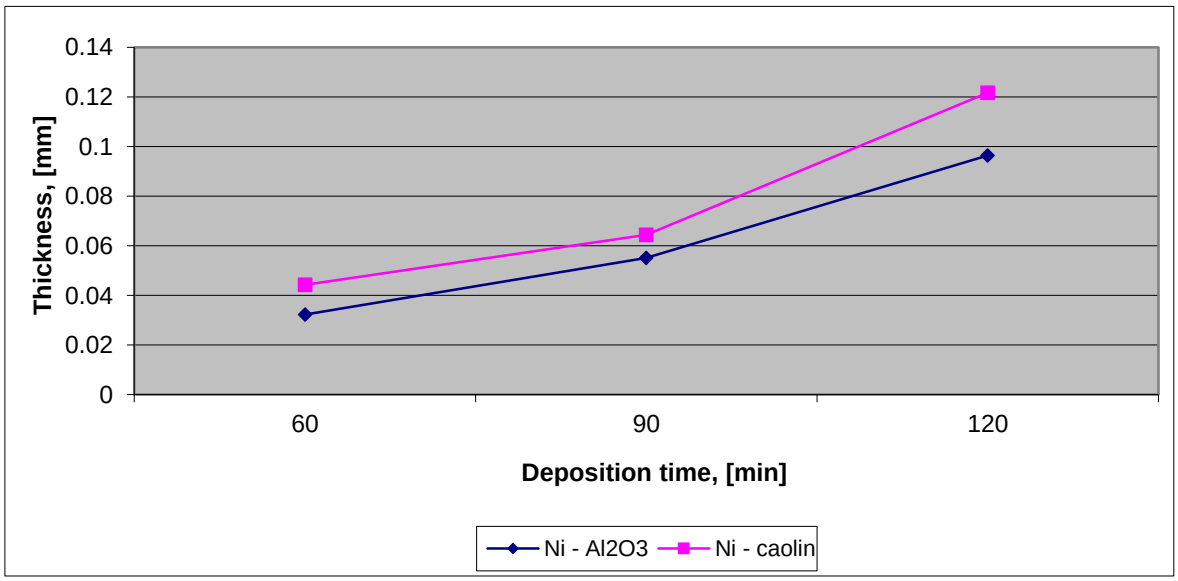

Fig. 7. *The influence of deposition time on the thickness of layer composite coatings electrochemically produced by using nickel matrix as dispersed phases Al_2O_3 particles and kaolin*

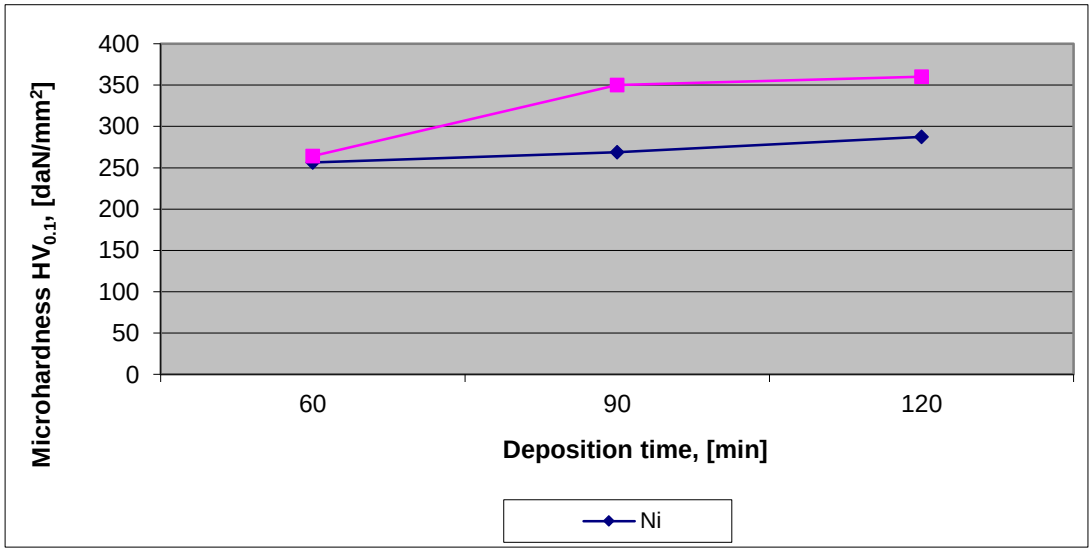

Fig. 8. *The influence of deposition time on microhardness of composite coatings electrochemically obtained in nickel matrix using as dispersed phases kaolin particles*

Fig. 9 shows the influence of deposition time on the microhardness of composite coatings electrochemically obtained in nickel matrix using as dispersed phases particles of kaolin and alumina compared with pure nickel coatings. It can be seen that the composite coatings obtained by means of using the electrochemical nickel matrix as dispersed phases particles of kaolin and alumina present higher microhardness compared to pure nickel coatings. However, due to the tendency to agglomerate larger particles of alumina compared to particles of kaolin, the higher the deposition times, the higher microhardness was obtained.

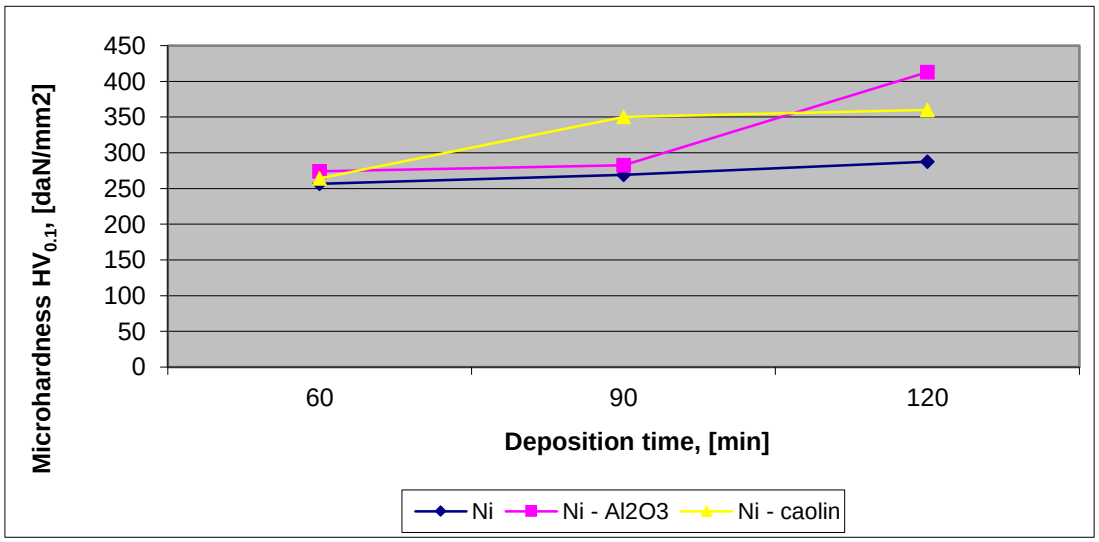

Fig. 9. *The influence of deposition time on microhardness of pure nickel coatings and on composites electrochemically produced in nickel matrix using as dispersed phases particles of kaolin and alumina*

Fig. 10 shows the effect of deposition time on thickness of the composite coating layer obtained electrochemically using the nickel matrix as a dispersed phase particle of kaolin and alumina as compared to pure nickel coatings. It can be seen that by increasing the deposition time, it increases the thickness of deposited layers, the influence of complementary phase particles gets stronger at longer deposition times.

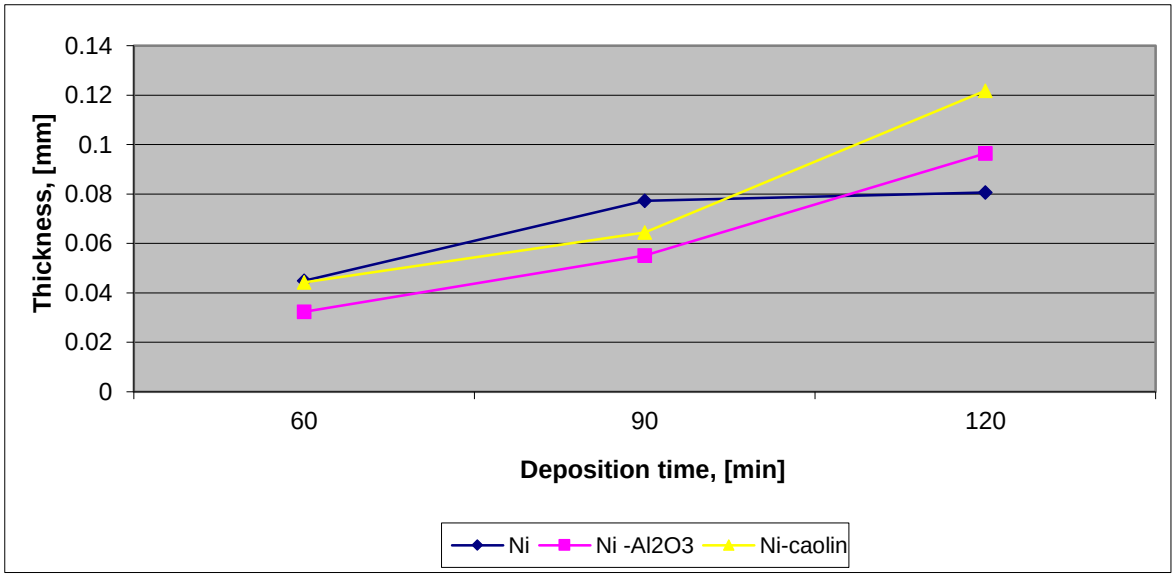

Fig. 10. *The influence of the deposition time on the thickness of the electrochemically obtained composite coating layer using the nickel matrix and as dispersed phases particles of kaolin and alumina as compared to pure nickel coatings*

4. Conclusions

By following the experimental researches, we can highlight the following conclusions:

❖ nickel coatings obtained are uniform, no crackings and a good adhesion to substrates of copper; the best coverage corresponded to the deposition time of 120 minutes;

❖ composite coatings electrochemically obtained in nickel matrix using as dispersed phases Al_2O_3 particles show good adhesion to the substrate, uniformity and compactness; the best inclusion particle dispersion was conducted at a deposition time of 90 minutes;

❖ composite coatings electrochemically obtained in nickel matrix using as dispersed phases kaolin clay particles are homogeneous, no crackings and a good adhesion to substrates of copper; the smaller size particles of kaolin has led to their inclusion in coating better than the Al_2O_3 dispersed phase coatings; the best matched sample has been obtained at a deposition time of 90 minutes;

❖ by increasing time of electrodeposition, the layer's coating thickness achieved increases from 0.0449 mm to 0.0806 mm to pure nickel coatings from 0.0323 mm to 0.0964 mm for ACE Ni - Al_2O_3, and from 0.443 mm to 0.1217 mm for ACE Ni - kaolin, current density and stirring rate being maintained constant;

❖ the layer thicknesses of the obtained coatings ACE Ni - kaolin are better than in the coatings of ACE results Ni - Al_2O_3; the smaller size of the kaolin particles has led to their improved inclusion in the deposited layer;

❖ composite coatings obtained by means of the electrochemical nickel matrix using as dispersed phases particles of kaolin and alumina present higher microhardnesses compared to pure nickel coatings, Such microhardness increases from 126.7 daN/mm^2 to copper support from 256.5 to 287.3 daN/mm^2 for pure nickel coatings, from 274.18 to 413 daN/mm^2 for ACE Ni - Al_2O_3 coatings, from 264 to 360 daN/mm^2 for ACE Ni-kaolin coatings, current density and stirring rate being maintained constant; this increase is due to the increasing tensions in the layer during deposition, and, on the other hand, good embedding of the dispersed particles in the deposited layer and its hardening.

References

[1]. Yahia H. Ahmad, Adel M. A. Mohamed., *Electrodeposition of Nanostructured Nickel-Ceramic Composite Coatings: A review*, International Journal of Electrochemical Science, 9, 2014.
[2]. Raul Novac, *Composite Coatings with Special Properties*, Teză doctorat, Galaţi, 2011.
[3]. Davies Nathan, *Applications of Clay Sedimentation: Deposition of CIGS Photovoltaic Inks*, Institute of Mathematics and Physics Aberystwyth University, 2014.
[4] Pavlov A. I., *Influenţa tratamentelor electrochimice a suprafeţelor (straturi nanocompozite în matrice de nichel) asupra rezistenţei la coroziune şi uzură*, Teză de doctorat, Galaţi, 2012.

THE ANNALS OF "DUNAREA DE JOS" UNIVERSITY OF GALATI
FASCICLE IX. METALLURGY AND MATERIALS SCIENCE
N°. 3 - 2016, ISSN 1453 – 083X

THE DIFFERENT PRACTICAL APPLICATION OF NIOBIUM CARBIDE COATINGS ELABORATED BY CVD PROCESS

Stela CONSTANTINESCU
"Dunarea de Jos" University of Galati, Romania
e-mail: stela.constantinescu@email.ro

ABSTRACT

In this paper, the different application of niobium carbide coatings onto hard carbide substrate was investigated using scanning electron microscope (SEM), X-ray diffractometer (XRD) and micro-hardness. The paper conducted a study on the friction coefficient and wear resistance as a function of load friction couple, for a series of NbC type thin layers; micro-hardness value measured in the coating layer was 29.800 MPa.

Scanning Electron Microscope was used to investigate the coating morphology and interface structure. X-ray mapping was also performed to characterise the elements in a semi-quantitative analysis. A Dron X-ray diffractometer with Mo Kα radiation operating was used for phase(s) identification. Adherence was assessed using a layer fingerprinting method using Rockwell hardness testers. CVD NbC coatings usually show only moderate or even poor corrosion protection for hard carbide substrates.

KEYWORDS: decorative, thin layer, wear resistance, adherence, corrosion

1. Introduction

Niobium carbide coatings find extensive applications in tribological, mechanical and even decorative applications. CVD, NbC coatings usually show only moderate or even poor corrosion protection for hard carbide substrates. The poor corrosion performance is not due to the intrinsic corrosion behaviour of the carbide coating itself. It results from small structural defects, pores and crack formed during or after deposition, which act as channels for the corrosion of substrate. We investigated the corrosion tests in water of niobium carbide coatings elaborated by CVD process.

If the vapour chemical deposition takes place within a tubular continuous reactor, a gas carrying the reacting species is passed over the sub-layer. At the sub-layer surface, the reacting elements undergo a number of chemical reactions leading to product formation. Part of the products are deposited on the sub-layer and part of it goes back to the gas stream [1, 2].

The thin layers developed inside of the NbC, were frequently used, when we talk about multi functionality. This aspect is correlated with the special properties of the films, which gives to the products, in the superficial area, performant properties and the possibility for tuning properties by variation of compositional ratio NbC.

From tribological point of view, the NbC layers are characterized by performant properties, including high hardness, good wear, high temperature stability and nice decorative appearance etc. Thus, from this point of view, these compounds are widely studied in the present, becoming important for applications such as the tribological ones.

Thin layers NbC can be deposited in an efficient mode, by using different procedures deposition of the Chemical Vapour Deposition (CVD) method. For preparing of these compounds as thin films, it is necessary a very attentive control of reactive gas flow, taking into account that this flow influences the final properties of the layers through the participations of the atomic elements present in the composition. As a conclusion, based on an intelligent approach of the fabrication of these materials, there is a possibility to tune their properties in the required direction, for certain industrial applications [4, 5].

Regarding the different practical application possibilities of these layers, one which can be considered are the niobium carbides (NbC) films which are used on a large scale for improving the tribological properties of different cutting tools manufactured from high speed carbured, WC with 6%

Co type. The tribological investigation of these superficial treated tools led to the conclusion that using CVD process for obtaining the layers, concurred to increase the durability. The NbC layers offer to the tools surface finishing, in addition to a high wear resistance and low friction coefficient (roughness low) [2, 3].

On the other hand, during the cutting process, temperatures developed at tool-piece interface (due to the friction) are around 450-500 °C. There is no risk of tool-steel substrate deformation in the steel, and also there is no risk of modifying the specific mechanical properties of the deposited layer.

Measurements of surface defects, friction characteristics and wear coefficient made on NbC, layers, revealed that using Chemical Vapour Deposition (CVD) method for obtaining these layers, can contribute effectively to reduce wear process and to minimize components loss.

Regarding the abovementioned purposes, the different deposition processes of thin films, belonging to CVD and PVD deposition methods have played an important role in Surface Engineering sector.

2. Experimental

Experimental were made of NbC thin films by CVD method, using as raw material pure niobium and ferroniobium. While heat treatment was used concentrated HCl vapour and CH_4 to obtain $NbCl_4$ and NBC as reactions below:

$$Nbs + 4HCl = NbCl_4 + 2H_2$$
$$NbCl_4 + CH_4 + H_2 = NbC + 4HCl + H_2$$

Characterisation of coating deposed by CVD method was done using scanning electron microscope (SEM), X-ray diffractometer (XRD) and Micro-hardness.

Was conducted a study on the friction coefficient and wear resistance as a function of load friction couple, for a series of NbC type thin layers. The thickness of these layers was 6, 8, 10 μm and these ones were obtained through the Chemical Vapour Deposition – CVD process.

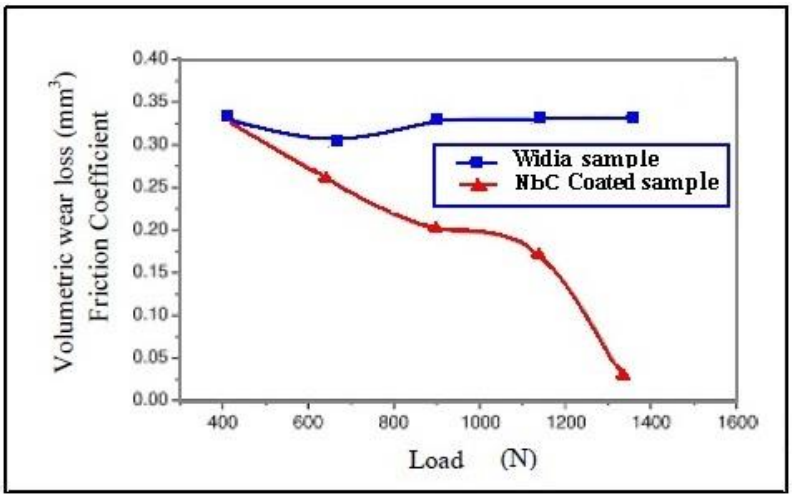

Fig. 1. *The friction coefficient of both surfaces, layers of NbC and widia sample against loads applied to the contact*

This study was done in friction conditions, in a comparative mode, based on samples coated and uncoated samples with NbC.

The friction couple was designed from the coated sample (fixed) and another mobile half-couple made from bearing steel, under conditions of linear motion "come and go", with the linear speed of 0.5 m/s. Thus, regarding the coated samples with NbC, according with Figure 1, with increasing friction couple load, the friction coefficient decreased significantly [6].

For higher loads (more than 900 N), it has been registered a slight positioning at a constant level of friction coefficient value; after this, it was registered an important decrease of this parameter till values of approximately 0.025 when the load reached 1350 N.

Friction coefficient values of widia sample, uncoated samples remained broadly constant, at values of approximately 0.33, for the entire load interval 400 - 1350 N.

Therefore, the friction behaviour of the coated samples is superior to the same one, specific of uncoated samples in a load dry friction conditions.

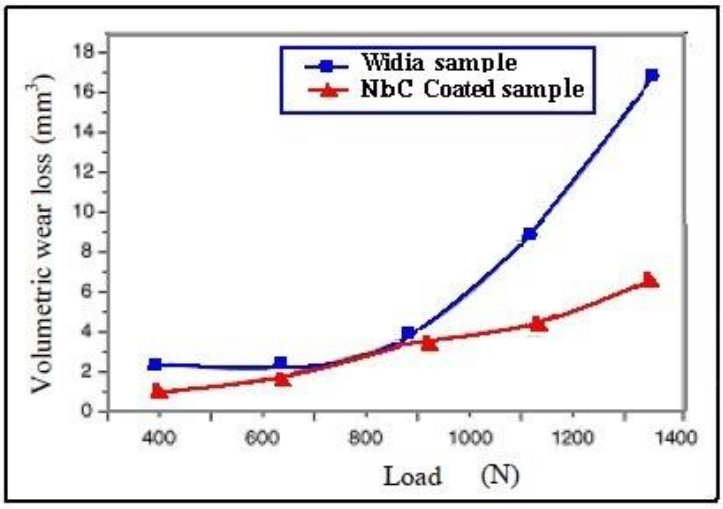

***Fig. 2**. Volumetric wear loss of samples against loads applied to the contact*

Figure 2 shows the dependence between the mass material loss and the applied contact load.

For smaller loads (400-900 N), the mass loss was not significant, but for values over than 900 N (900 N to 1350 N), the mass loss increased. It can be underline that this increasing of wear is more significant for the uncoated samples (17 mm^3) in comparison with those coated with NbC which reached a maximum of 6.8 mm^3 mass loss [7, 8].

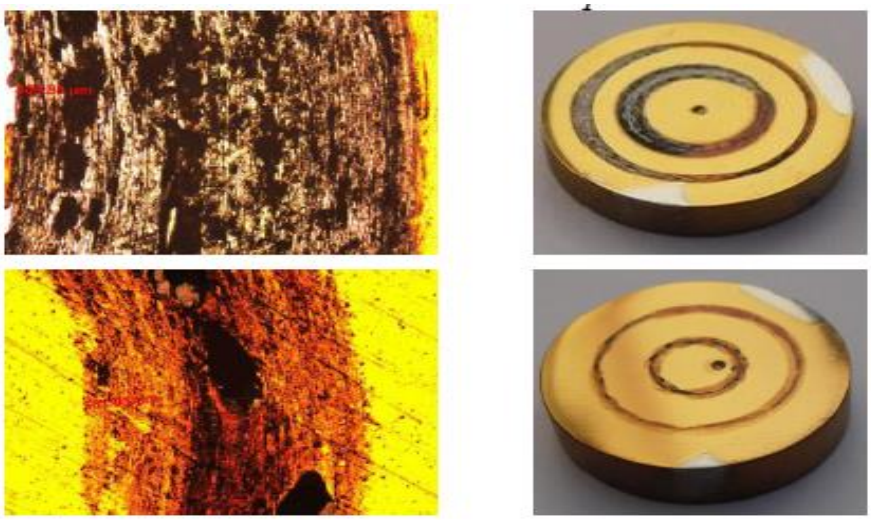

***Fig. 4.** Optical images (a) and photo (b) of traces of wear on the samples*

The NbC coated plates feature higher endurance capabilities than those uncoated for the same cutting speed both for steel and white cast iron.

The parameters of the cutting conditions were chosen in the range of the values used on the working machines at the Arcelor Mittal Steel Galati.

In Figure 3 is represented wear to plates coated with NbC thickness of 6, 8, 10 μm in the process of cutting. The graph wear over time (VB = f (τ)) was traced at intervals of time corresponding to a part of the processing passage, the second and third passes. First passage time is 7.1 min to 14.2 min for second and 21.3 min for third passage

The operation of the latter is based on a housing which cuts the deposited NbC layer. Samples for metallography were prepared by polishing, this prevented damage to the dissimilar interface (strate – substrate) during polishing SEM was used to investigate the coating morphology and interface structure. X-ray mapping were also performed to characterise the elements in a semi-quantitative analysis. Dron X-ray diffractometer with Mo Kα

radiation operating was used for phase(s) identification.

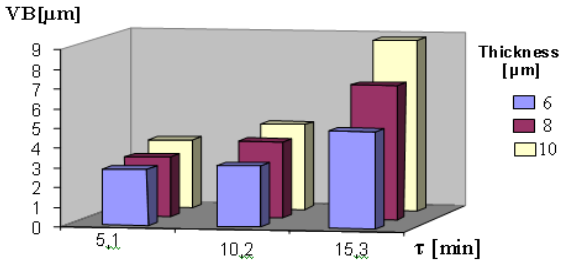

Fig. 3*. Variation wear VB = f (τ) to plates coated with NbC thickness of 6, 8, 10 µm in the process of cutting*

Analysing graph wear over time (Figure 3) it is noted that the character of these curves, in all cases, is normal, especially in working with smaller cutting speeds for using plates coated with NbC [9].

Using a "ball-on-disc" type tribometer, it was evaluated and compared the tribological performance of NbC films. These layers were deposited on widia plate, WC 94% and 6% Co type, by Chemical Vapour Deposition Process – CVD.

In Figure 4 are represented optical images (a) and photo (b) of traces of wear on the samples.

3. Results and discussion

The optimum layers in the cutting process are the NbC layers having thickness within 4 – 10 µm above these values, the layer's loose tenacity and become fragile. As result of the thermal treatment which means heating up to 1068 ºC degrees for various exposure times, layer thickness within 3 – 10 µm was achieved [10]. The thickness of the thin layers increases with the time of exposure to the working temperature as illustrated in Figure 5.

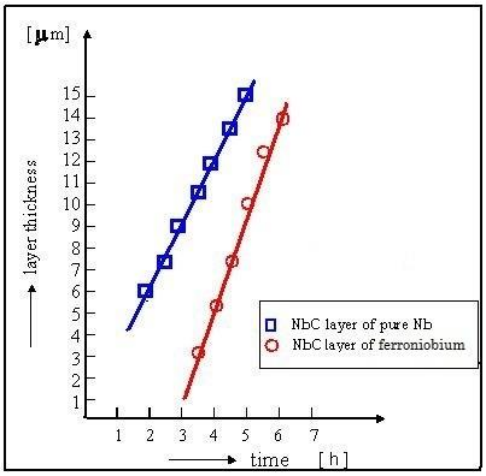

Fig. 5. *The thickness of the thin NbC layers increases with the time*

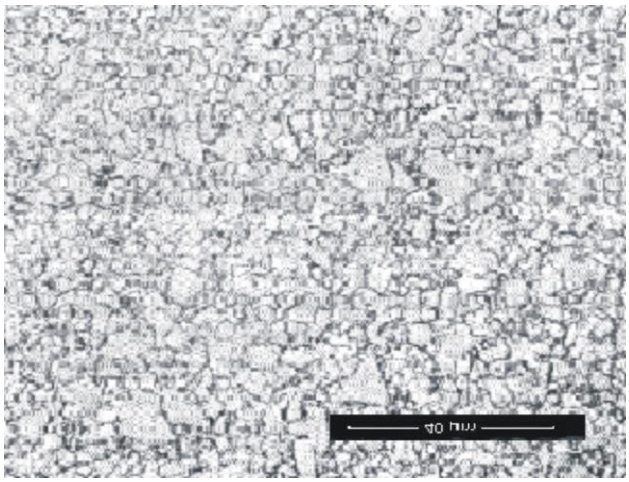

Fig. 6. *Metallographic appearance of alloy with 94 %WC, 6%Co, x1500*

Figure 6 shows the alloy structure metallographic with 6% Co and 94% WC, fine grained. In this figure the basic constituent - tungsten carbide - the form recrystallized called α2. Cobalt is presented in Figure 6 more crowded between WC crystals, showing the structure and some porosity.

WC crystals have a stable structure appearing in the form of equilateral triangular prism or parallelepiped with rectangular base.

Figures 7 and 8, superficial aspects of the layers are deposited CVD compared to monolayer NbC uncovered a plate appearance, classic, studied by electron microscopy. It is clear difference in size of crystals of layer size and size uniformity and surface roughness [13, 14].

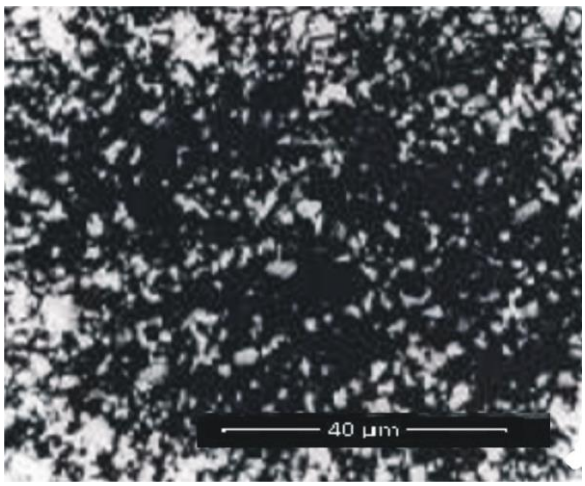

Fig. 7. *Uncoated plate surface appearance - SEM electron microscopy*

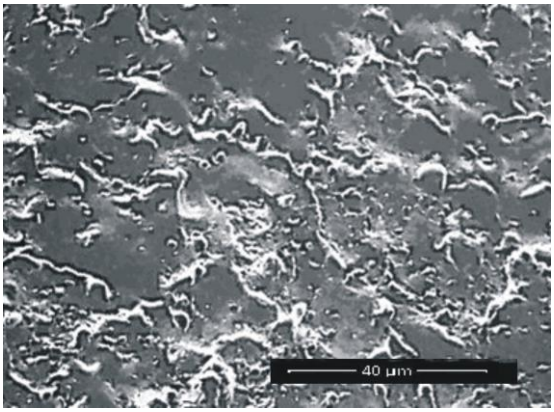

Fig. 8. *Monolayer covered surface plate appearance NbC-electron microscopy SEM*

The uncoated plate surface is rough, because carbide crystals are visible. NbC coated plates germination is observed through nodular much smoother surface thus, the surface is smooth, not slippery and practically with no apparent crystallization. For this reason, coatings provide scope for a much better behaviour from cutting and greater resistance to wear.

Grades are pursued to achieve coatings are out good surface roughness and a good layer purity combined with high uniformity of grain layer.

In Figure 9 metallographic appearance is set for a good quality coated plate. NbC coating is composed of uniform thickness and the grain, having crystal columnar layer. Niobium carbide coating is uniform and adherent throughout its thickness as shown by the metallographic analysis.

Almost isomorphic layer uniform particle size and purity to ensure good behaviour on cutting premises.

The micro-hardness was measured by the Vickers method. The micro-hardness measurements were carried out on plates coated with thin layers of niobium carbide with a thickness of 6 µm different, 8 µm and 10 µm. Micro-hardness is not a constant like Vickers hardness, in spite of the geometrical

similarity, but decreases with higher testing charges depending on the size of the print. The micro-hardness tests show that we have NbC, value HV 0.05 = 29 800 MPa is in good agreement with the data from the literature.

Adherence was assessed by thin layer fingerprinting method using Rockwell hardness testers (diamond cone), the press load 1491 N (150 kgf). This method is used for rapid evaluation of thin film adhesion. Good adhesion on NbC layer by bonding HF4 index shows that interfacial region remains as in normal [15, 16]. In Figure 10 are shown optical fingerprint images after Rockwell indentation for determining adherence NbC films.

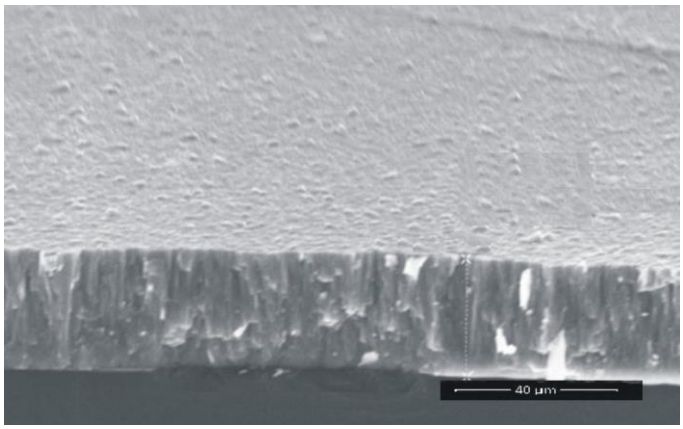

Fig. 9. *SEM images of NbC layer*

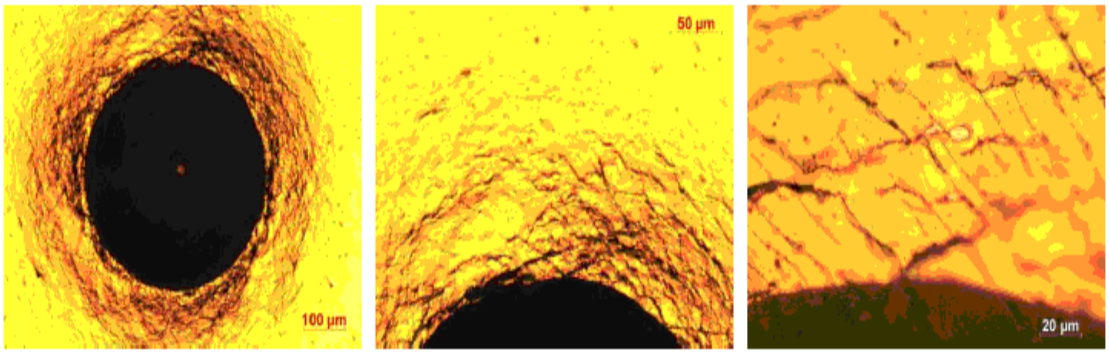

Fig. 10. *Damages formed on NbC coatings during Rockwell C testing*

XRD investigation revealed that it could be obtained a cubic crystallographic arrangement (Figure 11). The result is favourable and certify existing thin NbC layer (the maximum curves diffractometer) [17, 18]. The conclusion drawn from the analysis is that the diffractometer NbC layer which is not susceptible of cracking during tense operation.

CVD NbC coatings usually show only moderate or even poor corrosion protection for hard carbide substrates. The poor corrosion performance is not due to the intrinsic corrosion behaviour of the nitride coating itself. It results from small structural defects, pores and crack formed during or after deposition, which act as channels for the corrosion of substrate [19, 20]. We investigated the corrosion tests in water of titanium nitride coatings elaborated by CVD process.

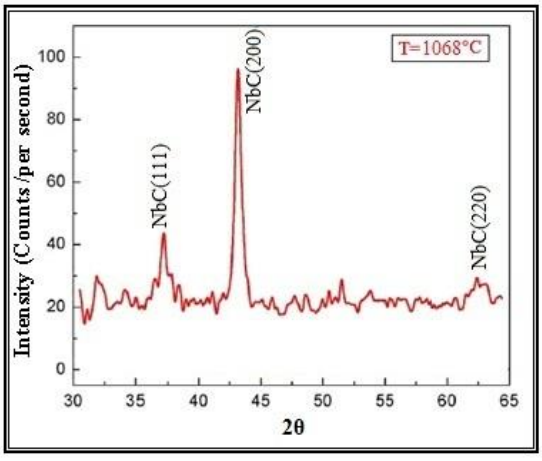

Fig. 11. *X- ray diffraction spectrum of NbC coating*

Fig. 12. *Surface appearance of uncoated NbC samples after corrosion*

a b

Fig. 13. *Surface appearance of covered NbC samples after corrosion a) 6 μm; b) 8 μm*

As seen in Figures 13a, 13b uncoated surface NbC samples have surface oxides by 40% if the samples coated with the thickness of 6μm NbC have slight traces of surface oxides on 5% non-stick surface and covered with NbC samples with thickness of 8μm surface shows no oxides.

Uncoated samples and coated with thin layers of NbC were exposed to corrosion in water for 600 h. In uncoated samples, the corrosion rate increases with time, and in the case of the samples coated with NbC corrosion rate decreases over time. It was noted that in corrosion test in water, samples covered with NbC channel are stronger compared with uncoated samples NbC.

4. Conclusions

These coatings have good wear resistance, abrasion resistance, corrosion resistance and a strong strate-substrate interface. This leads to formation of thick and rough coating. The coating is finely grained, adherent, dense and free from cracks. However, some porosity is observed in the coating layer.

The thin layers NbC with a thickness of approx. 10 μm, obtained by Chemical Vapour Deposition – CVD process on widia substrates, presented a better wear resistance and a lower friction. Graphs wear over time, VB = f (τ), are the normal character.

Diffractometer analyses certify the existence of a thin NbC layer, and it is not likely crack sticky in operation.

Good adhesion on NbC layer by bonding HF4 index shows that interfacial region remains as in normal situation.

Micro-hardness is not a constant like Vickers hardness, in spite of the geometrical similarity, but

decreases with higher testing charges depending on the size of the print efficient value.

The layer begins losing its tenacity if its thickness increases considerably exceeding the thickness 10 μm mainly due to the lower strength characteristics. This together with the increase in the inner tensions results in cracks and breakings in the layers. This has been attributed to poor wetting characteristics.

In corrosion test in water, samples covered with NbC channel are stronger compared with uncoated samples NbC.

References

[1]. Constantinescu S., *Studies on Thin Carbide and Nitride Layers Deposition on Metal Basis, Based on Chemical Reaction at High Temperatures*, Academic Thesis, Galati, 1998.
[2]. Constantinescu S., *Nitride coatings on widia substrate for mechanical applications*, Journal Surface Engineering, vol. 1, p. 77-81, 2009.
[3]. Constantinescu S., Radu T., *Advanced methods of obtaining thin coats*, Ed. Științifică F.M.R., București, 2003.
[4]. Yasuharu O., Shinya K., Kazuhide O., Hideki A., Hideki N., Kenji H., Osamu M., Thin Solid Films 497, 2006.
[5]. Sista V., Kahvecioglu O., Erylmaz O. L., Erdemir A., Timur S., Thin Solid Films, 520, 1582, 2011.
[6]. Bemporad E., Sebastiani M., Pecchio C., De Rossi S., *High thickness Ti/TiC multilayer thin coatings for wear resistant applications*, Surface and Coatings Technology, vol. 201, issue 6, p. 2155-2165, 2006.
[7]. Staia M. H., Perez-Delgado Y., Sanchez C., Castro A., Le Bourhis E., Puchi-Cabrera E. S., Wear, 267, 1452, 2009.
[8]. Yasuda Y., Kano M., Mabuchi Y., Abou S., *Research on Diamond-like Carbon Coatings for Low-friction Valve, Lifters*, Special Publications. Society of Automobile Engineers SP-1744, p. 77-82, 2003.
[9]. Polcar T., Evaristo M., Cavaleiro A., Wear, 266, p. 388, 2009.
[10]. Zhecheva A., Sha W., Malinov S., Long A., *Enhancing the microstructure and properties of titanium alloys through nitriding and other surface engineering methods*, Surface and Coatings Technology, vol. 200, issue 7, p. 2192-2207, 2005.
[11]. Choy K. L., *Chemical vapour deposition of coatings*, Progress in Materials Science, 48, p. 57-170, 2003.
[12]. Bemporad E., Sebastiani M., Pecchio C., De Rossi S., *High thickness Ti/TiC multilayer thin coatings for wear resistant applications*, Surface and Coatings Technology, vol. 201, issue 6, p. 2155-2165, 2006.
[13]. Caicedo J. C., Amaya C., Yate L., Nos O., Gomez M. E., Prieto P., *Hard coating performance enhancement by using [Ti/TiN]n, [Zr/ZrN]n and [TiN/ZrN]n multilayer system*, Mater. Sci. Eng. B, vol. 171, p. 56-61, 2010.
[14]. Yasuharu O., Shinya K., Kazuhide O., Hideki A., Hideki N., Kenji H., Osamu M., Thin Solid Films, 497, 218, 2006.
[15]. Notter I. M., Gabe D. R., *Porosity of Electrodeposited Coatings: Its Cause, Nature, Effect and Management*, Corrosion Reviews, 10 (3-4), p. 217-280, 1992.
[16]. Munemasa J., Kumakiri T., *Effect of the Surface Roughness of Substrate on the corrosion properties of fims coated by Physical Vapour Deposition*, Surface and CoatingsTechnology, 49, p. 496-499, 1991.
[17]. Krawitz A. D., *Introduction to Diffraction in Materials Science and Engineering*, Wiley, New York, p. 165-167, 2001.
[18]. Krawitz A. D., *Introduction to Diffraction in Materials Science and Engineering*, Wiley, New York, p. 165-167, 2001.
[19]. Man A., Aubert P., Mercier F., Khodja H., Berthier C., Houdy P., Surf. Coat. Technol., 194, p. 190-195, 2005.
[20]. Sista V., Kahvecioglu O., Erylmaz O. L., Erdemir A., Timur S., Thin Solid Films, 520, 1582, 2011.

THE ANNALS OF "DUNAREA DE JOS" UNIVERSITY OF GALATI
FASCICLE IX. METALLURGY AND MATERIALS SCIENCE
N°. 3 - 2016, ISSN 1453 – 083X

ENVIRONMENTAL RISKS ASSESSMENT BY QUALITATIVE AND QUANTITATIVE METHODS

Tamara RADU
"Dunarea de Jos" University of Galati, Romania
e-mail: tradu@ugal.ro

ABSTRACT

The paper presents qualitative and quantitative methods, applicable on environmental risks, and conditions of application. The principles of the two classes of risk assessment methods and the advantages and disadvantages of their application in environmental risk assessment are presented. For both methods, there is a wide range of techniques and tools with applicability more or less specific to certain types of risks. The risk matrix method with its many application forms and examples are presented. Also, it analysed the environmental risk associated thermal plants by risk matrix method.

KEYWORDS: environmental risk, qualitative and quantitative methods, risk matrix

1. Introduction

Globalization of environmental problems raise increasing concerns internationally. Production processes require natural resources which, integrated into an appropriate technology [1-3], lead to useful or recyclable products [4, 5], and also to unusable products which return to the environment and contaminate it [6, 7]. Environmental risk arises from such interactions between human activities and the environment. This risk has begun to occupy an increasingly important place in the environmental management of an organization. Environmental policies of organizations with significant environmental impact include more and more commitments to environmental risk.

The scope of the environmental risk assessment may however be much broader, including environmental risks (such as those relating to biodiversity, species extinction, etc.), risks of environmental factors (e.g. depletion of water resources, desertification, ozone depletion, global warming, etc.) or the occurrence of environmental hazards (risk of floods, earthquakes, storms, etc.).

2. Characteristics of qualitative and quantitative methods

Environmental risk assessment is relevant whenever installations or technological operations can interact with the environment and there is the possibility of adverse effects.

For this purpose, two main classes of methods may be used: qualitative methods and quantitative methods.

2.1. Qualitative risk analysis

Qualitative risk analysis involves using qualitative criteria, in order to both appreciate the consequences of a hazard and to determine the frequency of its occurrence. Also, qualitative decisions are taken based on the expertise in the field, for risk classification [8].

Hazard identification is based on various qualitative methods such as check lists, inspections of installations, preliminary hazard analysis, analysis of human errors, method "but if", analysis of the properties of hazardous substances, HAZOP (Hazard and Operability Study) studies, environmental audits, etc. [9]. After rigorously identifying the hazards, it is proceeded to determine the gravity of the consequences and the occurrence probability of that risk by establishing classes of suggestive names (e.g. small, medium, large) to which numbers may be assigned, or not (e.g. 1 - low, 2 - medium, 3 - large) and the risk is to be calculated, in the latter case, numerically. Qualitative methods are valuable mainly for the assessment of risk in complex systems such as the environment.

The *benefits* of applying qualitative methods [10]:

- are easy to apply;
- are effective;
- can be tailored to the situation subject to risk assessment (simplified or enriched);
- can be applied by non-specialists as well;
- are inexpensive;
- do not require complicated databases;
- have a general nature hence broad applicability.

As major *disadvantages*, we can mention:

- are subjective, depending much on the interpretation of the person who applies the method;
- can have a high degree of ambiguity;
- have a high probability of "lost" risk (unidentified);
- are less useful in characterizing the magnitude of risk.

Because of these restrictions, these methods will not be used to exclude dangers from further consideration, but only for their ranking purpose.

The literature presents various qualitative methods for assessing environmental risk such as: risk matrix, events tree, error tree, analysis of source-path-receiver, model of pollutants conveyance etc.

2.2. Quantitative risk analysis

Quantitative risk analysis is an expensive specialized method requiring background data and analysis and may also include formal mathematical modeling. Quantitative analysis means to assess the number of variables, parameters and states of the system subject to risk assessment and provides quantitative results. This approach is more objective and accurate. Quantitative quantifying of the environmental risk is made especially for extremely rarely occurring events, very severe with possible catastrophic consequences [9]. It should be noted that the quantitative results can be greatly affected by the accuracy and validity of the input parameters. Uncertain, complex and variable data affect and make considerably difficult the analysis and adversely affect its outcome. For this reason, quantitative results in risk analysis should not be considered as exact numbers, but estimated on a variable scale depending on the quality of the data used in the calculations.

Where possible, a detailed and quantified analysis made by competent persons provides a better understanding of risk and its management opportunities, as compared to a purely qualitative analysis. The strength of the quantified approach is not its accuracy, but the benefits of a more rigorous analysis [8]. A trap of the quantitative analysis may be unjustified confidence in the accuracy of numerical results. These are not absolute, because the results of the analysis may be based on inaccurate information and usually require generalization and simplification of assumptions [8].

Quantitative analysis benefits from special techniques such as modern statistical and probabilistic methods or simulation method. Among the well-known methods, we may include: DOW method, Monte Carlo method, errors tree, events tree, Mond Index etc. The quantitative methods are generally complex, their application requiring specialists with relevant expertise.

2.3. The application of qualitative and quantitative methods in environmental risk

For both quantitative and qualitative approaches, there is a wide range of techniques and tools applicable more or less specifically to certain types of risks. Also, tools and techniques of risk assessment are developed continuously. Most experts in the field of risk are for an initially qualitative analysis followed, if the situation requires, by a quantitative analysis, as shown in Figure 2 [11]. Qualitative risk assessment techniques are used when risks cannot be quantified or when insufficiently reliable information is available for the quantitative assessment, or when collection of data is not efficient in terms of time required for study or costs. Quantitative assessment techniques are usually used in more complex activities to supplement qualitative techniques.

As it can be seen from the diagrams shown in Figure 1, the two types of analyzes aim, in different terms, at dimensioning the two factors which determine the risk, i.e. the likelihood and the consequences of a danger.

Determining the probability of an event in environmental risk assessment can be a very simple or very difficult approach. There may be many situations where the probability of an event is 1 (so it will happen for sure). For example, once it was decided to build a bridge and the necessary resources were allocated, the construction will be done for sure and with all environmental consequences (loss of habitats, landscape elements and structures in the area). In this case, the important parameters to be considered are: the *likelihood* and *magnitude of the consequences* to the *likelihood of the event* (building) itself. There are as many situations, especially those caused by accidents, when the probability of the trigger event becomes very important. These events usually have a probability of less than 1 and it will be necessary to determine it. For example, in certain situations of malfunction or accident, the planned release of pollutants into the air from various industrial activities can exceed the allowed limits with significant consequences on the environment [6].

In this case, it is necessary to establish the likelihood of the triggering event through various techniques and methods available.

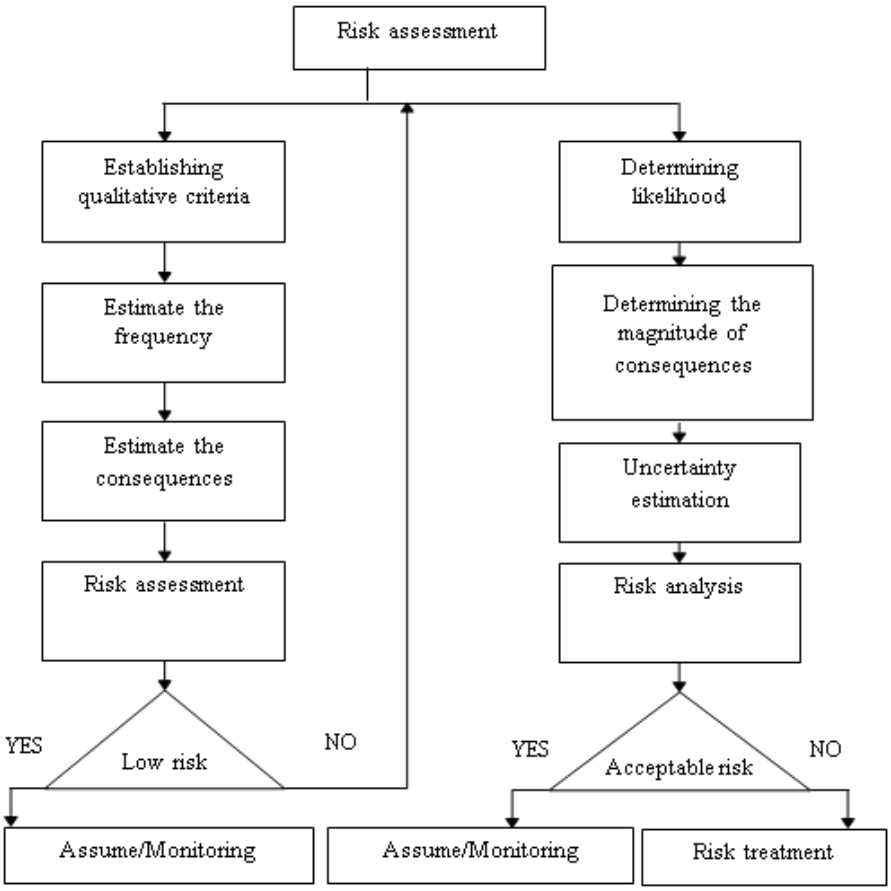

Fig. 1. *The application of qualitative and quantitative methods to assess environmental risk* [11]

Estimating the extent and probability of consequences. In some cases, especially in the environmental risk assessment, there will be a high level of uncertainty in estimating the magnitude of the consequences. Ecosystems are often complex, with many food chains or other interdependencies between species that require costly or lengthy investigations to establish the extent of the consequences of a hazard. In such cases, measures of optimal cost / efficiency ratios will be taken, even in the presence of uncertainty regarding the magnitude of the consequences in order to avoid serious or irreversible damages. However, in most cases it is possible to quantify the magnitude of the consequences and even conversion into a monetary value that will facilitate the socio-economic analysis. For example, there are well-developed techniques to estimate the probability that a chemical product released into the environment adversely affect organisms. This assessment is based on a comparison of a known concentration at which side effects occur and a concentration predicted or measured in the environment. If no data are available on the consequences of a hazard or the risk assessment uncertainty is unacceptable, use may be made of various models, assumptions, extrapolation techniques, etc. For example, to assess the dispersion and concentration of a substance accidentally released into the environment, its physico-chemical properties and details of the amounts released can be analyzed.

3. Risk matrix method- case study

Most commonly, a qualitative analysis refers to a matrix approach. Risk matrix presents columns for frequency and lines for the consequences extent. The analyst or group of specialists classifies the identified hazard depending on the effect size and frequency, setting its appropriate place into the matrix. The literature shows different types of matrices from the simplest, with three levels on each axis, to various combinations: three to four, four to four, four to five, five to five, etc. Experience suggests that five classes for each axis should be minimal because analysts find it difficult to take decisions to establish rank risk with

a smaller number of options [9]. A larger number than five levels may be useful in some complex systems for which other analytical tools are not available, but may induce the false sense of precision of such a risk analysis. The magnitude of risk can be dotted inside the risk matrix also by suggestive colors such as green - low risk, yellow - medium risk, and red - for high risk.

The best, however, matrices are those of five classes for consequences, five classes for risk frequency and five levels of risk: Table 1 [8, 9, 12].

Table 1. *Risk Matrix with five classes for each axis*

	Severity of the consequences					
Frequency		Insignificant	Minor	Moderate	High	Very high
	Very low	Very low	Very low	Very low	Very low	Low
	Low	Very low	Low	Low	Low	Medium
	Medium	Very low	Low	Low	Medium	High
	High	Very low	Low	Medium	High	Very high
	Very high	Low	Medium	High	Very high	Very high

In literature are presented the models detailing the five levels of risk and probability and severity expressed only in suggestive words [13,14,15]. Much more advantageous are the methods using risk matrices whose severity and probability classes are accompanied by specifications to guide assessors to a more accurate risk assessment [9, 12].

Let us consider the major environmental hazards caused by specific processes and operations of a thermal plant using coal and natural gas as fuel [16], namely:

h1 - the emission, transport and dispersion of SO_2 in the air over the accepted norms;

h2 - the emergence of acid rain caused by SO_2 and SO_3 by reaction with rainwater;

h3 - CO_2 emissions with major influence on climate change;

h4 - NO_x emissions over the accepted norms;

h5 - formation, due to NO_2, of the nitric acid and the ammonium nitrate aerosols;

h6 - formation of the ozone; having as precursor of NO_2;

h7 - emissions diffuse / fugitive of CO;

h8 - emissions diffuse / fugitive of dioxins and furans;

h9 - soil pollution in the slag dump;

h10 - soil pollution by coal dust in the storage of raw materials;

h11 - soil pollution by oil products;

h12 - pollution of groundwater;

h13 - pollution by wastewater;

h14 - fly ash;

h15 - slag and ash particles shattered of the air currents;

h16 - radioactive slag and ash;

h17 - transfer and dispersion of pollutants in aquatic environments;

h18 - noise pollution;

h19 - production of the fires;

h20 - production of the explosions.

These hazards, depending on the frequency and probability evaluated, we will place a risk matrix, shown above, to determine for each hazard the level of risk - Table 2.

Table 2. *Environmental Risk Matrix for hazards specific of a thermal plant**

	Severity of the consequences					
Frequency		Insignificant	Minor	Moderate	High	Very high
	Very low	-	-	Very low risk h4	Very low risk h5	Low risk h6, h7, h16, h20
	Low	-	-	-	Low risk h2	Moderate risk h8, h19
	Medium	-	-	-	Moderate risk h1	High risk h12, h13, h17
	High	-	-	Moderate risk h10, h11	High risk h3, h14	Very high risk h15
	Very high	-	-	High risk h18	Very high risk, h9	-

* The matrix presented is in the first place an example of the method without claiming a well-documented assessment as required by such an approach.

Environmental risk analysis for the heat plant shows mainly large and very large severity of the consequences. Risk occurrence frequency covers all classes. The risk levels of the hazards are concentrated on moderately large and very large risk.

4. Conclusions

Environmental risk assessment can be a very simple or very difficult approach depending on the complexity of the issue being analyzed and the available data. When the environmental hazards cannot be quantified or are not available sufficiently reliable information necessary for quantitative assessment, or collection of data is not efficient in terms of time required for study or costs, qualitative assessment techniques will be applied. A widely-applied method for this purpose is the risk matrix method. The best matrices are those with at least five classes for serious consequences, five classes of frequency and five levels of risk. Most experts in the field of risk are in favor of an initial qualitative analysis followed, if necessary, by a quantitative analysis. Quantitative assessment techniques are expensive and complex but wherever possible, a detailed and quantified analysis made by competent persons provides a better understanding of risk and its management opportunities as compared to a purely qualitative analysis. Both methods have established methods and techniques that can be applied to environmental risk assessment. Environmental risk analysis for thermal power plant shows mainly large and very large severity of the consequences. Risk occurrence frequency covers all classes.

References

[1]. Vlad M., Radu T., Mitoseru O., Potecasu F., *Environment Quality Improvement at Hot-dip Galvanisation and the Recycling of Zinc By-products*, Journal of Environmental Protection and Ecology 12, no. 3A, p. 1415-1423, 2011.

[2]. Radu T., Ciocan A., Balint S., DraganV., *Environmental friendly solution for the hot dip galvanized coatings*, SGEM2011 Conference Proceedings, June 20-25, vol. 3, p. 53-60, 2011.

[3]. Balint L., Istrate G. G., Balint S., Radu T., *Composite coatings with nickel matrix and silicon by clean technology*, SGEM 2011, Conference Proceedings, June 20-25, vol. 3, p.27-34, 2011.

[4]. Ciocan A., Radu T., Balint L., Balint S. I., *Recovery of precious and special metals from cell phone waste by pyrometallurgical processing of printed circuit boards*, SGEM2013 Conference Proceedings, June 16-22, p.749-756, 2013.

[5]. Vlad M., Movileanu G., Radu T., Balint L., *Recycling of zinc by products*, SGEM 2011, Conference Proceedings, June 20-25, 2011, vol. 3, p. 875-882, 2011.

[6]. Radu T., Ciocan A., Balint S. I., Balint L., *Dioxins and furans emissions in the primary steel sector*, SGEM2013 Conference Proceedings, June 16-22, p. 609-616, 2013.

[7]. Ciocan Anisoara, Florentina Potecasu, Veiga Joao Pedro, *Characteristics of the blast furnace dust in accordance with the conditions imposed by the valorization solution*, Metalurgia International, vol. 15, issue 10, p. 85-90, 2010.

[8]. Dryden P., Beer T., Lambert I., s. a., *Environmental risk management*, ISBN 0642546304, Australia, 1999.

[9]. Ozunu A., Anghel C. I., *Evaluarea riscului tehnologic şi securitatea mediului*, Ed. Accent, Cluj-Napoca, 2007.

[10]. Tamara Radu, Maria Vlad, Marius Bodor, Gelu Movileanu, *Managementul riscului de mediu*, Galati University Press, Colectia Stiinte Ingineresti, 2015.

[11]. ***, http://www.scribd.com/doc/31130364/Slide-Riscuri.

[12]. Radu T., Ciocan A., Vlad M., Balint S. I., Dragan V., *Environmental risk assessment in the galvanizing of steel sheets*, SGEM 2012, 12th International Multidisciplinary Scientific GeoConference Proceedings, vol. 5, p. 391-397, 2012.

[13]. ***, *Environmental Risk Assessment*, Environment, Health and Safety Committee [EHSC] of the Royal Society of Chemistry. Environment, Health and Safety Committee, www.rsc.org, 2008.

[14]. Green E., Short S., Taylor March M., *Guidelines for Environmental Risk Assessment and Management*, ISBN 0 11 753551 6, 1998.

[15]. ***, *Environmental Risk*, ACE European risk briefing, http://www.acegroup.com.

[16]. Radu T., *Environmental Risk Assessment for Thermal Power Plants*, The Annals of "Dunarea de jos" University of Galati, Fascicle IX. Metallurgy and Materials Science, no. 4, p. 38-42, 2015.

THE ANNALS OF "DUNAREA DE JOS" UNIVERSITY OF GALATI
FASCICLE IX. METALLURGY AND MATERIALS SCIENCE
N°. 3 - 2016, ISSN 1453 – 083X

OPTIMIZATION TECHNIQUES FOR THE NEUTRALIZATION OF THE POLLUTED WATERS FROM METAL PLATING

Ștefan DRAGOMIR, Marian BORDEI*
"Dunarea de Jos" University of Galati, Romania
*correspondent author
e-mail: mbordei@ugal.ro

ABSTRACT

The problems related to the protection of the environment are regarded especially as a result of the local pollution by the industry and agriculture or by the overcrowded areas, which have led to the disturbance of some ecosystems and to worse living conditions of people. The extensive use of chemical substances in the technological processes demands special measures concerning the protection of the environment. A major problem is the purification of industrial waste water.

KEYWORDS: metal plating, polluted water, purification

1. Introduction

In this paper, we will present a solution for the treatment of the cyanides water from galvanic industry.

The removal of the residual pollutants existing in the effluents from the mechanical - biological purification stations of waste waters implies the use of the electrolysis processes effects in order to resolve the issues of the related domain. A series of conditions, locally established in Romania, through the Technical Rules of Waters Protection (NTPA001 and NTPA002), and on the European plan for the member states through the CCEE Directives no. 271/91 and no. 676/91 are designed to fit within the specify limits the acceptable level of the pollutants in the effluents.

NTPA - 001 refers to the waste waters of any kind, namely to waste water, industrial waste, agro-zootechnical, of mine or deposits water, evacuated through arranged fire systems coming from own technological processes, as well as from the mixed used water, which were or not cleaned. The values shown in these norms are maximum admissible values.

NTPA - 002 refers to the quality of waste water, from both social and economic activities, which are to be evacuated in the sewerage networks of the towns and, directly, in the treatment plants. The establishment of technological process, the origin and the quality characteristics of the waste water requires the knowledge of the industrial process for a judicious design of the purification stations. Therefore, it is necessary to know the origin of the main flows and their main characteristics to define the method of purification. The reduction of waste water requires the use of new technologies. The main harmful substances of industrial waste water are the organic substances, the substances in the suspension, the toxic substances and the heavy metals, the synthetic detergents, etc. The recovery of the valuable substances from the waste waters is aimed at their reduction of the discharged harmful substances [1].

As a result of these chemical analysis we have chosen to preserve the existing neutralization process and following it, to apply an electrolytic oxidation followed by a process of adsorption on activated charcoal and a final filtration in a granular filter with sand.

2. Waste water neutralization

For the waste water in A basin (with cyanides):

- it is adjusted the pH of the solution between 7 ÷ 8: if the pH < 7, NaOH is added; if the pH > 8, HCl is added;
- 4 l sol. $CaCl_2$/ 4 t sol. tank is added (5 kg $CaCl_2$/100 l H_2O);
- stirred 15 minutes;
- 3 l $FeCl_3$/1000 l sol. tank is added;
- stirred for 15 minutes;
- add 2.5 l polyelectrolyte/1000 l sol. from the tank;
- mix 3 ÷ 5 minutes;
- after agitation 2 ÷ 3 hours are expected for sludge decantation.

For the waste water in B basin (with metallic ions):

- add the H_2SO_4 to pH = 0 ÷ 2;
- add sodium metabisulfite for reducing chromium hexavalent from +6 to +3 up to the point of change of color from red to blue-green;
- add, all the time, sodium metabisulfite (the solution is obtained by dissolving 10 kg quantity of sodium in 100 l hot water);
- after a primary settling, the water of the tanks 5 and 6 are entered in the tanks 7 where takes place the final decantation and, then, filtering.

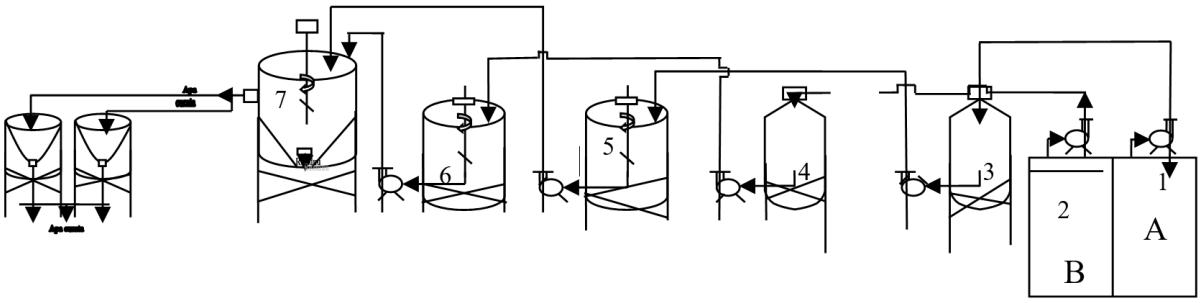

Fig. 1. *Electro chemical purification of waste water to metal plating*

In the mechanical engineering industry, there is the electro-metallurgy branch in aqueous galvanic-technical medium. The waste waters resulting from the washing of the galvanic covered pieces or electro-chemical treated contain toxic impurifications, often, non-biodegradables Cr^{6+}, CN^- etc. which require their cleaning before discharging in the natural circuit. The removal of the hexavalent chromium combinations will be carried out by chemical reduction or electro-chemical ions at Cr^{3+}, less toxic and whose combinations are mostly insoluble [2].

The chemical methods have the disadvantage of being effective in a pH-acid limited area and require reactants for carrying out the reduction reaction. The electrochemical methods eliminate these disadvantages and, in addition with the removal of ions containing Cr^{6+}, other harmful impurificators can be removed. The electrochemical treatment consists in subjecting the contaminated water to an electrolyze process with water-soluble anode made of alloyed aluminum with 0.01-1 % indium or gallium as well as of iron or ferrous material [3].

In the case of using iron anodes, as a result of the electrolysis process, the following processes take place:

- *on cathode*: a) the reduction of chloride H^+ ions and, therefore, the alkalinizing of the cathode space; (b) the reduction of Cr^{6+} at Cr^{3+} chloride ions, which together with the OH^- ions make forming an insoluble precipitate, $Cr(OH)_2$;
- *on anode*: the iron ionization in accordance with the reaction:

$$Fe \rightarrow Fe^{2+}+2e \quad (1)$$

The Fe^{2+} ions precipitate in the form of ferrous hydroxide, rough, which, in the presence of dissolved oxygen, passes, partly, in the ferric hydroxide. The total reaction product is an insoluble hydroxides complex that incorporates impurificator ions in the form of $Cr(OH)_3$.

The presence of iron complex determines that the chromium hydroxide, which normally require a specific pH domain for a full precipitation, should no longer be sensitive to pH, this can vary within broad limits (pH = 4-11).

The studies have been carried out on synthetic waters, containing 200 ppm Cr^{6+} and 20 g/L sodium sulphate necessary to increase the conductivity [4]. The original solution and the filtrate after the electrolysis process of have been subjected to the analysis for the Cr^{6+} and Cr^{3+} ions determination after the" iodometric" manganometrical method.

Is was used a parallelepiped shaped cell made of plexiglass, having a useful 0.3 l capacity. The anodes and cathodes have the dimensions 50 x 30 x 1 mm (the grilling surface - 30 cm^2) and they were made of the same carbon steel material [4].

The electrodes have been fitted in parallel and in series at a distance of 0.8 cm. In the case of fitting in parallel, the electrode number was variable, while in the case of fitting in series, we worked with a constant number of nine electrodes, which corresponds to eight electrochemical cells.

3. Experimental results

The experiments have pursued the effectiveness of the polluted waters purification and the specific consumption of energy, depending on the density of

the anode (number of anode manufacture) and the time of the electrolysis.

There have been made tests with a number of four anodes at smaller density and time electrolysis. It was found that, both anode current density decreases less than 0.2 A/dm^2, as well as of the electrolysis time reduction below 30 minutes have adverse effects on the treatment efficiency (Table 1); also, the efficiency of the purification at the parameters of the electrolysis of links the point A (anode surface 1.2 dm^2) is presented.

Table 1. *The efficiency of the purification*

The density of the anode current	**Time for electrolysis**	**Treatment efficiency**	**Obs.**
[A/dm^2]	[min]	[%]	
0.2	30	100	Point A
0.18	30	92.3	
0.15	30	83.9	
0.2	25	83.0	
0.2	20	64.2	

The dependence of the specific energy consumption on the current density for the variable anode areas is: 1-0.3 dm^2; 2-0.6 dm^2; 3-0.9 dm^2; 4-1.2 dm^2. In accordance with the fitting of the electrodes in parallel, a surface anode of 1.2 dm^2 (four anode manufacture) provides an effective way of 100% at a current density of 0.2 A/dm^2 and a treatment duration of 30 minutes, the energy consumption being 0.45 kWh/m^3.

The precipitate which was formed, includes the impurificator in the form of chromium hydroxide, and it has the appearance of powder and is easily filtered. The only disadvantage of this procedure consists in the relatively high treatment duration which does not allow the achievement of a continuous process.

The fitting in series of the electrodes allows the increase of the current anode density for a relatively low volumetric density, whereas total intensity in the circuit is equal to the intensity of a single electrochemical cell. Based on these grounds we aimed to reduce the time for electrolysis processes by increasing the density of the current on an electrode. Admitting that maintaining water during ten minutes in the electrolyzer leads to performing a continuous flux treatment we tried to find the optimum current density which will ensure a high efficiency and minimal power consumption for this time.

It is found that the efficiency of the treatment increases from 37 to 96.7% when the density of current increases from 0.2 to 1 A/dm^2, after which, the increase of current density two and three times, raises the efficiency only with few percent.

The energy consumption also has a high increase at the current densities by 2 and 3 of/dm^2, caused by the increase of the voltage at the terminals, a result of strong polarization of electrodes. Therefore, under the conditions of fitting of the electrodes in series a 10-minute treatment can be made, at a current density of 1A/dm^2, thus ensuring a efficiency over 95% with a power consumption of approximately 1 kW/m^3.

The optimal conditions were obtained in the conditions of an electrochemical treatment with steel carbon anodes fitted in series.

The use of higher concentrations of Cr^{6+} ions led to the drop in the efficiency of the method because of electrode passivation. If the case of parallel fitting electrodes, an anode surface of 1.2 dm^2/0.3 l solution at a current density of 0.2 A/dm^2 for 30 minutes allows to perform a treatment with an efficiency of 100% and a consumption of 0.45 kWh/m^3.

The fitting of an equal number of electrodes allowed the reducing of the electrolysis time to 10 minutes, the efficiency of the treatment being 96.7 % at the density of 1 A/dm^2, with a power consumption of 1.1 kWh/m^3. The water treatment containing Cr^{6+} ions in a cell with pads fitted in parallel is twice more economical than in the case of their fitting in series, but it shows the disadvantage of a higher duration and of the process discontinuity [5].

The option for a system or the other will depend on the quality of the waters which are to be purified, the need for a continuous process being imposed in the case of chroming installations with a higher production.

3.1. Electrolytic purification of industrial waste water

The development of the industry and in particular of the chemical industry imposes special measures concerning the protection of the environment; in this context, a major problem is the purification of industrial waste water.

The development and implementation of sewage technologies at a technical contemporary level require a modern process to ensure a more advanced impurificator removal at a low cost.

Among the processes applied at present for purification waste water, a special place is occupied by the electrochemical methods, because of the possibilities they can offer:

- a wide area of appliance;
- the advanced destruction of the biodegradable impurificators;
- the recovery or the regeneration of valuable products.

Depending on the way the removal of the impurificators is made, the electrochemical methods can be classified into three main processes: electrolysis, electrodialysis, electroflotation.

3.1.1. Electro-chemical treatment of waste waters containing different inorganic impurificators

The oxidation of electro-chemical cyanide from waste waters (destruction of free and complex cyanide), the destruction of CN^- ions, after the electrolysis, is the result of conduct of the following processes:

$$CN^- + 2OH^- \rightarrow CNO^- + H_2O + 2e \quad (2)$$
$$2CNO^- + 6OH^- \rightarrow HCO^-_3 + N_2 + 2H_2O \quad (3)$$

In order to intensify the process of oxidation, small quantities of chlorides are frequently added in the polluted waters. The chlorine released on anode exercises an oxidizing action on CN^-, according to the reaction:

$$CN^- + Cl_2 + 2\ OH^- \rightarrow CNO^- + 2\ Cl^- + H_2O \quad (4)$$

One of the methods of purification of the solutions containing the ferrous and potassium ferri-cyanide propose their treatment in an electrolyzer with graphite anode and steel cathode at a current density of by 0.8-30 A/dm^2.

In order to intensify the process, 3-6 g/l of $CaCl_2$ for 1 g ferrous and ferri-cyanide are introduced in solutions.

Thus, 500 ml of solution, containing 1 g/l $Fe(CN)_6^3$ to which 3 g $CaCl_2$ were added, were subjected to the electrolysis process at a current anode density of 7-8 A/dm^2, under a voltage of 5 V, at a temperature of 90 °C and pH = 3.

After 30 minutes of electrolyze time, the solution was pure, free of CN^- or Fe^{2+} and Fe^{3+} (ions which have been precipitated as hydroxides).

3.1.2 Removal of chloride As^{3+}

Removal of chloride As^{3+} from the leaks waters in the sulfuric acid industry can be achieved through electrolysis in a cell with two separate compartments through an orifice (cationic membranes a MK-40 type).

Water, containing As^{3+} (535 mg/l, pH = 1.5-3.5 is passed through the anodic space and through the cathodic space a conductive solution pass (3-5% NaCl or Na_2SO_4). In this process, the iron soluble anode it used. During the electrolysis process, the anode dissolution with Fe^{2+} ions formation and the oxidation of As^{3+} ions at As^{5+} ions take place, which, together with ferrous hydroxide, form an insoluble complex [4].

The degree of purification depends to a great extent on the density of the current. The optimum density is 1.9 A/dm^2, to which the degree of purification is 99.7 % (the arsenic concentration of decreases from 534 mg/l to 1.6 mg/l, after 30 minutes of electrolysis).

3.3. The recovery of iodine from the metal iodides contained in the waste waters

The residual solutions from the deposed titanium containing TiI_4 (5 g/l), to which 5% HNO_3 has added were subjected to the electrolysis with platinum pads at a current density of 3.5 A/dm^2, at 25 °C. The iodine formed on anode was precipitated and filtered [5].

The electro-chemical recovery of $FeSO_4$ and $FeSO_4$ resulting as sub-products in the manufacture of TiO_2, is done by the electrolysis in a cell with two separate compartments through a membrane able to avoid the passing of NH_4^+ cations from anodic compartment to the cathodic one and also to allow the passing of SO_4^{2-} ions from the cathodic compartment to the anodic one. After the electrolysis, the iron is deposited on the cathode on the anode $(NH_4)S_2O_8$ is formed.

4. Conclusions

Waste waters from metal plating contain between 1000 and 3000 mg/l metallic ions from various anions, complexion agents or shine agents, showing a high degree of toxicity.

The electrolysis of such waters, under certain conditions, allows their denoxiousness and metals recovery. The toxic metallic ions can be removed by reduction in the process of cathodic process, when their recovery is achieved by their embedding in hydroxides precipitations, resulting from the electrolysis with the water-soluble anode (usually of iron). At the same time, with the metallic ions removal, and the oxidation of some harmful anion is carried out, such as CN^- or some organic compounds present in the water.

Such toxic metals (Cr, Pb, Hg, Zn, Mn, Cd) and CN^- have been removed from waste water through electrolysis process, in the presence of the sodium chloride, using the soluble anode made of iron and cathodes made of an insoluble material.

The metals toxic ions have been precipitated as ferrites and removed by filtration, and CN^- has been oxidized to CO_2 and N_2.

For the recovery of metals from the diluted solutions, the electrolysis with a cathode made of current particles enclosed in a rotating perforated cylinder is carried out.

Waste water (the electrolyte) is circulated among the cathode particles using a pump.

References

[1]. Dan Ovidiu Ianculescu, *Staţii de epurare de capacitate mică*, Editura MatrixRom, Bucureşti, 2002.

[2]. Gh. Ionescu, Raluca Racoviţeanu, *Epurarea apelor uzate*, Editura MatrixRom, Bucureşti, 2003.

[3]. ***, *Normativ tehnic privind stabilirea limitelor de încărcare cu poluanţi a apelor uzate*, NTPA-001 and NTPA-002.

[4]. ***, *Staţii de epurare. Partea 3. Epurări preliminare*, SR EN 12255-3, 2002.

[5]. ***, *Staţii de epurare. Partea 16. Filtrare fizică*, SR EN 12255-16, 2002.

THE ANNALS OF "DUNAREA DE JOS" UNIVERSITY OF GALATI
FASCICLE IX. METALLURGY AND MATERIALS SCIENCE
Nº. 3 - 2016, ISSN 1453 – 083X

RESEARCH ON THE OPERATION OF COMMERCIAL VESSELS WITH COMPRESSED AIR

Ștefan DRAGOMIR, Marian BORDEI*
"Dunarea de Jos" University of Galati, Romania
*correspondent author
e-mail: mbordei@ugal.ro

ABSTRACT

Regarding the reduction of the carbon dioxide emissions in the atmosphere, this paper is going to present a system of propulsion with compressed air used for medium-sized commercial vessels. In the transport domain, Romania holds a key position at the eastern border of the European Union, a transit area, both in the east-west direction (connection with Asia via the Black Sea), and north-south (from the Baltic Sea to the Mediterranean Sea). Three of the priority axes TEN-T cross the territory of Romania. We believe that using compressed air instead of fossil fuels will also determine a fuel economy of approximately 42% leading to the improvement of the companies finances which use these systems.

KEYWORDS: air compressed engine, vessel

1. Introduction

The national transport systems existing in Romania consist in cargo and passengers transport. In these systems, the road, rail (on inland waterway and maritime), air, non-motorized and special (through pipes and air electrical transport) operate. As regards the transport by inland waterway, it is noted that the main ports of Romania are: Constanta, Mangalia, Midia-Navodari, Sulina, Tulcea, Galati, Braila. The use of compressed air for the propulsion for the coastal vessels proves to be effective from the point of view of consumption and autonomy.

The constructive advantage of using compressed air is the fact that can be introduced into a classic type engine by means of a relay and an electro-valve playing the role of a compressed air pressure regulator which is introduced with force into the engine cylinders placing both the crankshaft and the flywheel in rotating movement.

2. Experimental model

For the laboratory experiment an engine with a single piston was used (Figure 1).

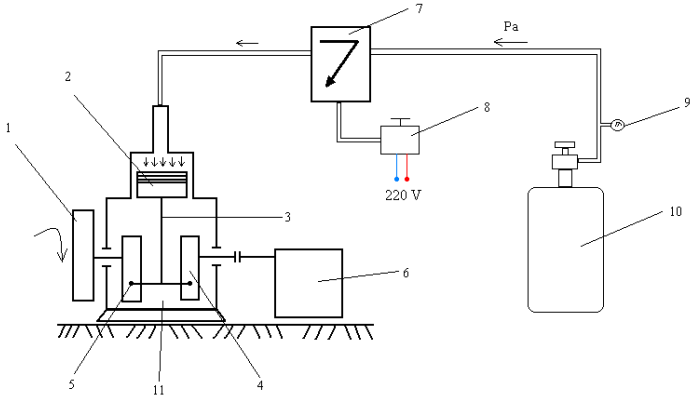

Fig. 1. *Propulsion system constructive schedule: 1 - flywheel; 2 - piston; 3 - con rod; 4 - crankshaft; 5 - button of the eccentric crank; 6 - working machine; 7 - electro-valve; 8 - relay; 9 - pressure gauge; 10 - compressed air tube; 11 - engine with a piston in the two-stroke engines*

The components necessary for making the experiments in optimal conditions are: engine itself - standard construction (with a piston, two-stroke engines); the elector-valve; relay; the cylinders with compressed air; the pressure gauge; the pipes in the high-pressure circuit. The engine itself has electronic ignition, the piston has 48 mm diameter and the stroke of the piston is 62 mm. The engine develops a power of 4.2 HP at 4800 rpm/min, its capacity being of 120 cc.

The prototype system can be used when moving a boat, the source of compressed air in this case being some tubes of oxygen having a pressure 150 bars, a capacity of 8 m^3 air and which at an average consumption of about 4 bar/sec a tube will consume in about two hours (Figure 2).

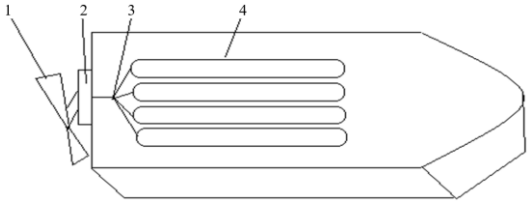

Fig. 2. *Vessel propulsion by compressed air: 1 - propeller, 2 - engine, 3 - joints, 4 - compressed air tubes*

In order to ensure the vessel autonomy for a period of four hours, four tubes of compressed air will be used.

The tubes can also help to a better floatation of the survival craft [1].

3. The engine operation

The compressed air from the gas tubes which forms the supply tank, is released by opening the gas cylinder tap.

The compressed air with pressure between 4 and 8 bar will penetrate into the electro-valve, which has also the role of pressure regulator (similar acceleration from a car), after which, passing through the electro valve, penetrate into the engine cylinder by pushing it.

The flywheel takes over and smoothes out the rotating movement obtained at the shaft of its own [3].

At the shaft of the flywheel, depending on the pressure in the cylinder of the engine, a torque M_{ac} and a speed of rotation will be obtained. The shaft is put in touch with the blades by means of a coupling bolts. The higher the pressure of instilling good will be, the higher the rotation speed and the torque will be, reaching the necessary value for the equipment functioning [2].

3.1. Calculation of engine torque

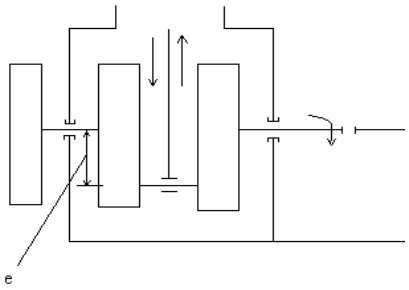

Fig. 3. *Schedule for eccentricity torque calculus*

Torque: $M_{ac} = F_p * e * \cos\alpha$ [Nm]

where: e - eccentricity; e = 0.06;

F_p - force measured using the pressure gauge;

$\alpha = 30°$; $\cos\alpha = 0.86$;

M_{ac} = 88.73 Nm (maximum torque value);

M_{ac} = 14 Nm (minimum torque value).

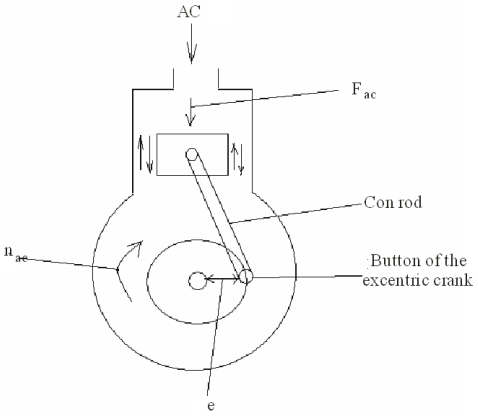

Fig. 4. *Compressed air engine section*

3.2. Rotation speed computation of engine crankshaft

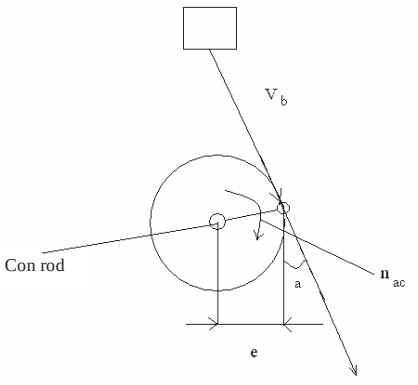

Fig. 5. *Calculus schedule rotation speed and tangentially speeds*

Tangentially speeds:

$$V_b = \omega * e = \frac{\Pi * n_{ac} * e}{30} \text{ [m/s]}$$

Crankshaft rotation speed:

$$n_{ac} = \frac{30\, V_b}{\Pi * e} \text{ [rot/min]}$$

Speed values for:

$P_{min} \rightarrow v_{min}$ = 60 rot / min
$P_{max} \rightarrow v_{max}$ = 150 rot / min

3.3. The power resulting from the motor shaft

$$P = k_d * \frac{M_{ac} * n_{ac}}{9550\, \eta} \text{ [kW]}$$

k_d – overload factor, k_d = 1, 2

$$M_{ac} = F_b * e * \cos\alpha \text{ [Nm]}$$

where: e = 0.06 m
α = 30°; cos α = 0.86
η = 80 %

Power values:

$$P_{vm\,\min} = 1.2\, M_{ac\min} * \frac{P_{\min}}{9550\, \eta} \text{ [kW];}$$

$P_{vm\,min}$ = 1.2 kW

$$P_{vm\max} = 1.2\, M_{ac\max} * \frac{P_{\max}}{9550\, \eta} \text{ [kW];}$$

$P_{vm\ max}$ = 1.8 kW

3.4. Measurements and recordings of the parameters for the prototype

There were measured and recorded the following parameters for the prototype: pressure, torque and speed of rotation, reported in Table 1.

Table 1. *The measured parameters for the prototype*

Parameter	t_1 = 0 s	t_2 = 10 s	t_3 = 20 s	t_4 = 30 s	t_5 = 40 s	t_6 = 50 s	t_7 = 60 s
Pressure after valve [bar]	4.1	4.4	4.6	4.9	5.2	5.8	6.4
Rotation speed [rpm/min]	60	82	96	110	125	136	152
Torque to the shaft to the engine [Nm]	88	93	113	128	145	163	184

It is noted that the same time with the increase of air pressure in the engine, the torque of the crankshaft and the rotating speed of the propeller increase too, meaning the speed of the vessel.

A good quality of the air is essential in order to achieve a maximum output of the pneumatic engine system as regards the capacity, torque, speed and performance. It is recommended that the air with which the supply is carried out to be filtered and regulated by the use of a filter, a pressure regulator and an air regulator.

4. Conclusions

From a technical point of view, the pneumatic motors are reliable and due to their mode of operation, they can be used in several types of applications. The engine is part of the pneumatic circuit, together with a pump, valve, filters, connectors and others. Each item has its role, or the compressed air from the reservoir is supplied under pressure to the engine, which is connected directly to the drive system. Pneumatic engines are precise forces in various applications because of their technical advantages. These systems are easier to maintain and have a greater longevity than the electric motors or the complex mechanical systems [4].

While the electric motors sizes are proportional to the power that develops, the pneumatic engines are much smaller, relative to the same task. The electric motors have constant need of electric power and must be placed directly on the axis of the movement, a difficult thing in different situations. For the same application, a pneumatic engine system with small dimensions can be easily connected to a pump through a system of flexible hoses that can be placed easily even in small spaces.

Pneumatic motors work even after the interruption of the pressure air source. The operating chamber, after being filled with compressed air, closes securely and loses the connection with the pressure source.

The compressed air expands, assigns its energy to the mobile component of the engine at the same time with its decrease in temperature. Such an engine is operated in such a way with the cycle of the expansion bottle. There are pneumatic engines which operate after a mixed cycle i.e. the first part of the cycle works with full pressure, so the engine is in connection with the source of the compressed air and the second part, after a cycle of expansion.

The efficiency of the pneumatic engines depends on the pressure and air flow rate with which the moving system is supplied. By adjusting the pressure and the flow of air, the torque and the pneumatic engine speedy can be adjusted.

References

[**1]. Demian Tr., Banu G.**, *Micromotoare pneumatice liniare si rotative*, Editura Tehnica, Bucuresti, 1984.
[2]. Stanescu A. M., Banu V., Atodiroaei M., Gaburici V., *Sisteme de automatizare a echipamentelor pneumatice*, Editura Tehnica, Bucuresti, 1987.
[3]. Radcenco V., Alexandrescu N., lonescu M., Ionescu M., *Calculul si proiectarea elementelor si schemelor pneumatice de automatizare*, Editura Tehnica, Bucuresti, 1985.
[4]. Lazea Gh., *Echipamente de automatizare pneumatice si hidraulice –indumator de laborator*, Editura Lito IPCN, Cluj-Napoca, 1982.

THE ANNALS OF "DUNAREA DE JOS" UNIVERSITY OF GALATI
FASCICLE IX. METALLURGY AND MATERIALS SCIENCE
N°. 3 - 2016, ISSN 1453 – 083X

METHODS TO REDUCE GAS EMISSIONS ONBOARD SHIPS

Ioan BOSOANCĂ
"Dunarea de Jos" University of Galati, Romania, Faculty of Naval Architecture, Galati,
47 Domneasca Street, 800008, Romania
e-mail: ioan.bosoanca@ugal.ro

ABSTRACT

Regarding the latest IMO requirements, the EEDI (Energy Efficiency Design Index) is mandatory to be limited as levels under IMO MEPC requirements.

The paper presents some paths to reduce EEDI as are applied onboard a 5550 TEU C/V and their effects upon ship's performances.

KEYWORDS: IMO MEPC, Energy Efficiency Design Index, innovative propeller, slow steaming, energy saving

1. Introduction

Greenhouse gas emissions lead not only to well-known global warming, but also to ocean acidification affecting aquatic biota [1]. Marine Environmental Protection Committee (IMO MEPC) introduced *Energy Efficiency Design Index (EEDI)* as an instrument to quantify these COx emissions, especially for new ships, even if this industry is responsible for only 3% of planetary gas emissions. Together with *Ship Energy Efficiency Management Plan (SEEMP)* they became mandatory under MARPOL Annex VI beginning with 1st January 2013.

This EEDI limitation addresses container ships, tankers, bulk carriers etc. but not passenger and RO-RO ships, even the EEDI must be calculated also for them, acc. to [2].

Having in mind the above considerations, the owners, charterers and ship's operators need to adopt measures to limit the gas emissions using different methods and technologies. This means that limiting environment pollution should be a part of the SEEMP, as by example, speed optimization.

2. Container carrier ships

Because container ships are the most important ships form the global warming standpoint, this paper presents the benefits of retrofitting the propeller onboard an existing vessel and lowering the revolution speed of Main Engine coupled directly with the propeller, so-called *slow steaming*. The ship's service speed with original arrangements is 25.0 kts. It was used a new innovative ESCAP propeller (MMG-Germany), see Fig. 1, acc. to [3]. The old FPP propeller (6 blades, 8.0 m diameter) was replaced with a new propeller (5 blades, but a greater diameter, 8.2 m) having fins for energy saving, mounted in aft side of propeller disk, similar the well-known type PBCF (*Propeller Boss Cap Fins*):

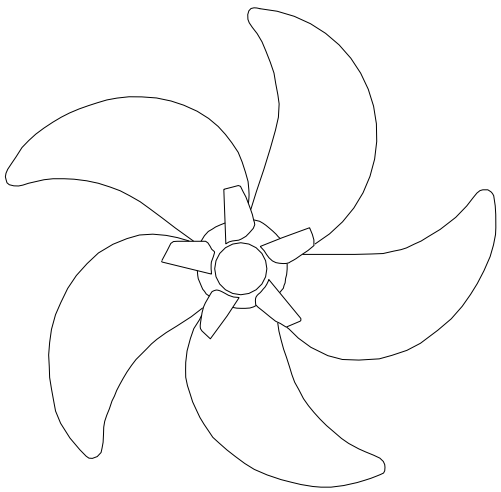

Fig. 1. *Re-design ESCAP propeller (MMG-Germany)*

Applying slow steaming concept, the MCR (Maximum Continuous Rating) power was reduced from 42140 kW @ 104 rpm to 27391 kW @ 91.3 rpm.

According to [4], the power-speed performances have been tested in progressive speed trials on Adriatic Sea, Rijeka area, in ballast condition, conducted by author.

There have been performed three double runs on north to south direction and vice versa, with the followings propeller rpm: 50, 65.0 and 91.3 rpm, applying the procedure of [5].

The corresponding speed – power diagram is shown in the bottom Fig. 2:

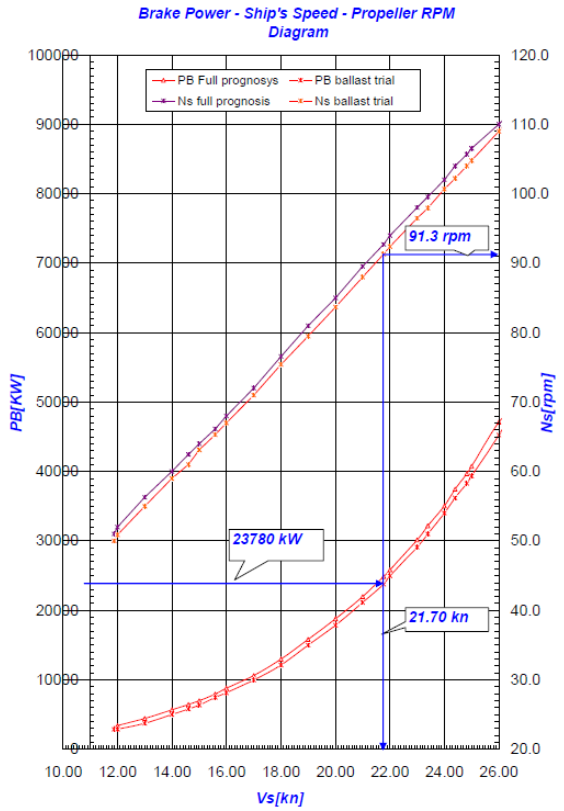

Fig. 2. *Power-Ship's Speed Diagram*

According to [6], attained EEDI it is:

$$\frac{\left(\prod_{j=1}^{n} f_j\right)\left(\sum_{i=1}^{nME} P_{MEi} \circ C_{FME(i)} \circ SFC_{ME(i)}\right) + (P_{AE} \circ C_{FAE} \circ SFC^{*}_{AE}) + \left(\left(\prod_{j=1}^{n} f_j \circ \sum_{i=1}^{nPTI} P_{PTI(i)} - \sum_{i=1}^{neff} f_{eff(i)} \circ P_{AEeff(i)}\right) \circ C_{FAE} \circ SFC_{AE}\right) - \left(\sum_{i=1}^{neff} f_{eff(i)} \circ P_{eff(i)} \circ C_{FME} \circ SFC^{**}_{ME}\right)}{f_i \circ f_c \circ Capacity \circ f_w \circ V_{ref}}$$

where:

f_j: correction factor for ship specific design elements;
P_{MEi}: power of main engines;
C_F: conversion factor between fuel consumption and CO_2 emission;
SFC: specific fuel consumption;
P_{AEeff}: auxiliary power reduction;
P_{PTI}: shaft motor;
f_{eff}: availability factor of innovative energy efficiency technology;
P_{AEeff}: auxiliary power reduction;
f_i: capacity factor;
f_c: cubic capacity correction factor;
Capacity: bulk carriers, tankers, gas carriers, ro-ro cargo ships and general cargo ships;
f_w: weather factor;
V_{re}; ship's speed.

Assuming:

- Type of ship: container carrier;
- one M/E;
- P_{ME} = 42140 kW;
- C_{FME} = 3.114 acc. to [5];
- SFC_{ME} = 165g/kWh;
- P_{AE} = 2310 kW;
- C_{FAE} = 3.206 acc. to [5];
- SFC_{AE} = 220g/kWh;
- $P_{PTI} = P_{AEeff}$ = 0;
- $f_j = f_{eff}$ = 0;
- f_i = 1;
- f_c = 1;
- Capacity = 74447 dwt;
- f_w = 1;
- V_{ref} = 25 kts.

In the below Tables (no. 1 and no. 2) the EEDI, both for original ship and updated ship are calculated:

Table 1.

	Ship's original data				
	MCR	=	42140	kW	
	Deadweight	=	74447	dwt	
	Ship's speed	=	25	kts	
	No. of M/Es	=	1		
75%	P_{ME}	=	31605	kW	
	C_{FME}	=	3.114		acc.to [6]
	SFC_{ME}	=	165	kWh	
	P_{AE}	=	2310	kW	
	C_{FAE}	=	3.206		acc. to [6];
	SFC_{AE}	=	220	g/kWh	
	$P_{PTI}=P_{AEeff}$	=	0		
	$f_j=f_{eff}=0$;	=	0		
	$f_i=1$;	=	1		
	$f_c=1$;	=	1		
70%	Capacity	=	52113	dwt	
	$f_w=1$;	=	1		
75%	V_{ref}	=	19	kts	
	EEDI orig	**=**	**18.29**	g - CO_2/ton mile	

In original version, the $EEDI_{orig}$ = 18.29 gCO_2/ton mile.

Table 2.

	Ship's new data				
	MCR	=	27391	kW	
	Deadweight	=	74447	dwt	
	Ship's speed	=	21	kts (after sea trials)	
	No. of M/Es	=	1		
75%	P_{ME}	=	20543	kW	
	C_{FME}	=	3.114		acc.to [6]
	SFC_{ME}	=	165	kWh	
	P_{AE}	=	2310	kW	
	C_{FAE}	=	3.206		acc. to [6];
	SFC_{AE}	=	220	g/kWh	
	$P_{PTI}=P_{AEeff}$	=	0		
	$f_j=f_{eff}=0$;	=	0		
	$f_i=1$;	=	1		
	$f_c=1$;	=	1		
70%	Capacity	=	52113	dwt	
	$f_w=1$;	=	1		
75%	V_{ref}	=	16	kts	
	EEDI new	**=**	**14.85**	g - CO2/ton mile	

In updated version (innovative propeller and de-ratted M/E) the $EEDI_{new}$ = 14.85 gCO_2/ton mile.

3. Conclusions

Reduction of gas emissions is an important task in maritime transport, both for designers, shipbuilders, owners, charterers etc. The legislation on sea and shore related to pollution uses different procedures, and is more and more updated in order to reduce the gas emissions.

In Fig. 3 below are shown the rules for new ships beginning with 2025 and the calculated EEDI for original and updated ship.

For the ship presented in this paper (already in operation since 2011) the calculated EEDI is greater than limit for new ship beginning with 2015, even after new propeller mounting and M/E de-ratted. This means the new values for gas emission are very low and great investment efforts should be made in the future for ships already being in operation to fulfill the new rules regarding the gas emissions.

Anyway, lowering maximum accepted level for gas emission means less pollution and a cleaner environment.

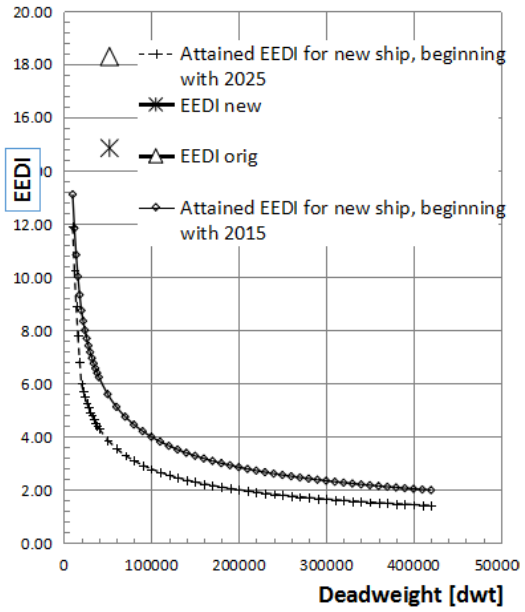

Fig. 3. *Attained EEDI for original propeller, new propeller and MEPC rules beginning with 2025*

References

[1]. Matthias Hofmanna, Hans-Joachim Schellnhubera, *Oceanic acidification affects marine carbon pump and triggers extended marine oxygen holes*, www.pnas.org_cgi _doi_10.1073_pnas.0813384106.

[2]. ***, *Implementing the Energy Efficiency Design Index (EEDI). Guidance for owners, operators, shipyards and tank test organisations* – Lloyd Register 2012.

[3]. ***, *FPP Manual, MMG Project no. 90.1427-00-8200*, 2014.

[4]. Bosoanca I., *Power – Ship's Speed onboard MSC Alicante, 5550 Teu Container Carrier*, Diagnose and Measurements Group, July 2016.

[5]. ***, ISO 15016-2015: *Ships and marine technology - Guidelines for the assessment of speed and power performance by analysis of speed trial data*.

[6]. ***, *Guidelines on the method of calculation of the attained energy efficiency design index (EEDI) for new ships, Resolution* MEPC.212(63) 2012.

MANUSCRISELE, CĂRŢILE ŞI REVISTELE PENTRU SCHIMB, PRECUM ŞI ORICE CORESPONDENŢE SE VOR TRIMITE PE ADRESA:

MANUSCRIPTS, REVIEWS AND BOOKS FOR EXCHANGE COOPERATION, AS WELL AS ANY CORRESPONDANCE WILL BE MAILED TO:

LES MANUSCRIPTS, LES REVUES ET LES LIVRES POUR L'ECHANGE, TOUT AUSSI QUE LA CORRESPONDANCE SERONT ENVOYES A L'ADRESSE:

MANUSCKRIPTEN, ZIETSCHRITFTEN UND BUCHER FUR AUSTAUCH SOWIE DIE KORRESPONDENZ SID AN FOLGENDE ANSCHRIFT ZU SEDEN:

After the latest evaluation of the journals by the National Center for Science Policy and Scientometrics (**CENAPOSS**), in recognition of its quality and impact at national level, the journal will be included in the B^+ category, 215 code (http://cncsis.gov.ro/userfiles/file/CENAPOSS/Bplus_2011.pdf).

The journal is already indexed in:

EBSCO: http://www.ebscohost.com/titleLists/a9h-journals.pdf

Copernicus: http://journals.indexcopernicus.com/karta.php

The papers published in this journal can be viewed on the website of "Dunarea de Jos" University of Galati, the Faculty of Engineering, pages: http://www.sim.ugal.ro/Annals.htm, http://www.imsi.ugal.ro/Annals.html.

Name and Address of Publisher:
Contact person: Elena MEREUȚĂ
Galati University Press - GUP
47 Domneasca St., 800008 - Galati, Romania
Phone: +40 336 130139, Fax: +40 236 461353
Email: gup@ugal.ro

Name and Address of Editor:
Prof. Dr. Eng. Marian BORDEI
Dunarea de Jos University of Galati, Faculty of Engineering
111 Domneasca St., 800201 - Galati, Romania
Phone: +40 336 130208
Phone/Fax: +40 336 130283
Email: mbordei@ugal.ro

AFFILIATED WITH:

- THE ROMANIAN SOCIETY FOR METALLURGY
- THE ROMANIAN SOCIETY FOR CHEMISTRY
- THE ROMANIAN SOCIETY FOR BIOMATERIALS
- THE ROMANIAN TECHNICAL FOUNDRY SOCIETY
- THE MATERIALS INFORMATION SOCIETY (ASM INTERNATIONAL)

Edited under the care of the FACULTY OF ENGINEERING

Annual subscription (4 issues per year)

Editing date: 15.09.2016
Number of issues: 200
Printed by Galati University Press (accredited by CNCSIS)
47 Domneasca Street, 800008, Galati, Romania